

**Temporal and Spatial Variations of the
Geomagnetic Field, up to a Timescale of 10^5
Years**

Ian Turton

A thesis submitted in fulfilment of the requirements
for the degree of Doctor of Philosophy
to the
University of Edinburgh
1992



Abstract

This thesis comprises two parts. The main part is involved with laboratory studies of the palaeosecular variation of the geomagnetic field as recorded in lake sediments. The natural remanent magnetization of the sediments cored from the two Italian maar lakes, Lago di Monticchio and Lago di Martignano, has been studied. Further studies were carried out on the sediments of Lago di Martignano to determine the cause of large variations in the magnetic intensity of the sediments with an age of ~ 6000 years BP and it was concluded that this was caused by the arrival of Neolithic man and the advent of agriculture in the catchment area. The directional record for this lake was also compared to the established record for north west Europe. Several declination and inclination features could be correlated between the two records. The record from Lago di Martignano can be accepted as a regional palaeomagnetic reference curve for central Italy.

Cores up to 50m long were taken from Lago di Monticchio. Whilst not yet firmly dated, it is agreed that this record spans the last 250,000 years. A relative palaeointensity record has been calculated and spectral analysis has been carried out. It is concluded provisionally that the palaeointensity recorded in the sediments was effected by the astronomical frequencies associated with precession of the Earth, the eccentricity and the obliquity of the Earth's orbit.

The second part of this thesis is concerned with modeling the palaeosecular variations as recorded in sediments around the world through the Holocene, i.e. the last 10,000 years. The properties of sequential secular variation records from sediments are compared with palaeosecular variation scatter determined from sets of lava flows. It is concluded that a comparison between PSV recorded in lava flows and lake sediments is valid.

Acknowledgments

This project was funded by the Natural Environment Research Council. My thanks to Prof. K.M. Creer for initiating this project and assisting me through out.

I must also thank Mr A. Pike for all his technical assistance both on field work and in the laboratory and Elizabeth Kroll for her help in measuring the ARM's and SIRM's of core D.

I am grateful to all my colleagues in the groups collaborating in the Euromaars project for their invaluable help and kindness on my visits to their labs.

Many thanks to all the staff and postgraduate students in the department for their often fruitful discussions and other input over the years.

I'd also like to thank my wife, Lesley, for all her support and help during the arduous task of writing up this thesis.

Contents

Abstract	i
Acknowledgments	iii
Abbreviations	vii
1 Introduction	1
1.1 Geomagnetic Secular Variations	1
1.2 Objectives	2
2 Palaeomagnetic Records from Lake Sediments	3
2.1 Introduction	3
2.2 Sources of Magnetic Grains	4
2.3 Detrital and Post-Depositional Remanent Magnetizations	4
2.3.1 Introduction	4
2.3.2 Time Scale for Grain Alignment	5
2.3.3 Interpretation of the Geomagnetic Record	6
2.4 Maar Lake Formation	7
3 Methodology	9
3.1 Coring techniques	9
3.1.1 Mackereth Corer	9
3.1.2 Livingstone Corer	9
3.2 Sub-sampling	10
3.2.1 Mackereth Cores	10
3.2.2 Livingstone Cores	11
3.3 Magnetic Measurements	11
3.3.1 Measurement of Natural Remanences	11
3.3.2 Measurement of Susceptibility	12

3.3.3	Demagnetization Procedures	12
3.3.4	Artificial Remanences	12
3.4	Variations in the Intensity of the Geomagnetic Field	13
4	Spectral Analysis Methods	14
4.1	Introduction	14
4.2	Methods	15
4.2.1	The Lomb–Scargle Method	15
4.2.2	Fourier Transform Spectral Analysis	16
4.2.3	The Maximum Entropy Method	17
4.3	Testing of the Methods	18
4.3.1	Synthetic Data	18
4.3.2	Results	18
4.4	Conclusions	25
5	Results from the Laghi di Monticchio	30
5.1	Introduction	30
5.2	Regional Geology and the Formation of the Lake	33
5.3	Palaeomagnetic Results from Lago di Monticchio	33
5.3.1	Mackereth Cores	33
5.3.2	Livingstone Cores	33
5.4	Initial Dating of the Core	49
5.5	Spectral Analysis of Core D	51
5.6	Discussion	57
5.7	Evidence for Seismicity in Lago di Monticchio	58
6	Results from Lago di Martignano	61
6.1	Introduction	61
6.2	Setting and Geology	61
6.3	Description of Palaeomagnetic Results	62
6.4	Construction of a Time scale	65
6.5	Description of the Secular Variation	66
6.6	Magnetic Mineral Studies on the Sediments of Lago di Martignano	69
6.7	Human Impact on the Palaeomagnetic Record and the Pollen Record	73
6.8	Conclusions	76
7	Modeling of the Palaeo–Geomagnetic Field	77
7.1	Introduction	77

7.2	Modeling Theory	78
7.2.1	Simple Drifting and Oscillating Dipole Models	78
7.2.2	Current Loop Models	80
7.2.3	Spherical Harmonic Models	82
7.2.4	The McFadden, Merrill and McElhinny Model	83
7.3	Results of Modeling	87
7.4	Test of Model G	102
7.5	Conclusions and Discussion	102
8	Conclusions	104
8.1	Introduction	104
8.2	Palaeosecular Variations in Italy and Europe	104
8.3	Geomagnetic Field Modeling, from Palaeosecular variations	105
A	Computer Programs	107
A.1	Palaeomagnetic Data Handling	107
A.1.1	Introduction	107
A.1.2	Data Entry	107
A.1.3	Data Processing	111
A.2	Modeling Programs	120
A.2.1	Introduction	120
A.2.2	Dipole Models	120
A.2.3	Single Site Models	120
A.2.4	World Models	127
B	Spherical Harmonics	137
	References	140

Chapter 1

Introduction

1.1 Geomagnetic Secular Variations

The first scientific studies of the Earth's magnetic field were undertaken by Gilbert in *De Magnete* in 1600. In 1635 Gellibrand recognised a steady progressive change in the angle between magnetic north and geographic north (Chapman and Bartels, 1940). Bauer observed that over a long period of time these changes are cyclic and that the details of the curves for Paris and London are similar (e.g. see Stacey, 1969). Thus it can be seen that secular variation occurs on a large scale.

In 1683 Halley published his conclusion that secular variation was due to a steady westward drift of the geomagnetic field (Bullard, 1956). Halley proposed that part of the field was due to magnetic poles situated in an inner core, and hence came very close to present ideas on the subject. He reasoned that if the core rotated more slowly than the outer part of the Earth then the field would appear to drift westward.

Until recent years geomagnetic studies have been limited to the last few centuries, i.e. to the historical period which man made instruments have been available, either in the form of compasses, dip-circles on sailing ships or latter in observatories.

One of the main objectives of the study has been to extend the temporal coverage of geomagnetic database to reveal more realistically the nature and evolution of the processes that cause the field. Lake sediment palaeosecular variation studies can be used to bridge the gap between the short term records available from magnetic observatories and satellites and the extremely long period records from the reversal stratigraphy of the ocean floor. The method depends on magnetic grains contained by sediments becoming aligned along the ambient magnetic field at the time of deposition (or soon after). Lake sediment sequences can be found to provide records of a few thousand to hundreds of thousands of years long, which are the characteristic time scales for the

non-dipole field (Bullard *et al.* 1950). Marine sediments, because of their much slower rates of deposition are not able to resolve secular variation patterns with characteristic times of the order of a few thousands of years.

1.2 Objectives

This work falls in to three parts:-

1. the broadening (in the geographical sense) the European palaeosecular variation database by the measurement of palaeosecular variation at two sites in Italy
2. an attempt to model secular variation of the geomagnetic field using lake sediment palaeosecular variation records as data.
3. The question of whether the secular variations recorded in lake sediments during the Holocene has any similarities to that recorded in lava over the last 5 Myrs can be approached by comparing scatter of VGP's recorded in lake sediments with the predictions made by 'Model G' developed by McFadden *et al.* (1988).

The two lakes studied were Lago di Monticchio and Lago di Martignano. This work is detailed in Chapters 5 and 6 respectively. Both lakes are maar lakes. This type of lake has been found to provide a good environment for recording geomagnetic and climatic changes. The relatively high sedimentation rate complements the marine record by providing much higher resolution. Chapter 5 discusses the possibility that the geodynamo may be forced by astronomical periods. Chapter 6 makes use of data from a series of shorter cores from Lago di Martignano to look at the impact on the catchment area of the lake by changes in the climate and by man's arrival in the region following the end of the last ice age. The results from this lake are also presented as a preliminary palaeomagnetic type curve for this region.

A long term objective of this work is to obtain a sufficiently large amount of secular variation data from Europe to allow the creation of contour maps of field parameters (D, I, J) through time, for the Holocene. This is however an ambitious project which will take a considerable amount of time. But if a smaller amount of data can be added to the modeling programme discussed in chapter 7 for Europe, then it may be possible to model the field for Europe which would allow an informed decision to be made about where further sites of interest could be obtained.

Chapter 2

Palaeomagnetic Records from Lake Sediments

2.1 Introduction

This chapter presents a short background to palaeomagnetic studies of lake sediments. Palaeomagnetic records from lake sediments fill the gap in the geomagnetic power spectrum between historical records of hundreds of years and the record in the sea floor of polarity reversals on an order of tens and hundreds of thousands of years. Lake sediments allow the recovery of palaeosecular variations (PSV) in the scale of thousands of years, depending on rates of sediment deposition.

Only a small proportion of lakes so far studied have provided a good record of PSV. The lake dynamics must be of sufficiently low energy to allow quiet deposition of magnetic grains (see section 2.3.2): strong water currents cause systematic and strong turbulence cause random errors in the alignment of the grain magnetic moments to the geomagnetic field. This means that small isolated lakes are to be preferred.

Many small maar-type lakes (see section 2.4) fulfill these conditions with a deep, flat centre and steep sides, small, easily defined, catchment areas and are usually not connected to the local ground water table. This last consideration means there is less chance of the lake being affected by local drying during warmer periods, thus increasing the chances of a continuous record being recovered.

It is also important that the grains are predominantly spherical as a high aspect ratio can cause alignment of grain shape rather than magnetic moment during deposition. A third factor in the implantation of a faithful record of the palaeomagnetic is the source rock of the sediment (see section 2.2) which should be strongly magnetic to provide a good source of carrier grains.

Creer (1985) reviewed the state of lake sediment palaeomagnetic data; he shows that it is possible to correlate PSV features in both declination and inclination between several European lakes over large distances, for at least the Holocene. As more long records have become available since then, these correlations have been extended back through the last glacial (Weichselian) and the glacial cycles preceding this.

2.2 Sources of Magnetic Grains

The magnetic minerals present in a sediment can be classified into three groups (Thompson and Oldfield, 1986) authigenic, diagenetic and allogenic. Authigenic magnetic minerals are formed *in situ* by chemical or biological action after deposition of the sediment. Diagenetic minerals are the result of the conversion of magnetic or non-magnetic minerals to new magnetic minerals during deposition and compaction of the sediment. Allogenic minerals are carried into the lake from outside, either from within the lake catchment area or from more distant areas. The majority of magnetic minerals in maar lakes are allogenic in source, most often being the result of erosion of the bed rock or soils in the limited lake catchment area. One important source of allogenic magnetic minerals from outside the lake catchment area is wind borne volcanic debris, these tephras will form compact layers within the sediment column but can be considered instantaneous events compared to the other sediments. It is not usually possible to recover a palaeomagnetic direction from tephras, due to their fast deposition and poor consolidation.

2.3 Detrital and Post-Depositional Remanent Magnetizations

2.3.1 Introduction

The direction of the present geomagnetic field has been found to have been recorded by detrital grains in unconsolidated sediments. The primary remanence of these sediments occurs from the statistical alignment of these magnetic grains. This process has been termed detrital remanent magnetization or DRM (McNish and Johnson, 1938, Tucker, 1983). This DRM can be subsequently altered by physical misalignment of the magnetic grains, viscous remagnetization and/or chemical growth of a new magnetic phase.

When an unconsolidated sediment acquires a DRM, no change occurs to the individual magnetic moments of the detrital grains, as when a thermal remanent magnetization (TRM) is acquired. Instead the whole grain is rotated due to the torque between the

magnetic moment of the grain and the Earth's magnetic field. The grain alignment is locked in by the physical constraints of the grains forming the matrix of the surrounding sediment. If the sediment is subsequently disturbed, e.g. by water pressure applied during coring, slumping, etc., then the constraining forces can be relaxed and the grains can become realigned along the new ambient geomagnetic field direction, resulting in a post-depositional remanent magnetization (PDRM).

2.3.2 Time Scale for Grain Alignment

The simplest case to consider is that of a small spherical grain rotating freely. The equation of motion for such a grain is given by Nagata (1961) as:

$$I \frac{d^2\theta}{dt^2} = -\lambda \frac{d\theta}{dt} - mB \sin \theta - L \quad (2.1)$$

where θ is the angle between the grain moment (m) and the external field (B), I is the moment of inertia and λ is the viscous drag. L is any mechanical torque which might act on the grain, possibly over time. To solve equation 2.1 we must make some simplifications, in general the inertial term is negligible compared to the other terms (Colinson, 1965), if L is set to 0 the solution becomes:

$$\cos[\theta_t] = (1 - A)/(1 + A) \quad (2.2)$$

where $A = \tan(\theta_0/2)e^{(-2KT)}$, (θ_t is the angle after time T) $K = (mB/\lambda)$ and θ_0 is the initial grain orientation.

From equation 2.2, Tucker (1983) calculated that the time for a grain to become aligned to the Earth's magnetic field while falling through water is of the order of a few seconds. Hence it is reasonable to assume that even if the grain's orientation is completely randomized during the fall through the lake water, they would become aligned during their passage through the laminar flow region found at the water-sediment interface, before settling on the bottom.

Once in the sediment the proximity of other grains will increase the effective viscosity and hence increase the alignment time for a grain. Hamanno (1980) considered this effect theoretically and showed that as a critical void ratio is approached alignment time increases dramatically and the grain can be considered to have become blocked in. Since this decrease in void size is usually caused by compaction of the sediment, blocking will occur at a finite depth, controlled by sedimentation rate. This result is confirmed by Lovlie's experiments (1974) in which he found a depth of a few cm for slowly deposited laboratory sediments.

The PDRM can only be reset if the physical constraints preventing grain rotation are relaxed or physically moved. In the upper part of the sediment column physical perturbations may lower the blocking constraints. If the non-magnetic matrix, which is blocking the rotation of the magnetic grains, is disturbed, this may allow the magnetic grain to rotate towards the direction of the ambient magnetic field. Physical disturbance can occur as a result of gas bubbles passing through the sediment or by bioturbation and slumping. These perturbations are generally local in scale and will be random and accumulate over time. Deeper in a sediment when the grains are more firmly blocked, compaction may cause a shallowing of the inclination of the magnetic grains.

If the coring method used to recover the core is not a 'gentle' method then it is possible that the sediments will be disturbed and become unblocked. Therefore most coring techniques have developed to leave the sediment as undisturbed as possible (see section 3.1).

2.3.3 Interpretation of the Geomagnetic Record

Sub-samples of sediment taken for palaeomagnetic analysis span a period of time which depends on the deposition rate of the sediment. For example, with a lock in thickness of 10cm and a deposition rate of 1mm/yr, the lock in time would be 100 yr. Palaeomagnetic samples are normally 2cm thick hence it must be remembered that if the magnetic field changes significantly during either of the periods represented by these two critical thicknesses that there will be a smoothing of this change as recorded by the sediment. A further problem is introduced by the application of alternating field (AF) demagnetization to the samples. This will remove the contribution of low coercivity grains which are the largest and hence probably suffered most from gravitational torques during deposition, and any viscous components present. However the effect of a range of blocking times or depths due to the range of grain sizes present must be considered. The last grains to be blocked are the smallest grains which will be able to rotate in the smallest voids. These grains will have the highest coercivities and as such will contribute the high coercivity vector measured after AF demagnetization. In an undisturbed sediment this will be the component that is sought, however the smallest gains are also the first to be unblocked by any disturbance and may well carry a non-contemporaneous PDRM.

2.4 Maar Lake Formation

A maar lake is defined (Lorenz, 1973) as a large volcanic crater cut into country rock, possessing a low rim composed of pyroclastic debris (tuff or lapilli-tuff). The size of maar lakes varies from about 100 m to 2 km with a depth in proportion to the width ($\sim 10\text{m}$ to $>200\text{m}$). A maar is formed when ground or stream water enters a newly formed fissure and contacts the magma rising in the fissure. The water forms a column above the magma and becomes heated, essentially under constant volume (see figure 2.1a). The pressure rises until the water flashes to steam, the steam then rises rapidly towards the surface, ejecting chilled and fragmented juvenile rocks, country rock debris and water (figure 2.1b). The pressure at the eruption source then decreases and becomes lower than the surrounding lithostatic pressure. This leads to the wall-rocks bursting into the fissure and gives rise to an increase in the size of the fissure. The enlarged fissure will then again fill with water from above and magma from below. The eruption process will then repeat (up to several hundred times in a few weeks). With passage of time an 'explosion chamber' will form. At a critical pressure difference depending on the size and shape of the eruption chamber, the overlying wall-rocks will become unstable, causing the formation of a ring-fault. The wall-rocks enclosed by the ring-fault will then subside, along with any overlying subaerially deposited pyroclastics (figure 2.1c).

During subsidence the eruptions will continue for as long as there is a supply of water and magma in good contact. Subsidence will effectively close the vent allowing high pressures to continue to form.

The eruptions will finally cease, either due to a shortage of water or magma. The tuff-ring will then be rapidly eroded into the base of the crater, which will also fill with water to form a maar lake. The presence of a lake will increase the rate of erosion of the side walls by undercutting the tuff-ring by wave action (figure 2.1d).

Eventually the slopes will stabilise and become covered with plants and a slower sedimentation rate will occur. The result of this initially rapid sedimentation is to fill the centre of the lake and produce a lake with steep sides and a flat bottom. This type of lake is ideal for palaeomagnetic investigations as it provides a very low energy sedimentation environment at the centre of the lake and a steady input of sediment from a small, closed catchment area.

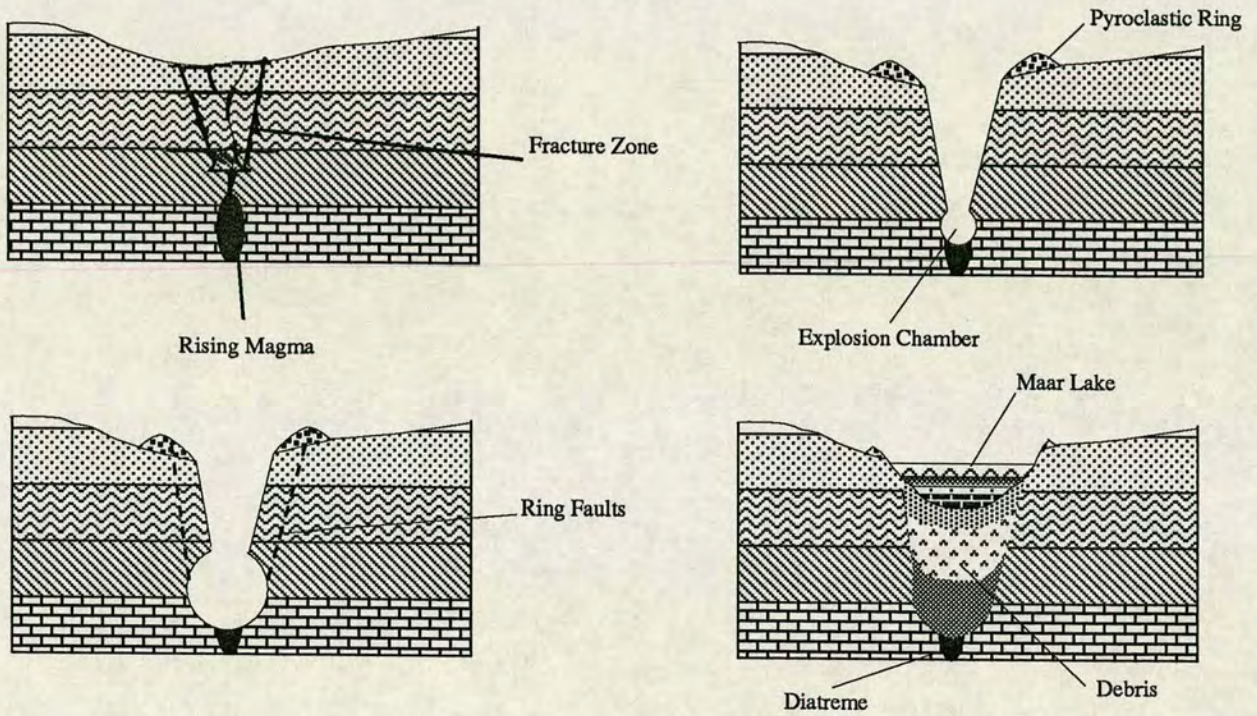


Figure 2.1. Maar Lake Formation, showing a) the initial contact between the rising magma and ground water, b) formation of an explosion chamber, c) the onset of ring faulting and d) the end of the explosions and the maar lake.

Chapter 3

Methodology

3.1 Coring techniques

3.1.1 Mackereth Corer

This is a pneumatically powered corer designed and developed by Mackereth (1958), which has the advantage of penetration of the sediment at a slow and controlled manner. This tends to limit the disturbance to the outer most edges of the core.

The corer can be used from a small inflatable boat by 2 or 3 people. The air supply is provided by a standard diving compressed air cylinder, at a pressure of 220 atmospheres, reduced to about 50 atmospheres at the corer.

Cores are recovered in a single section, so the cores are 6 or 9m long and 55mm in diameter. This means that the relative azimuthal orientation of each palaeomagnetic sub-sample is known with respect to all others. However the direction of true north relative to a core is not known, though the inclination of the core can not be far from the vertical or coring will fail (A. Pike, *Pers. Com.*). However it is possible for a core tube to bend during coring. Hence it is necessary for several cores to be taken from a lake to allow the removal of this effect.

3.1.2 Livingstone Corer

Livingstone (1955) discusses the design of a piston corer which is pushed into the sediment manually using a long rod made up of one or two metre sections screwed together.

Coring is carried out from a large fixed raft, by a team of people numbering between 5 and 20 depending on the depth of coring and the number of cores to be recovered. Cores are taken by making successive drives of 2 or 1m into the sediment, after each

drive the corer is brought back to the surface and the core is labeled and stored, a new core tube is then fitted to the corer. The corer is then reinserted into the core hole and pushed down to the coring depth, the fixed piston at the head of the core tube is then released and the core tube is pushed into the sediment, after required amount of sediment has been acquired the corer is again withdrawn. Since individual sections of the core are unorientated horizontally it is necessary to take at least 2 cores (with a few metres lateral separation) from each location with a vertical offset of section end to allow comparison of the two declination records and to provide continuous, uninterrupted sediment recovery as sediment is lost from section ends.

3.2 Sub-sampling

Sub-sampling should be carried out as soon as possible after coring to minimise damage to the samples, though in the case of the Italian cores a delay of between three to five weeks was unavoidable due to the time required to transport the cores from Italy to Edinburgh or Trier, FRG, where subsampling was carried out. The procedure was different for the two types of cores and will be described separately below.

3.2.1 Mackereth Cores

The PVC coring tubes were cut into two or three metre sections at the lake side. These sections were transported from the lake to the laboratory in Edinburgh. Later, just prior to sub-sampling these sections of core were further cut down into one metre sections for ease of handling. The core tubes were then sawed, almost through, with a circular saw along their length on both sides. The final layer of plastic was then cut through with a sharp knife taking care not to damage the sediment which was then cut through using a length of copper wire and the two equal halves were eased apart. Great care was taken at this point not to introduce shavings of PVC tube mixed into the sediment or spread across the surface of the core where the wire was pulled through.

One of each pair of halves was continuously sub-sampled for palaeomagnetic measurements in clear plastic cubic boxes of side 2.25 cm, giving approximately 40 cubes to the metre. All cubes were marked with a unique code, made up of a lake identifier, core number, section number and sample number (e.g., Mart9.1.030), in waterproof ink. An orientation arrow indicating "up" was also marked on each box. The depth of the sample from the top of each section was measured and recorded before the samples were extracted. Lids were placed on the boxes which were sealed in air tight boxes for storage in a magnetic field free environment prior to measurement.

The other half of each core was sealed in a plastic bag and stored in a cool room for later reference if required.

3.2.2 Livingstone Cores

These cores were collected in 1m and 2m lengths. The sections were transported to Trier. Since the steel coring tubes are precision made and hence are expensive, a method of sub-sampling had to be devised to allow their reuse.

A close fitting stainless steel piston was inserted into the upper end of each core tube which was held in a jig. The core section was then pulled gently past the piston which was held fixed. A thin wire placed vertically across the open end of the tube split the sediment as it was extruded. The two halves were caught in plastic gutters and sealed in plastic tubing for storage. One half of each section was photographed and used for microsedimentology and the other half was used for palaeomagnetic work. The 2 m core sections were divided into two 1 m lengths referred to as ober (upper) and unter (lower).

As the core tubes are made of mild steel precautions must be taken against rusting. Great care must also be taken against denting or distorting the tubes as this causes the piston to become stuck during extrusion of the sediment.

Sediment containing large amounts of sand or tephra were difficult or in some cases impossible to extrude since these layers expanded radially when compressed. Application of excessive force for extrusion would clearly compress and otherwise damage the sediment. When extrusion proved impossible the tubes were carefully sawn down each side and the sediment split with a wire in a similar manner to the Mackereth cores, and the steel tubes had to be scrapped.

3.3 Magnetic Measurements

3.3.1 Measurement of Natural Remanences

NRM's were measured on one of two cryogenic magnetometers after storage in 'zero' field generated by a set of Helmholtz coils for at least a week and often a month to reduce the effects of VRM. The samples from the first campaigns were measured using a Cryogenic Consultants 3-axis superconducting cryogenic magnetometer, using control software written by Smith (1985). Later samples were measured on a 2-G superconducting magnetometer controlled from an IBM compatible computer using software supplied by the company.

In both cases the control program of the machine stored the intensity of magnetization in three perpendicular directions in a disk file for later processing, using the programs described in Appendix A.

3.3.2 Measurement of Susceptibility

A Bartington Susceptibility Bridge was used to measure the magnetic susceptibility of all the samples taken. Susceptibility is a measure of the quantity of magnetic minerals present in the sample whereas NRM is an indication of the statistical alignment of the magnetic minerals as well as the quantity present. As a result susceptibility provides a useful proxy climatic indicator.

3.3.3 Demagnetization Procedures

Alternating Field (AF) demagnetization is carried out by applying a weak alternating magnetic field to the sample, which causes the magnetization of the low coercivity grains to follow the applied field. As this is reduced the magnetization of the particles is left in random positions, i.e. the easy axes directions of the grains. As there will be a large number of grains affected the magnetization of these grains is effectively randomized, leaving only the remanence of the grains with a coercivity greater than the applied field. Successive increments of the applied field combined with measurements of the remanence allow the coercivity to be analyzed up to the maximum field applied.

All samples were AF demagnetized. The samples from the initial campaign using a single shielded coil in fields upto 100 mT. For the later samples demagnetization upto 30 mT was carried out using the inline coils mounted on the 2-G magnetometer.

For all the cores a series of pilot samples were selected from the cores and stepwise demagnetized at fields of 5, 10, 15, 25 and 30 mT. Following this the remainder of the samples in the cores were demagnetized at a field of 10 mT for the first series of cores and 10 and 20 mT for the second series. This removed any remaining viscous remanence from the samples.

3.3.4 Artificial Remanences

ARM

Anhyseretic magnetizations are acquired when a sample is placed in a direct field and superimposed by with an alternating field. The remanence remaining after the sample is removed from the field is known as an Anhyseretic Remanent Magnetization (ARM).

The samples from core D were given an anhyseretic remanent magnetization (ARM)

in an AC field of 100mT, biased by a DC field of 0.1mT, to allow the determination of the magnetic mineral concentration and size distribution. These ARM's were AF demagnetized with a 10mT peak field to allow the comparison of the stabilities of ARM's and NRM's.

SIRM

Isothermal Remanent Magnetization (IRM) is the magnetization acquired by a sample when it is placed in a direct magnetic field. If the external field is large then this may cause a saturation of the sample which is termed a Saturated Isothermal Remanent Magnetization (SIRM). Selected cores were given SIRM's in a DC field of 1T.

3.4 Variations in the Intensity of the Geomagnetic Field

The recovery of palaeointensities from lake sediments has been attempted by several authors in the past (e.g. King *et al*, 1982, Tucker, 1981 and Thouveny, 1987). It has been concluded that while the intensity recorded in the sediments (NRM) can be normalized to allow for variations in the magnetic mineral concentration it is impossible to recover an absolute value for the ancient field strength.

There are two main factors which control the recorded intensity, the first is the strength of the geomagnetic field which will control the alignment of the magnetic particles as they are deposited (see Chapter 2), the second is the quantity and type of magnetic particles in each sample. These are controlled by the environment at the time of deposition. If the climate is warm, there will be an increase in vegetation within the catchment area which will lead to an increase in the organic input to the lake. This will result in a reduced magnetic mineral concentration by simple dilution effects and also as a result of slope stabilisation by the plants, lowering runoff and mineralogenic input.

Chapter 4

Spectral Analysis Methods

4.1 Introduction

In lake sediment palaeomagnetism several problems are likely to be encountered during spectral analysis:

1. The time scale for the data is poorly defined.
2. That there are gaps in the record caused by incomplete coring, i.e. where core sections join, or where the sediment was not sampled for some reason, such as slumping.
3. Even if the sampling on the depth scale is perfectly even, it is unlikely that this spacing will be retained once the depths are transformed to the timescale, if any but the simplest linear transform function is used.
4. Often the periods searched for are of the order of the length of the record, causing problems of resolution in the spectral analysis.

Different solutions can be applied to avoid some of the problems above, though obviously nothing can make up for the fact that a time scale is wrong. Two solutions can be used to help with the second two problems mentioned above. The first is to interpolate the data on to an evenly spaced time function and create data points which are evenly spaced through time. The second is to use a method that can cope with unevenly sampled data.

Three different methods of spectral analysis were tested for this work:

- The Fast Fourier Transform
- The Maximum Entropy Method

- The Lomb–Scargle Method

The first two methods (FFT and MEM) rely on the data being evenly spaced, which can introduce shifts in the frequencies found in the data. The third was developed by astronomers to avoid the necessity of regridding data.

4.2 Methods

4.2.1 The Lomb–Scargle Method

The Lomb–Scargle method performs spectral analysis on unevenly sampled data, and is known to be a powerful way to find, and test the significance of, weak periodic signals. Press and Rybicki (1989) showed that the method can be implemented using a fast fourier transform (FFT) as an order $10^2 N \log N$ operation, making it much faster than the method originally implemented by Horne and Baliunas (1986) which was of order $10^2 N^2$. Note that despite the use of the FFT, the algorithm is in no way equivalent to conventional FFT periodogram analysis.

Given a set of data values $h_i, i = 1, \dots, N$ at observation times t_i , the Lomb–Scargle Periodogram is constructed as follows. First compute the data's mean and variance by:

$$\bar{h} = \frac{1}{N} \sum_{i=1}^N h_i, \quad \sigma^2 = \frac{1}{N-1} \sum_{i=1}^N (h_i - \bar{h})^2 \quad (4.1)$$

Second for each angular frequency $\omega = 2\pi f > 0$ of interest compute a time offset τ by

$$\tan(2\omega\tau) = \frac{\sum_j \sin 2\omega t_j}{\sum_j \cos 2\omega t_j} \quad (4.2)$$

Third the Lomb–Scargle normalized periodogram is defined by:

$$P_n(\omega) = \frac{1}{2\sigma^2} \left\{ \frac{[\sum_j (h_j - \bar{h}) \cos \omega(t_j - \tau)]^2}{\sum_j \cos^2 \omega(t_j - \tau)} + \frac{[\sum_j (h_j - \bar{h}) \sin \omega(t_j - \tau)]^2}{\sum_j \sin^2 \omega(t_j - \tau)} \right\} \quad (4.3)$$

Lomb (1976) showed that equation 4.3 is identical to the equation that one would obtain if one estimated the harmonic content of a data set by linear least-squares fitting to the model:

$$h(t) = A \cos \omega t + B \sin \omega t \quad (4.4)$$

This gives an insight into the superior results of the method on unevenly sampled

data; it weights data on a 'per point' rather than a 'per time interval' basis.

It should be noted that the method allows spectral information to be obtained for frequencies significantly higher than the Nyquist frequency that would apply if the data were evenly spaced over the same record length.

4.2.2 Fourier Transform Spectral Analysis

A fourier transform converts a function $h(t)$ in the time domain to a function $H(f)$ in the frequency domain, i.e.:

$$H(f) = \int_{-\infty}^{\infty} h(t)e^{2\pi ift} dt \quad (4.5)$$

$$h(t) = \int_{-\infty}^{\infty} H(f)e^{-2\pi ift} df \quad (4.6)$$

The practical application of fourier transforms on discrete data makes several assumptions:

- That the signal $h(t)$ is discretely sampled at evenly spaced intervals.
- That this interval is sufficiently small to give 2 points per cycle at the highest frequency of interest.
- That the signal sampled is stationary (i.e. not changing) and is infinitely repeating.

The fourier transform of this discrete data at discrete frequencies of:

$$f_n = \frac{n}{N\Delta} \quad n = \frac{-N}{2}, \dots, \frac{N}{2} \quad (4.7)$$

gives:

$$H(f_n) = \int_{-\infty}^{\infty} h(t)e^{2\pi if_n t} dt \quad (4.8)$$

$$\approx \sum_{k=0}^{N-1} h_k e^{2\pi if_n t_k \Delta} \quad (4.9)$$

$$= \Delta \sum_{k=0}^{N-1} h_k e^{2\pi i k n / N} \quad (4.10)$$

Most practical implementations of the fourier transform make use of a Fast Fourier Transform (FFT) which is a $N \ln N$ order operation, whereas a normal fourier transform is of order N^2 . Most algorithms that are used are based upon the work of Cooley and Tukey.

It is possible to estimate the power spectrum of the signal $(c(t))$ using the FFT:

$$C_k = \sum_{j=0}^{N-1} c_j e^{2\pi i j k / N} \quad (4.11)$$

then the periodogram estimate of the power spectrum is defined at $N/2 + 1$ frequencies as:

$$P(0) = P(f_0) = \frac{1}{N^2} |C_0|^2 \quad (4.12)$$

$$P(f_k) = \frac{1}{N^2} [|C_k|^2 + |C_{N-k}|^2] \quad k = 1, 2, \dots, (N/2 - 1) \quad (4.13)$$

$$P(f_c) = P(f_{N/2}) = \frac{1}{N^2} |C_{N/2}|^2 \quad (4.14)$$

This gives a window function of

$$W(s) = \frac{1}{N^2} \left[\frac{\sin(\pi s)}{\sin(\pi s / N)} \right] \quad (4.15)$$

over which $P(f_k)$ is average of $P(f)$. This window falls off as $(\pi s)^{-2}$, which is not rapid and leads to significant leakage from one frequency to another. This leakage can be reduced by multiplying the data by a window function which is 0 at the ends and rises smoothly to one in the center. But there is a trade off between the narrowness of the spectral peaks and the leakage.

4.2.3 The Maximum Entropy Method

Burg (1967) developed this method of spectral analysis. If the complex f -plane is transformed on to a new plane, called the Z -plane by the relation

$$Z = e^{2\pi i f \Delta} \quad (4.16)$$

where Δ is the sampling interval.

The power spectrum estimate of a signal transformed in this way can be written as:

$$P(f) = \frac{1}{|\sum_{k=-M/2}^{M/2} b_k Z^k|^2} \quad (4.17)$$

$$= \frac{a_0}{|1 + \sum_{k=1}^M a_k Z^k|^2} \quad (4.18)$$

By considering the Laurent series in Z , which is equivalent to the power spectrum of the autocorrelation (ϕ_j)

$$\phi_j = \phi_{-j} \approx \frac{1}{N+1-j} \sum_{i=0}^{N-j} C_i C_{i+j} \quad j = 0, 1, \dots, N \quad (4.19)$$

leads to:

$$\frac{a_0}{|1 + \sum_{k=1}^M A_k Z^k|^2} \approx \sum_{j=-M}^M \phi_j Z^j \quad (4.20)$$

M is the order of the approximation and can be any integer up to N , but is usually much smaller than N , as the total operation count is of the order NM .

The choice of M is critical to the power spectrum obtained, if M is too low then the spectrum is over smoothed, however if M is too high then spurious peaks will be introduced as well as peak splitting and movement. The program used in these tests made use of Berryman's (1978) suggestion that $M = 2N/\ln 2N$.

4.3 Testing of the Methods

4.3.1 Synthetic Data

Two sets of synthetic data were created for the tests, the first a pure sine wave with a period of 50 Kyr (0.02 cycles/Kyr), sampled at 500 years intervals and a record length of 300 Kyr. The second a linear combination of 3 sine waves 100 Kyr, 45 Kyr and 20 Kyr (0.001 cycles/Kyr, 0.022 cycles/Kyr and 0.05 cycles/Kyr), with the same sampling interval and record length.

The data sets were "degraded" by adding random fluctuations of up to 50% of the signal strength to the data (figures 4.1a & 4.2a). Further degradation was achieved by randomly removing $\sim 50\%$ of the "noisy" data points (figures 4.1b & 4.2b) and finally removing $\sim 70\%$ of the data (figures 4.1c & 4.2c). The final data set could be considered comparable to "good" palaeomagnetic data.

4.3.2 Results

Figures 4.3 and 4.4 show that for the clean signal all three methods work well with the exception of MEM in the case of the complex signal where it can only pick one of the frequencies expected.

Again once noise is added (figures 4.5 & 4.6) all three methods are successful and the MEM estimate improves on the complex wave finding all three frequencies.

Once data points are removed only the Lomb-Scargle method can correctly identify

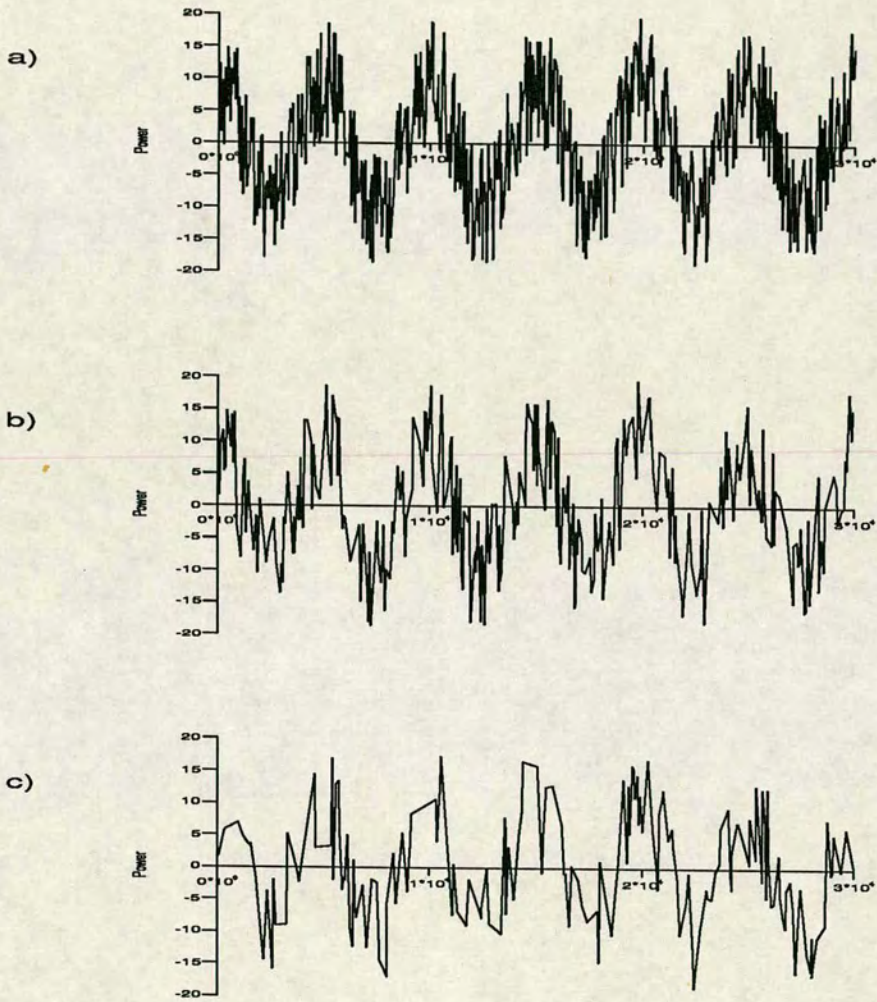


Figure 4.1. Initial data sets used to test the Spectral Analysis Programs

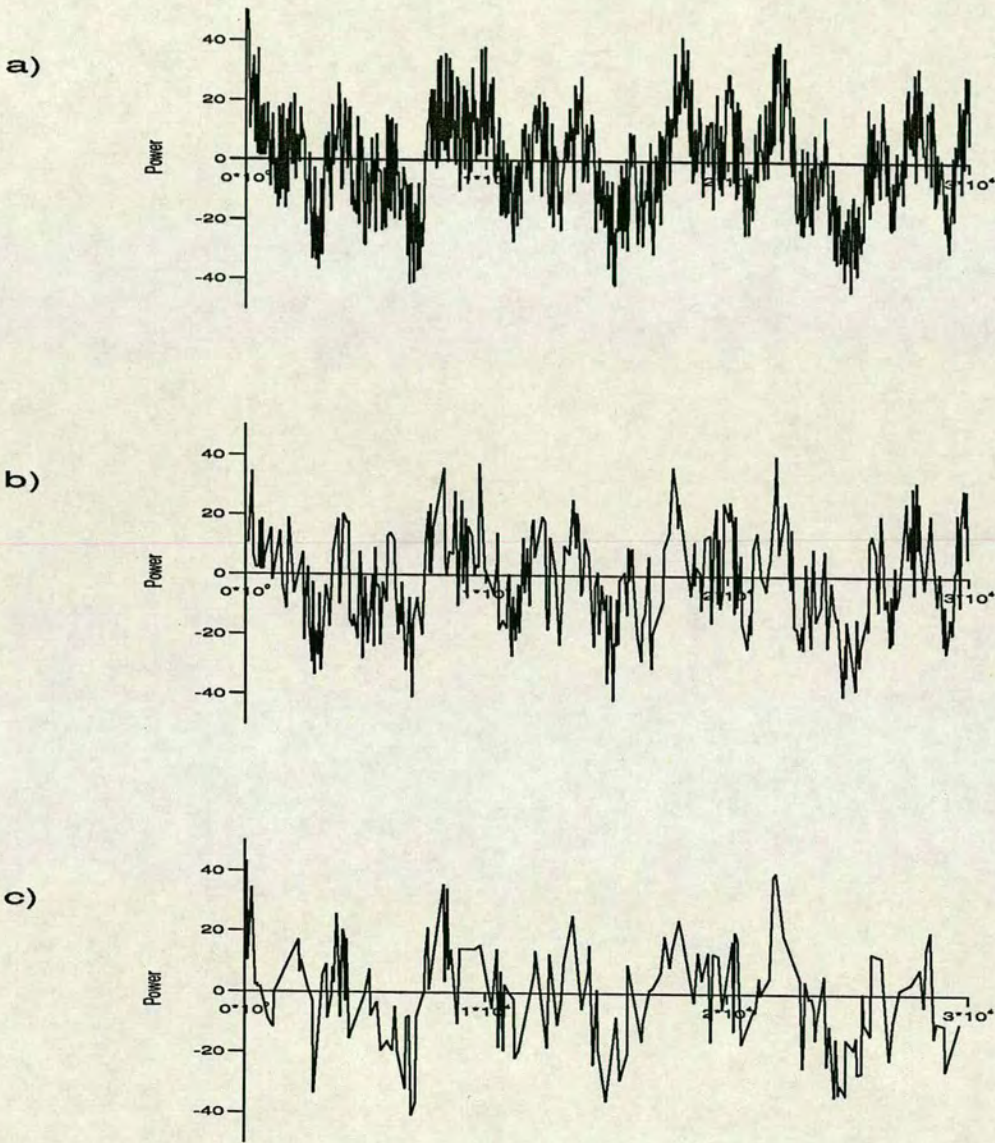


Figure 4.2. The more complex data set used for the second part of the testing

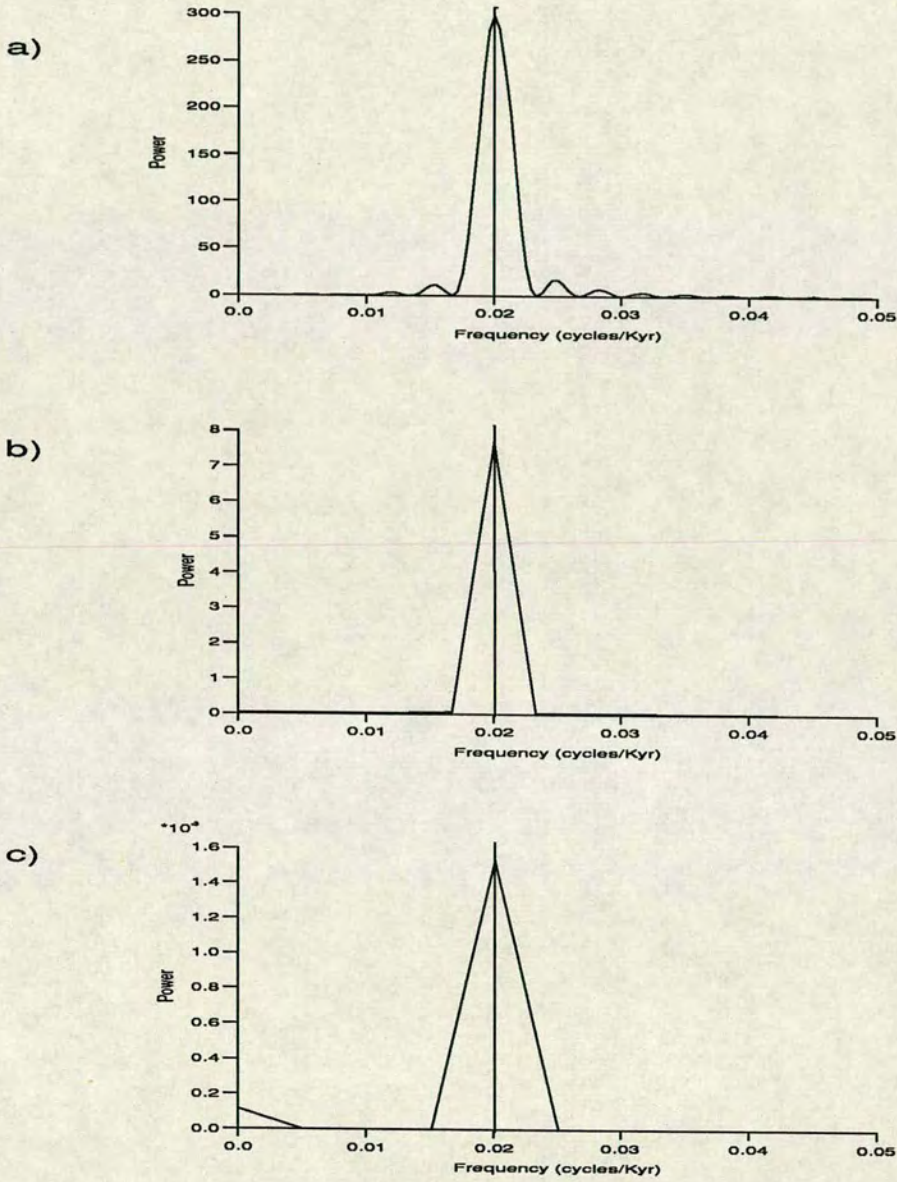


Figure 4.3. Periodograms of the pure sine wave; a) Lomb-Scargle analysis, b) Fourier analysis, c) MEM analysis

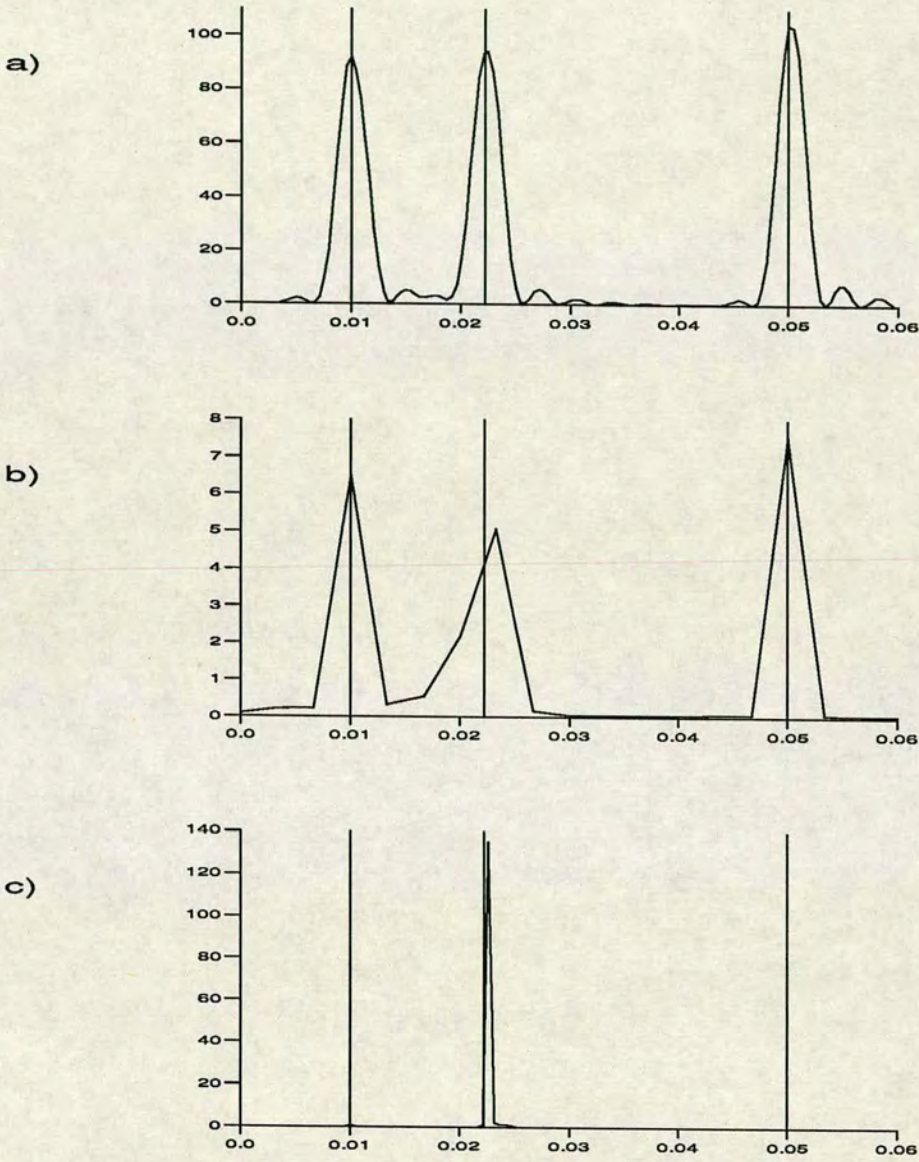


Figure 4.4. Periodograms of the sine waves; a) Lomb-Scargle analysis, b) Fourier analysis, c) MEM analysis

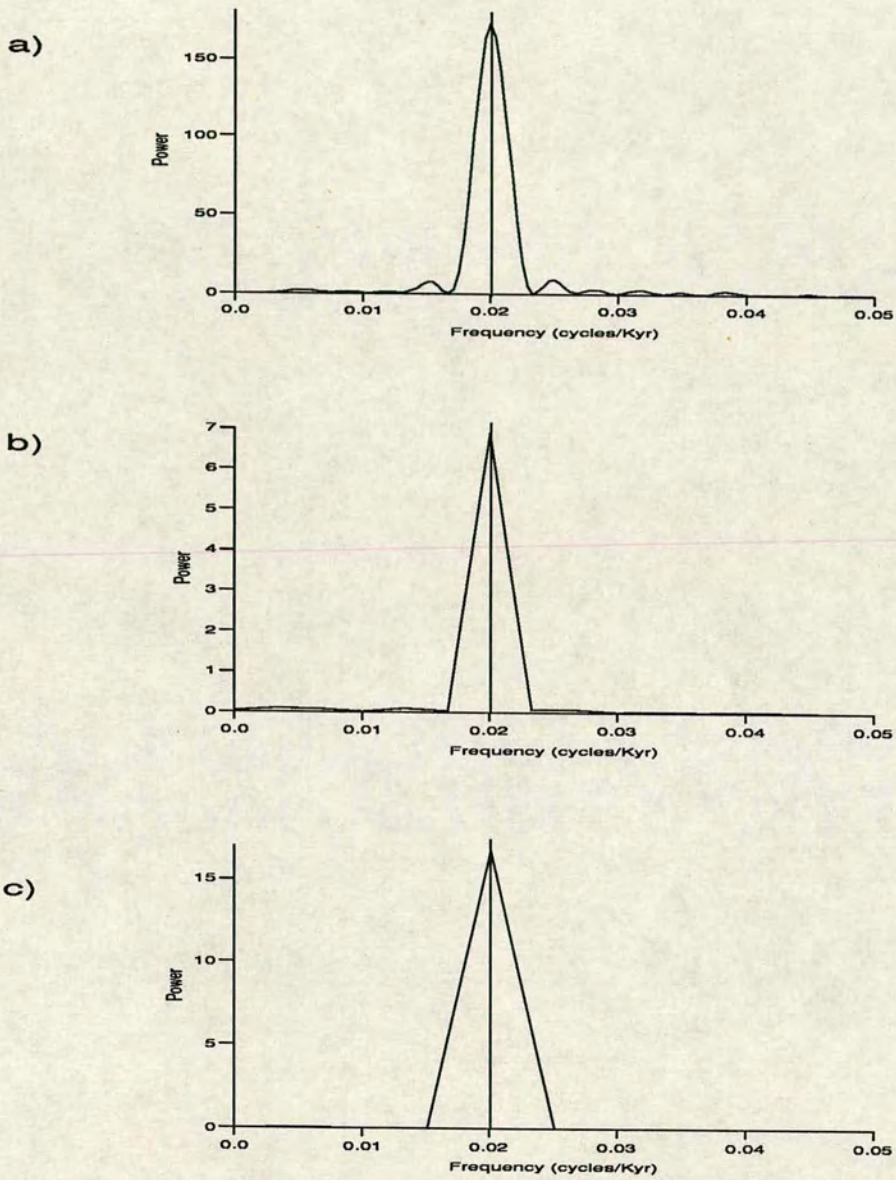


Figure 4.5. Periodograms of the noisy sine wave (figure 4.1a); a) Lomb-Scargle analysis, b) Fourier analysis, c) MEM analysis

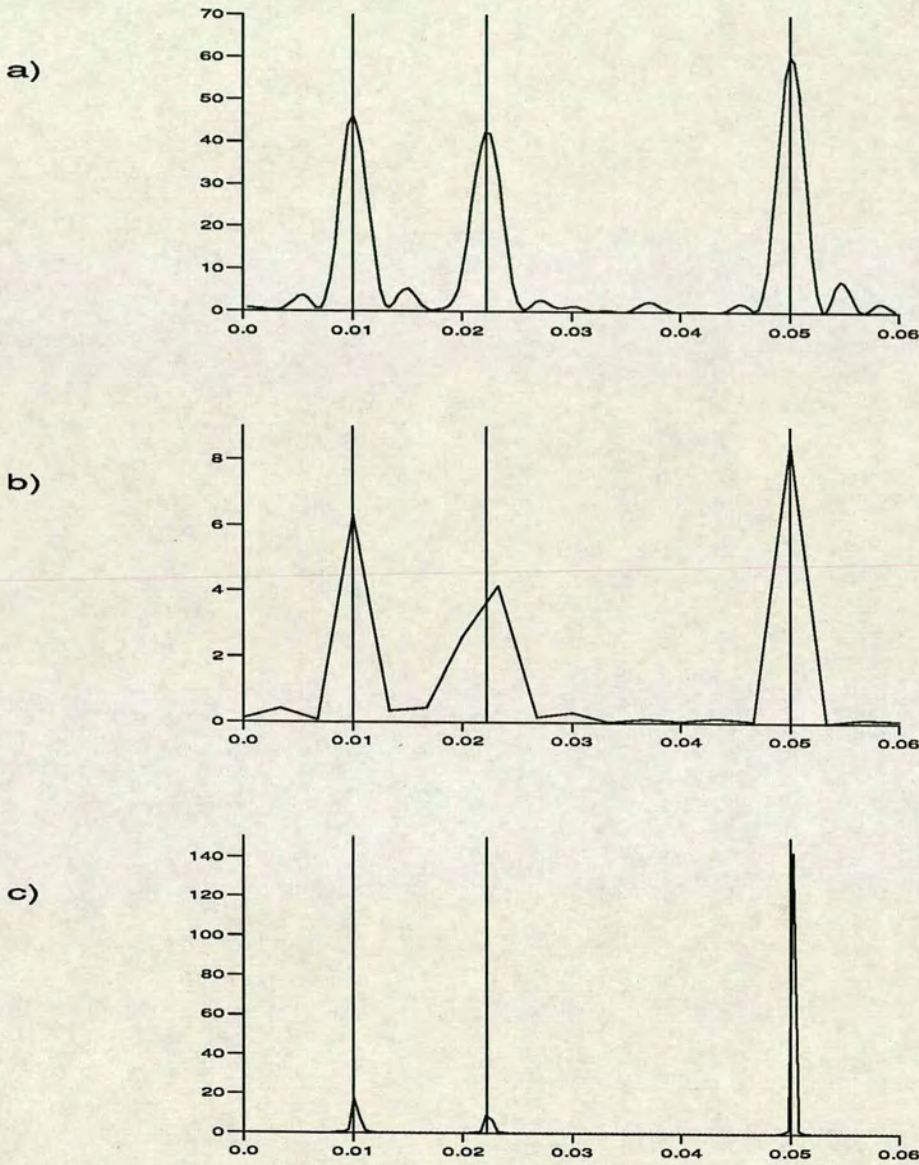


Figure 4.6. Periodograms of the noisy sine waves (figure 4.2a); a) Lomb-Scargle analysis, b) Fourier analysis, c) MEM analysis

the frequencies present in the data, figures 4.8 & 4.9. This is possibly due to the need to interpolate the data back on to an evenly-spaced time series for the fourier and MEM.

In the worst-case (figure 4.10) the Lomb-Scargle method has correctly identified the three frequencies, the lowest peak (0.01 cycles/Kyr) is twice the height of the highest spurious peak, and would possibly be discarded in a real analysis. But the other peaks are clearly present and could be used with confidence.

4.4 Conclusions

It seems clear that the Lomb-Scargle method is superior to conventional spectral analysis making use of FFT's or MEM. The method appears to cope with very poorly defined data, with uneven sampling and low signal to noise ratios. It is also possible to determine frequencies that are beyond the extremes of the frequency ranges that could be normally examined, this allows tentative analysis of records that are shorter than the period being sought.

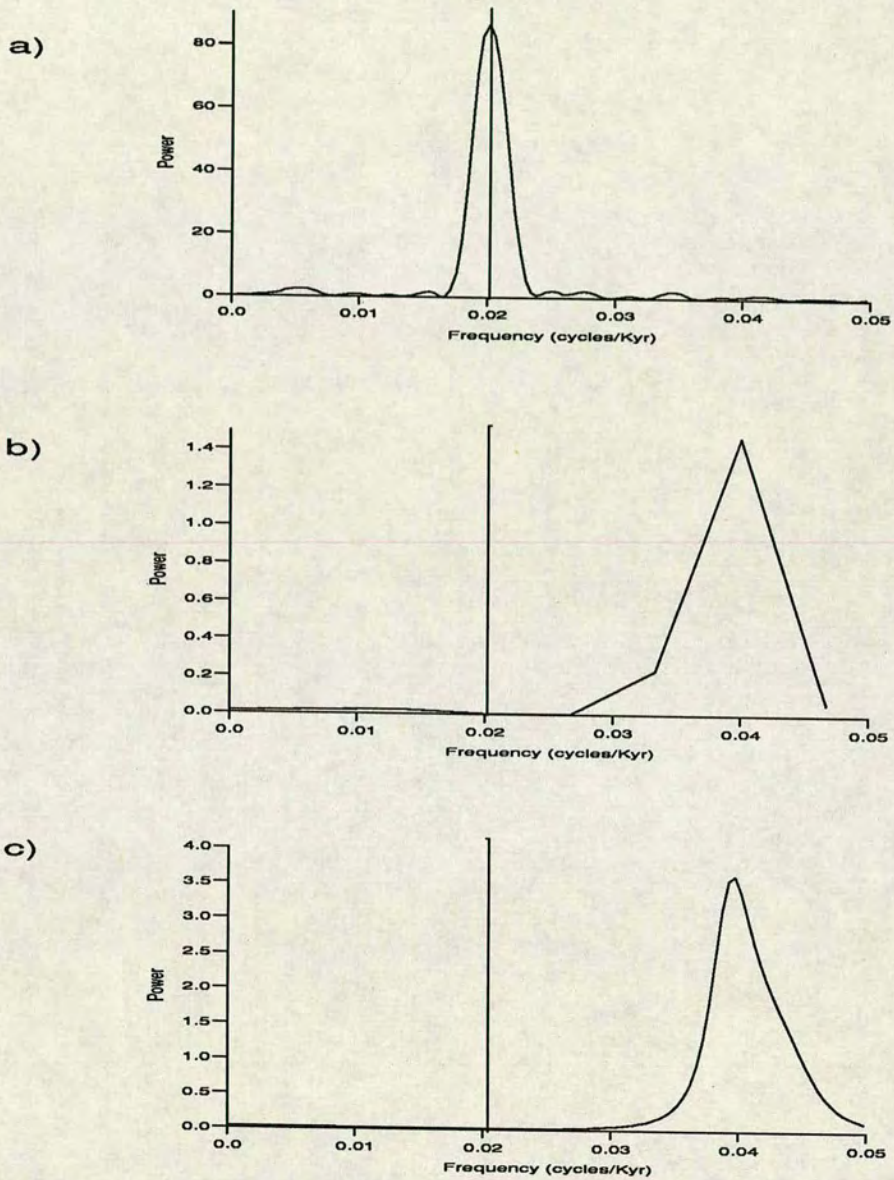


Figure 4.7. Periodograms of the noisy sine wave after deletion of 50% of data points (figure 4.1b); a) Lomb-Scargle analysis, b) Fourier analysis, c) MEM analysis

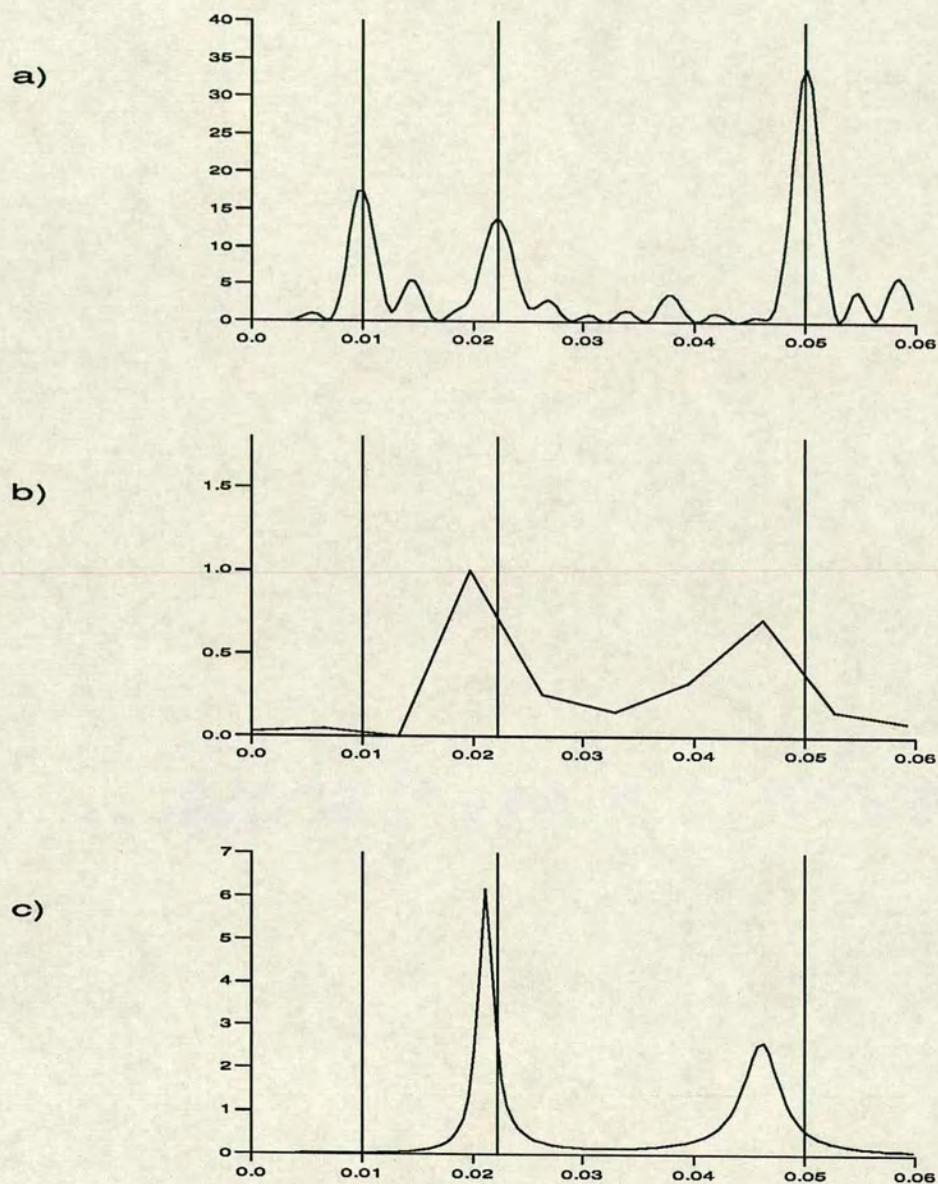


Figure 4.8. Periodograms of the noisy sine waves after deletion of 50% of data points (figure 4.2b); a) Lomb-Scargle analysis, b) Fourier analysis, c) MEM analysis

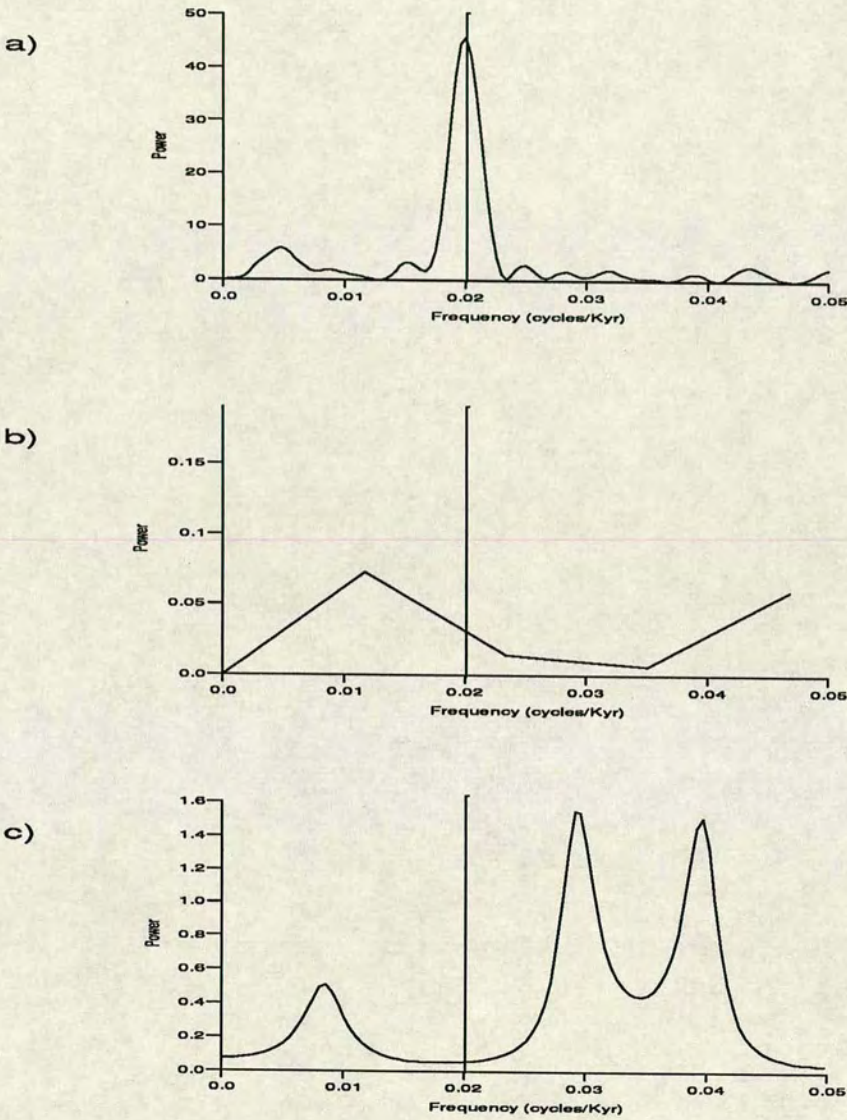


Figure 4.9. Periodograms of the noisy sine wave after deletion of 70% of data points (figure 4.1c); a) Lomb-Scargle analysis, b) Fourier analysis, c) MEM analysis

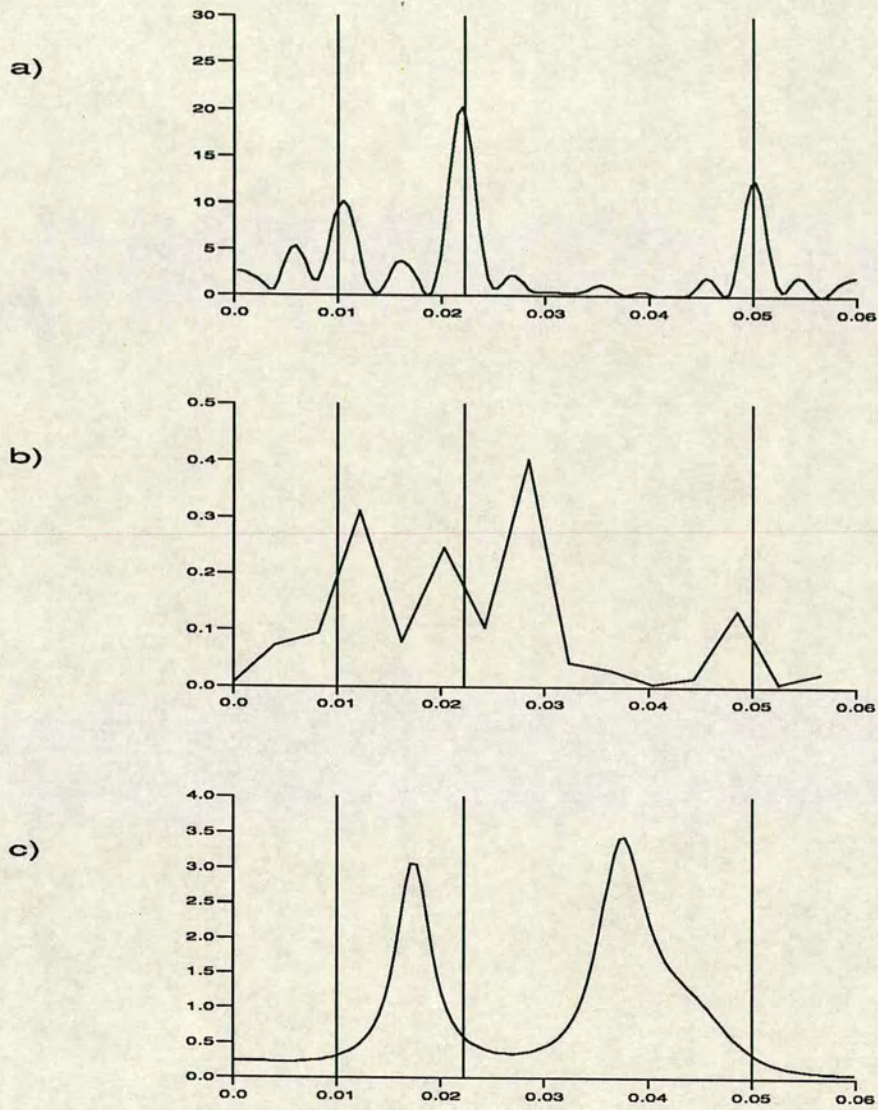


Figure 4.10. Periodograms of the noisy sine waves after deletion of 70% of data points (figure 4.2c); a) Lomb-Scargle analysis, b) Fourier analysis, c) MEM analysis

Chapter 5

Results from the Laghi di Monticchio

5.1 Introduction

The Laghi di Monticchio are a pair of lakes situated in the caldera of Monte Vulture. The lakes form the deepest part of the basin of this caldera. The lake surfaces are at about 656m above sea level and approximately 100km east of Naples (see figure 5.1).

Initially, in 1989, four 6m cores were collected from Lago Grande di Monticchio (figure 5.1) using a Mackereth corer, (Mackereth, 1959). These cores were taken from the centre of the lake (point M, figure 5.2) under about 25 m of water. The cores were then transported to Edinburgh and sub-sampled as described in section 3.2. Sub-samples for pollen analysis were also extracted at the same time so that the results would be directly comparable to the palaeomagnetic results.

In 1990 a second series of cores were collected using a Livingstone type corer, modified by Dr Usinger of Kiel University, FRG. The first of these coring operations (point A, on figure 5.2) was abandoned due to the extreme hardness of the sediments at a depth of only 4 m below the lake bottom. The raft and coring equipment were then moved to shallower water and a further three cores were obtained (points B, C & D on figure 5.2). Core B was 40 m long, core C was 14 m and core D was 51 m long. These cores were transported to Trier University, FRG, for subsampling for geochemical, micro-sedimentology, pollen and ostracod analysis, as well as palaeomagnetic work.

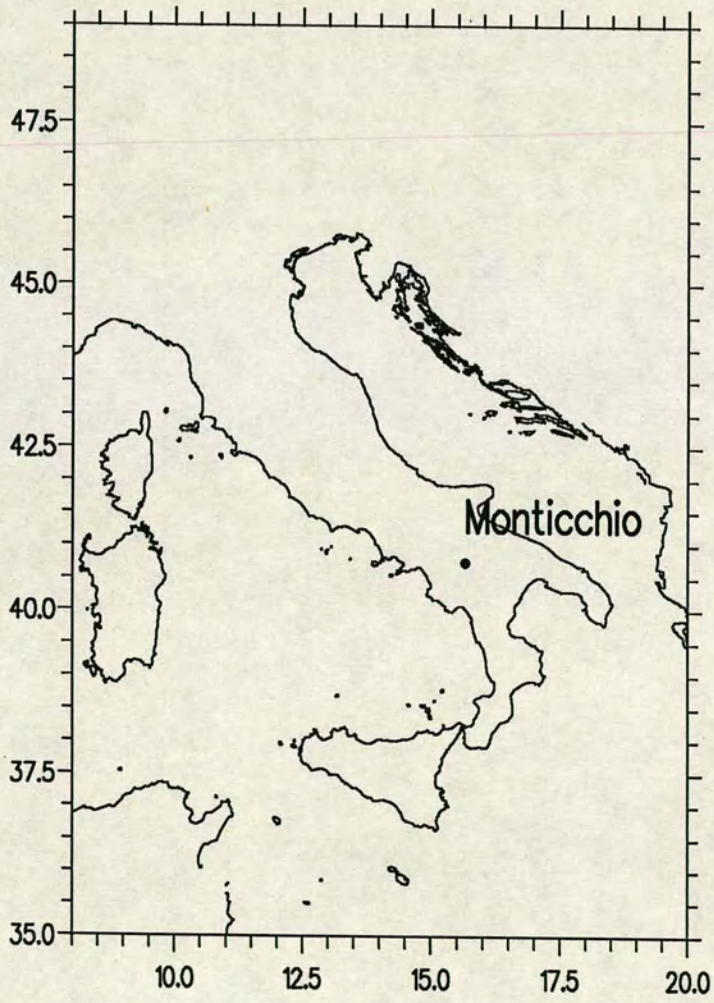


Figure 5.1. Location of Laghi di Monticchio

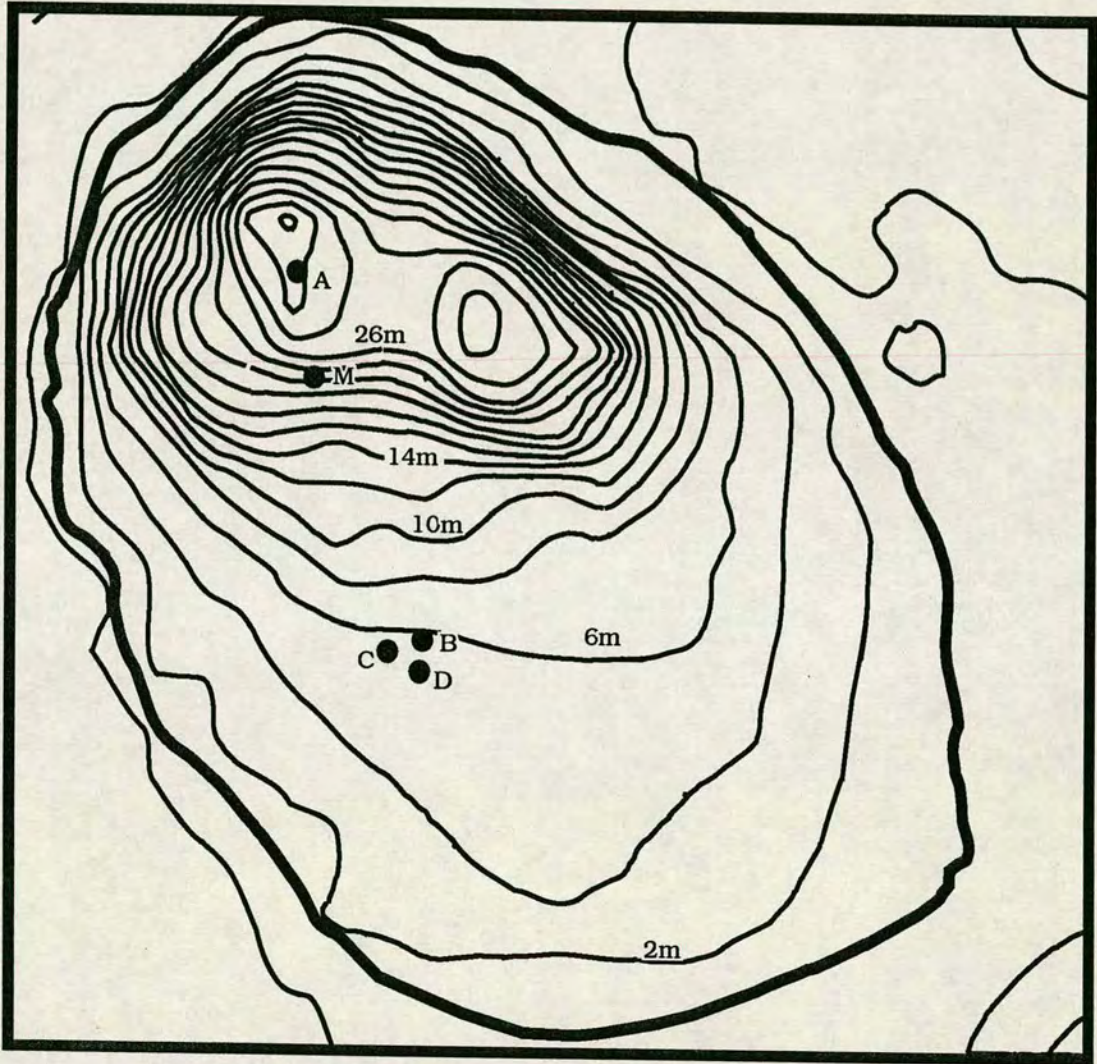


Figure 5.2. Bathymetry of Lago Grande di Monticchio

5.2 Regional Geology and the Formation of the Lake

Monte Vulture sits atop the sedimentary plateau which forms the southern Appenines orogenic complex (du Riche Preller, 1923). This massif evolved during the late Triassic, with the onset of continental separation and the formation of the Calabrian Arc (Scadone, 1979). This was followed by a period of sedimentation during the remainder of the Triassic, Jurassic and Cretaceous, forming a thick sequence of limestones. This sequence is overlain by an Eocene flysch and then Miocene and Pliocene marine conglomerates and sands. These sediments are associated with the opening and closure of the Tethys Ocean. The final tectonic phase in this region was a period of crustal thinning with associated igneous emplacement, resulting in a number of volcanos in southern Italy, including Monte Vulture. Lago di Monticchio was formed by a phreato-magmatic eruption during the early Quaternary, though no firm date exists for this eruption.

5.3 Palaeomagnetic Results from Lago di Monticchio

5.3.1 Mackereth Cores

Six cores were collected using a Mackereth corer in 1989; of these four were sub-sampled for palaeomagnetic study (1, 3, 4 & 5). The natural remanent magnetization (NRM) of the sub-samples from all four cores were measured. An initial examination of the directional results (declination and inclination) showed that they were very scattered for three of the cores (1, 3, & 5) but more coherent for core 4 (see figure 5.3). All the sub-samples were then bulk demagnetized in a field of 10mT, following pilot studies on ~10% of the samples from each core. The pilot samples confirmed the initial observation that three of the cores were too badly disturbed to recover any directional data. The results of core 4 showed some improvement with demagnetization as can be seen in figure 5.4

Subsequent examination of the cores showed signs of seismites and other earthquake induced failures within the sediment record. This is discussed further in section 5.7.

5.3.2 Livingstone Cores

Natural Magnetizations

Of the Livingstone cores collected, the two longest (B & D) were sampled for palaeomagnetic study. The natural remanent magnetizations (NRM's) of both cores were

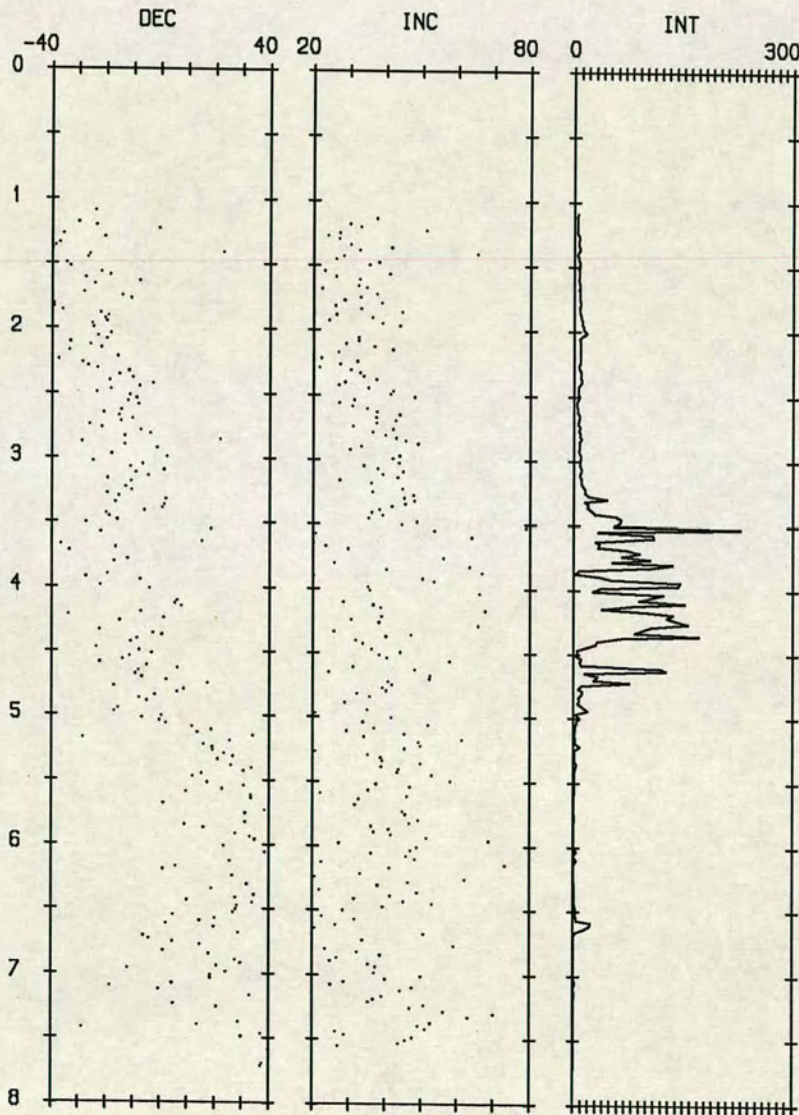


Figure 5.3. NRM results for core 4 from Lago di Monticchio. Declination and inclination are in degrees, intensity is in mA/m. The highly organic sediments are very weakly magnetized resulting in a poorly defined directional record.

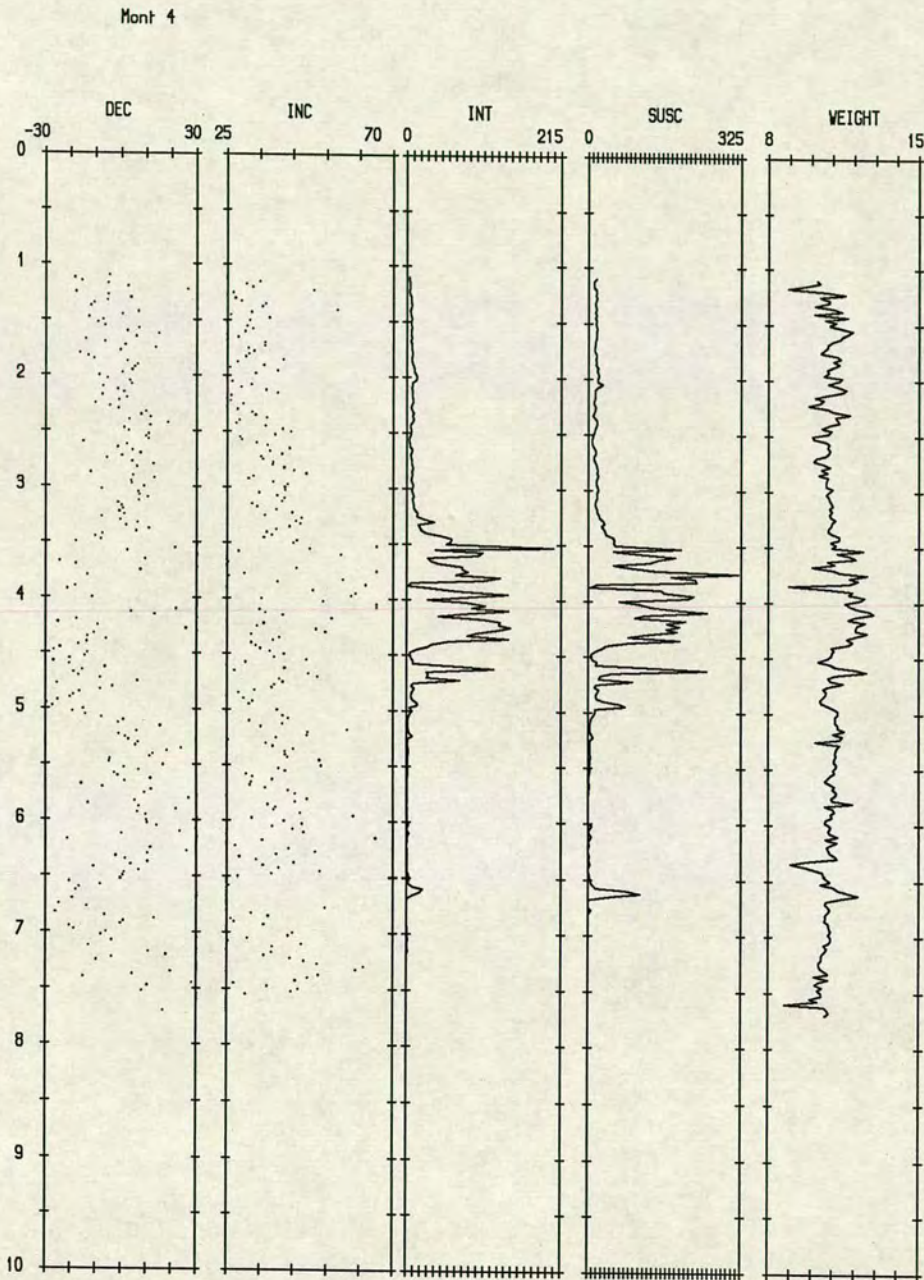


Figure 5.4. NRM results for core 4 from Lago di Monticchio, after AF demagnetization at 10mT. Declination and inclination are in degrees, intensity is in mA/m, susceptibility is in SI units and weight is in grams.

measured on a 3-axis Superconducting Rock Magnetometer produced by 2-G, California (figures 5.5 and 5.6). Each sample was also weighed and the NRM's were normalized by the weight of each sample (figures 5.5 and 5.6).

Some core sections were not sub-sampled as they had been disturbed in coring or during the extrusion process, or because they contained only slumped sediments which would not provide a reliable palaeomagnetic signal. This disturbance was easily recognised by visual inspection of the cores which were normally horizontally laminated.

It can be seen that the NRM of samples from the upper 10 m of the core are very weak and that both the inclination and declination are very scattered. However below this depth the intensity of the NRM increases and the directions are more coherent. The thin peaks in intensity are identified with tephra layers, and can be used for inter-core correlation because tephra provide instantaneous marker horizons. The magnetic susceptibility of all samples was also measured on a Bartington Bridge, down both cores. Figure 5.7 shows a comparison of intensity and susceptibility for each core and shows some of the "tie-points" used to convert the two cores to a common depth scale.

A series of pilot samples (5%) were selected from core D. The tenth and thirtieth samples from each metre section of core (approximately 40 samples) were chosen and alternating field (AF) demagnetization was applied in a series of steps at peak fields of 5, 10, 15, 20, 30 mT, using the demagnetizing coils built into the 2G magnetometer. Some of the results are shown in Figure 5.8, and it can be seen the samples can be divided into two groups. The first group, from the upper part of the core, have low intensities and give generally scattered directions during demagnetization. The second group, from the lower sections of the core, produce much better demagnetization plots. There is very little scatter and once a small viscous component has been removed they tend to produce straight lines towards the origin on the Zijderveld plots, which represents the direction of stable remanence.

The remainder of core D was demagnetized only in 10 and 20 mT and the results are shown in figures 5.9 and 5.10, which start at a depth of 10m since the upper weak sections were not remeasured.

The quality of the demagnetization was determined by comparing the declination and inclination directions after 10mT and 20mT AF demagnetization steps. If the directions differed by more than 20° the sample was numbered 0, if the difference was more than 10° then the sample was numbered 1, more than 5° a 2, more than 2° a 3, between 1° and 2° a 4, and less than 1° a 5. The results of this analysis are shown in figure 5.11. It can be seen that for the inclinations the remanence direction is very good, with more than half of the samples varying by less than 1° and three quarters of the samples differing by less than 2° . The declinations are slightly more scattered

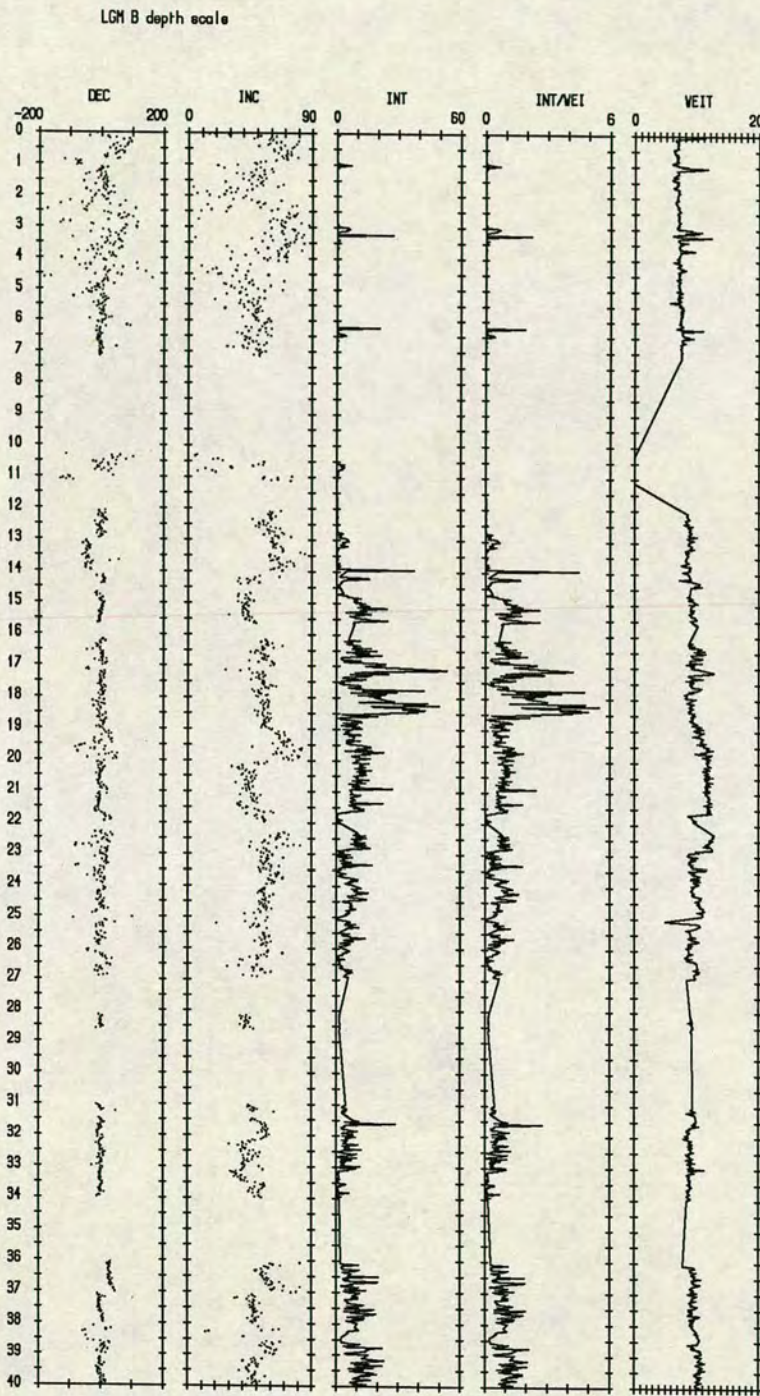


Figure 5.5. NRM measurements of Core B. Declination and inclination are in degrees, intensity is in mA/m and weight is in grams.

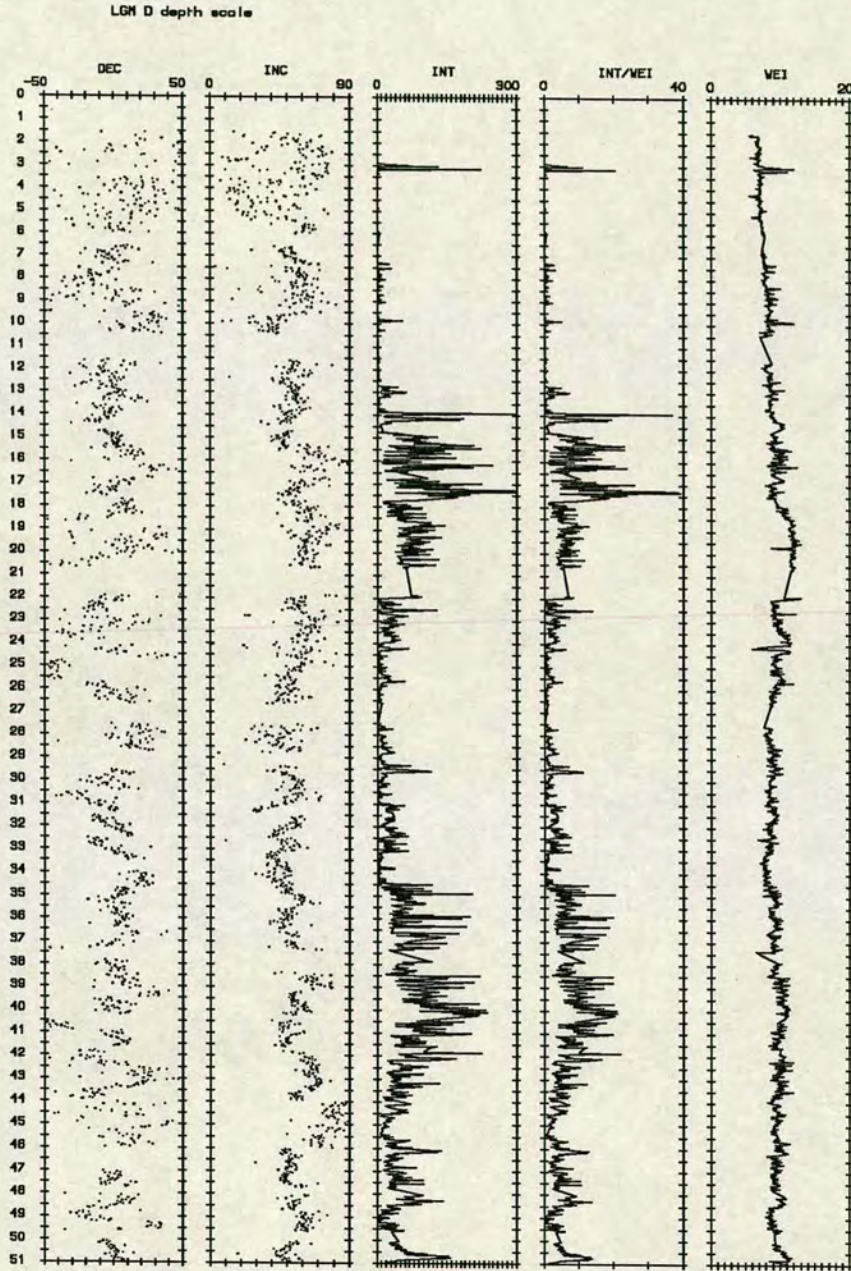


Figure 5.6. NRM measurements of Core D. Declination and inclination are in degrees, intensity is in mA/m and weight is in grams.

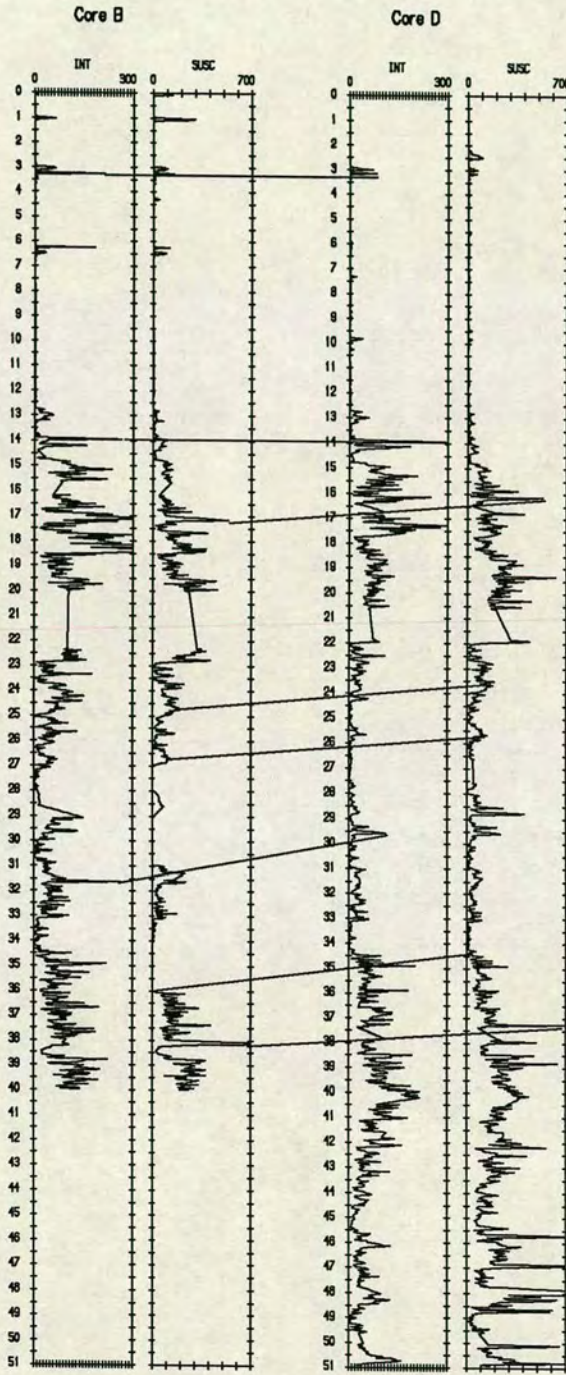


Figure 5.7. The intensity of the NRM and Susceptibility of cores B and D with some of the tie-points used to calculate the common depth scale.

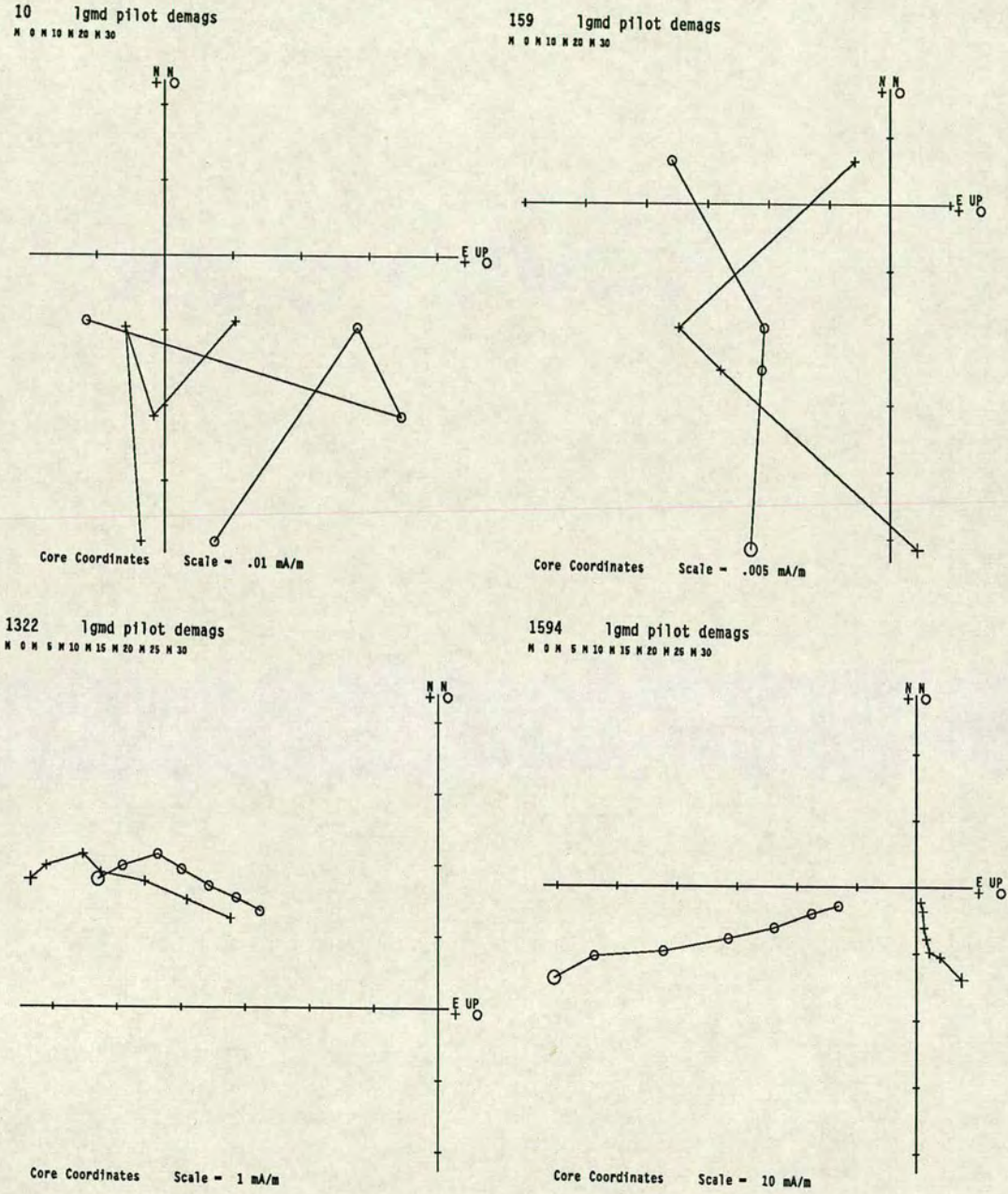


Figure 5.8. Pilot demagnetization plots of Core D

with under half of the samples varying by less than 2°.

Laboratory Induced Magnetizations

The samples from core D were given an anhysteretic remanent magnetization (ARM) in an AC field of 100mT, biased by a DC field of 0.1mT, to allow the determination of the magnetic mineral concentration and size distribution. These ARM's were AF demagnetized with a 10mT peak field to allow the comparison of the stabilities of ARM's and NRM's. Each sample was given a saturated isothermal remanent magnetization (SIRM) in a DC field of 1T.

Climate effects are seen most easily in measurements of parameters which are only effected by the concentration of magnetic minerals rather than by their alignment. Three magnetic parameters can be used for this – susceptibility, ARM and SIRM. It can be seen (figure 5.12) the downcore variations of these are all similar for the sediments of Monticchio. The crosscorrelation coefficients for these curves are all of the order of .68 which is a highly significant correlation with this many points. See page 101 for more details of this type of analysis.

In an attempt to determine more information about the magnetic mineralogy of the core ratios of χ_0 /ARM, ARM/SIRM and χ_0 /SIRM were calculated. As described in Appendix A, all the programs used took great care to make sure that each measurement relates to a unique sample number so that ratios are formed from the measurements on the same cube.

A graph of χ_{ARM} versus χ (as defined by King *et al* (1982)) can be used to determine the magnetic grain size of the sample. The magnitude of susceptibility is controlled by the concentration of large grains of magnetite, whereas ARM and SIRM are affected by finer grained magnetic material. They show that if there is a significant susceptibility associated with the non-magnetic matrix there will be an offset of the abscissa, this appears to be absent from figure 5.13.

χ_0 /ARM and χ_0 /SIRM plotted down core (figure 5.14) show generally straight lines with very little variation in the sections which show high susceptibility, ARM's and SIRM's and more scatter in the sections where these parameters are low. This is most probably an instrumental effect in that the errors will be proportionally higher in the sections with lower values which will tend to increase the scatter. A straight line was fitted to the plot of ARM versus susceptibility (figure 5.16), this shows some deviation from the straight line expected if there was no variation of minerals down core.

ARM/SIRM (figure 5.14) also shows a similar steady value with no coherent signal

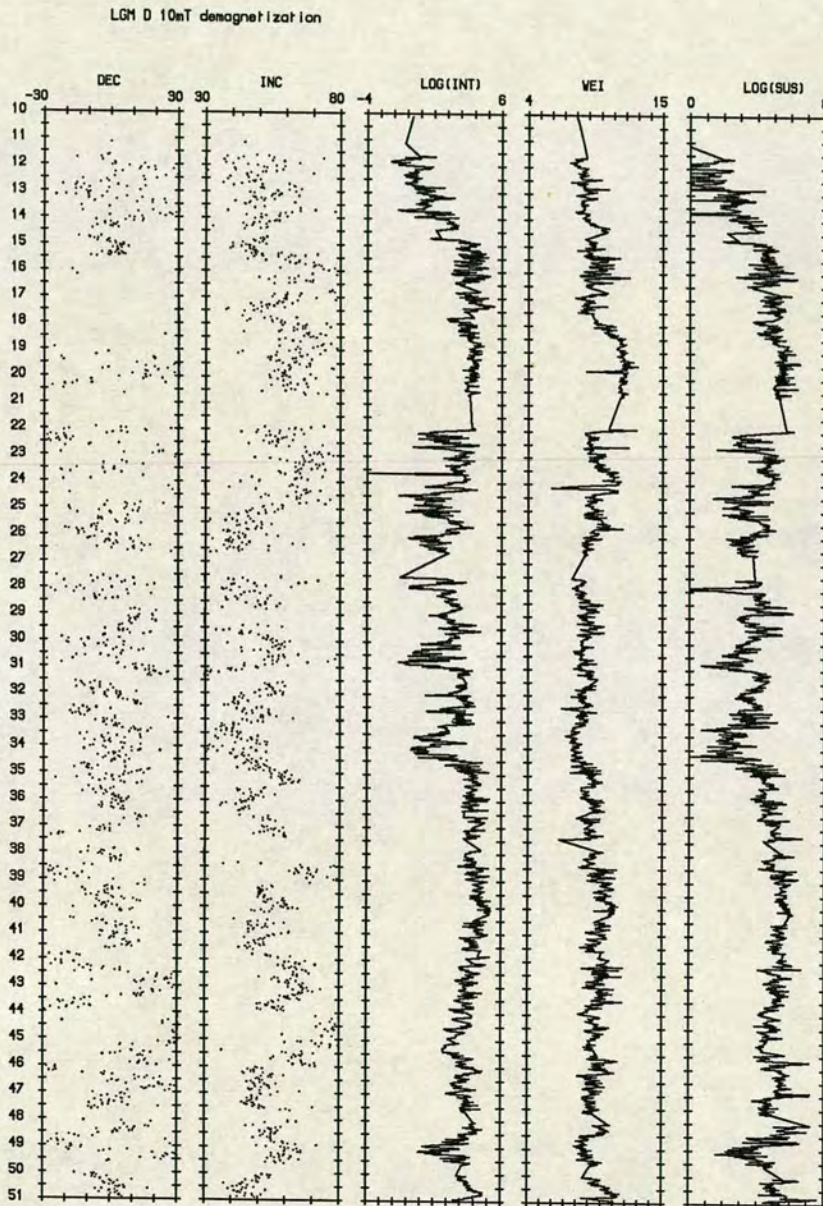


Figure 5.9. Results of Core D, after AF demagnetization in a peak field of 10mT. Declination and inclination are in degrees and weight is in grams.

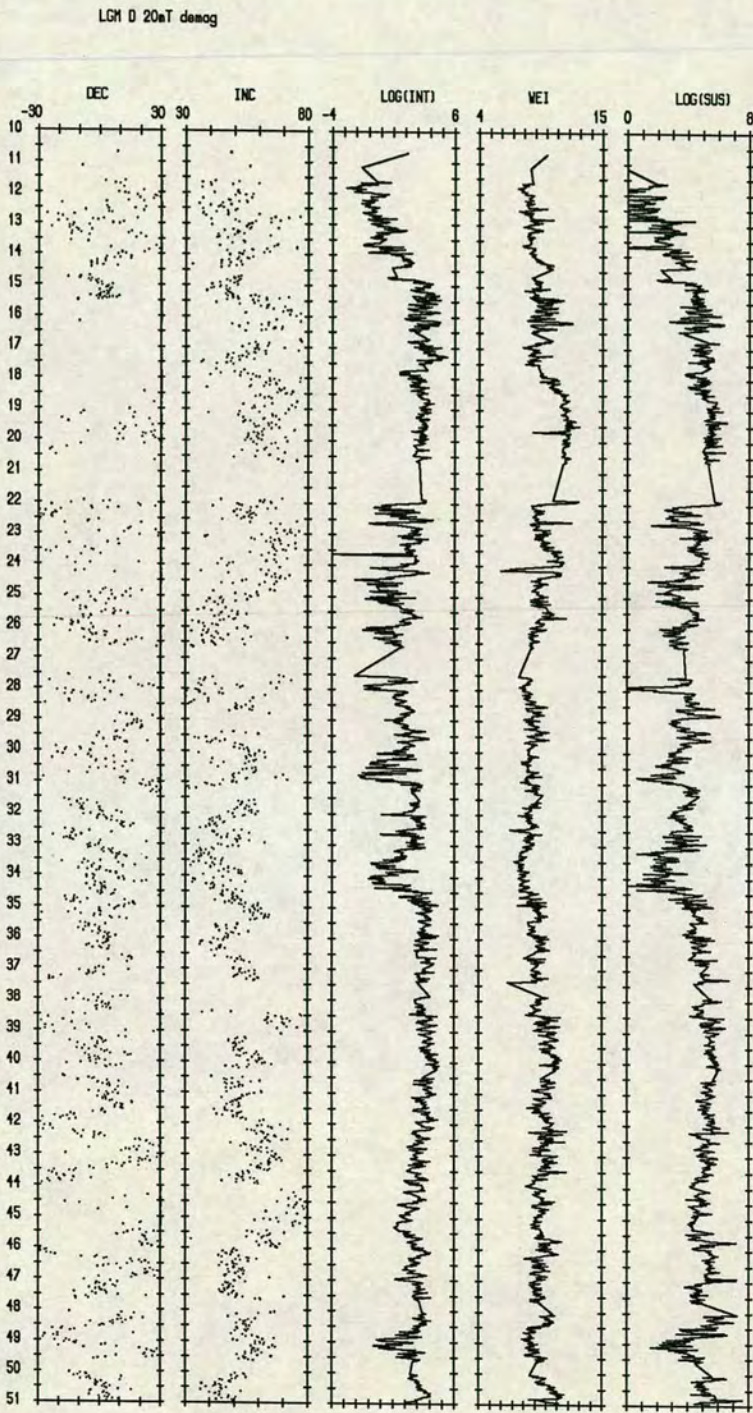


Figure 5.10. Results of Core D, after AF demagnetization in a peak field of 20mT. Declination and inclination are in degrees and weight is in grams.

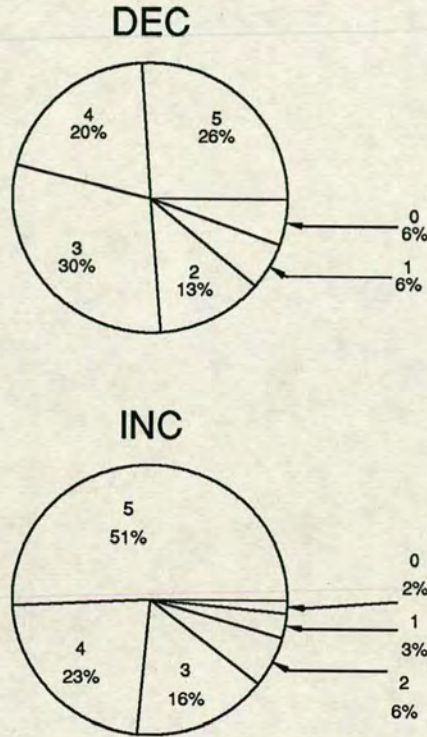


Figure 5.11. The directional quality of the remanence vectors of core D after 10mT and 20mT demagnetization steps. 5 signifies a difference of less than 1° between the two steps, 0 signifies a difference of more than 20° (see text for more details).

being present.

These three ratios indicate that there is very little variation in size or type of magnetic mineral down the length of the core. There may be some changes in the section of the core deposited during warm periods (low magnetic parameters), though the quality of the results at such low values leaves this interpretation open to doubt.

Palaeointensities

The uniformity of the mineral type and grain size validates an attempt to determine the relative palaeointensity of the geomagnetic field. This can be done by normalizing the NRM intensity by any of the parameters controlled by grain properties. Therefore three more ratios were calculated for the samples down the core, NRM/χ , NRM/ARM , NRM/SIRM (see figure 5.15). At this point any sample with a χ/ARM ratio of greater than 5 was removed as it was felt that these samples represented a mineral assemblage

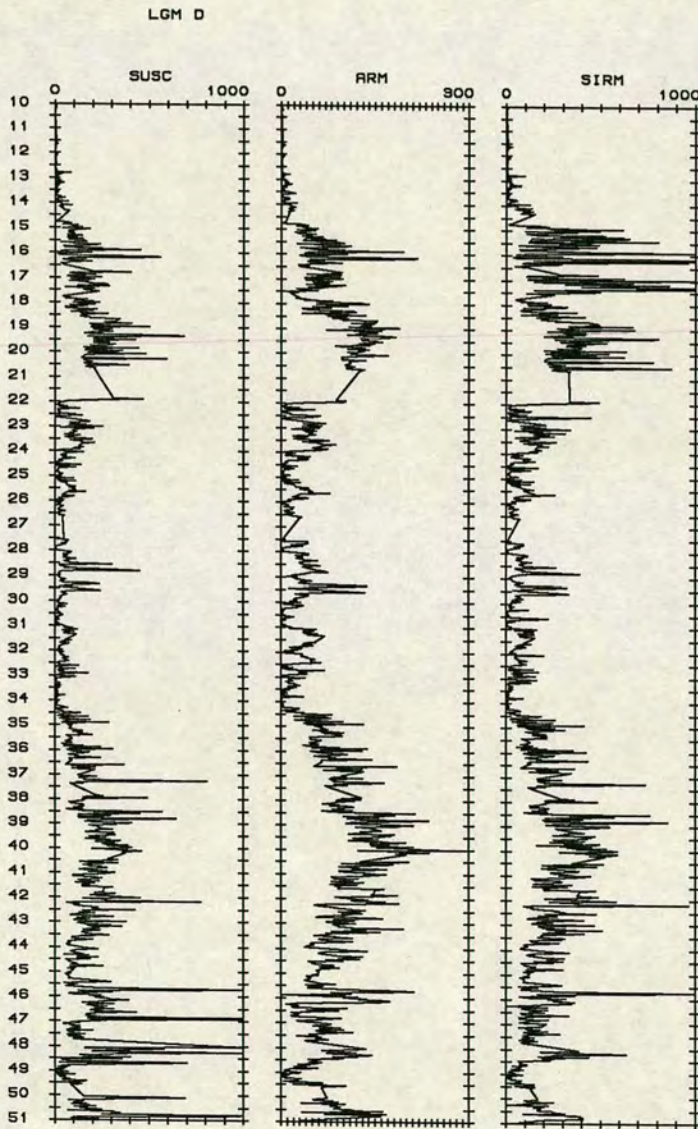


Figure 5.12. The magnetic parameters which are dependent on magnetic grain size and type, and are linked to the climate (see text for more details). Susceptibility is in SI units, ARM and SIRM are in mA/m.

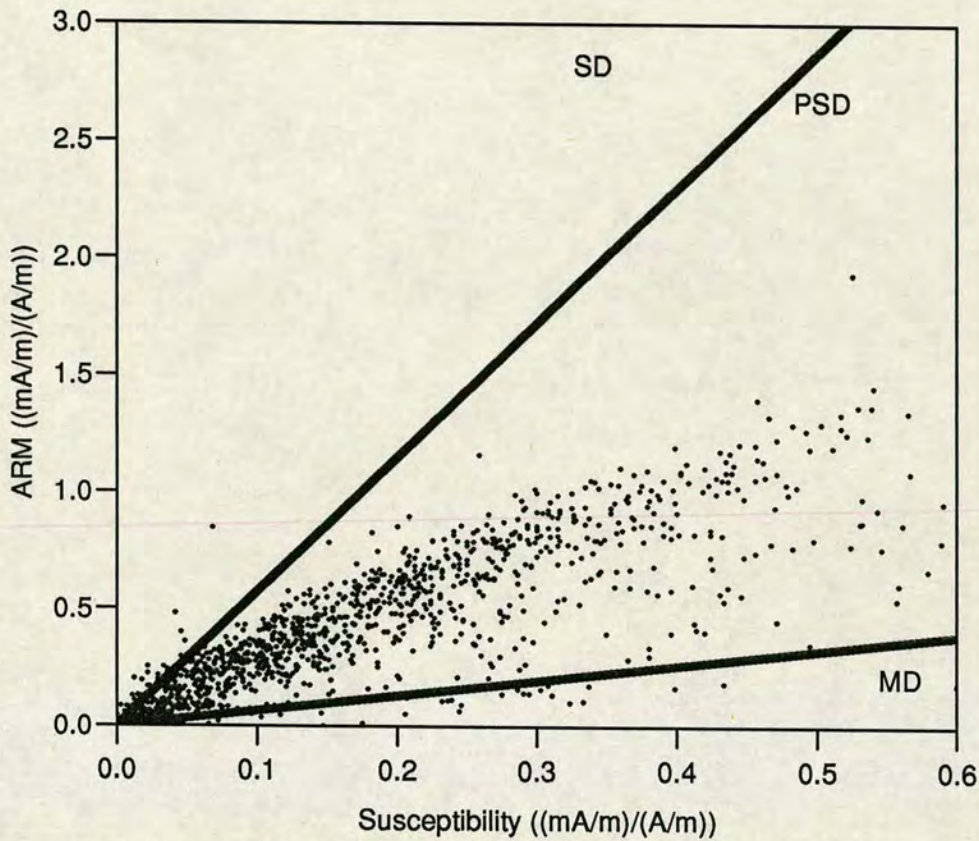


Figure 5.13. χ_{ARM} vs. χ as defined by King *et al* (1982)

too far from the straight line plotted in figure 5.16. This led to the removal of ~ 250 samples, the majority from the upper ten metres of the core but with some from the lower sections which corresponded to tephra layers, as recorded in the sedimentological description of the cores.

The NRM intensity and susceptibility are included in figure 5.15 for comparison. The similarity of the three ratios (correlation coefficients are all greater than .70) should be noted first. This is due to the stability of the magnetic minerals down the core. Therefore it is not really necessary to determine which of the three magnetic parameters is the best normalizing factor since they all appear equally good.

It should also be noted that in figure 5.15 that while the intensity of the NRM and the susceptibility show the periodicities noted above. The ratios calculated also show a strong periodicity but this is out of phase with the climate record (as shown by

r

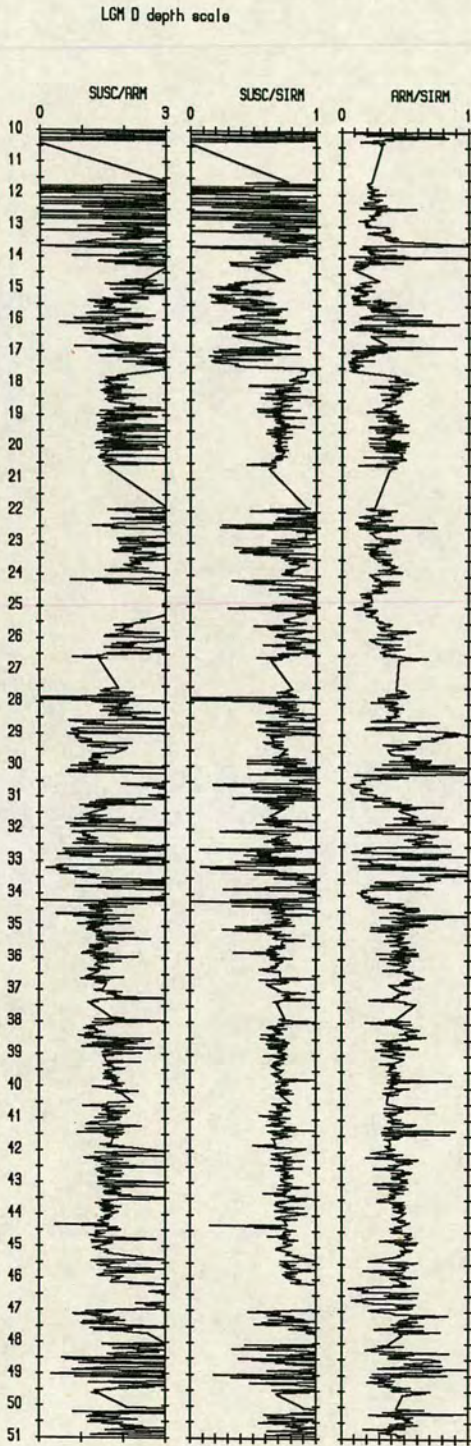


Figure 5.14. The three mineral magnetic ratios calculated for the core, all three are indications of the variability of magnetic grain type and size

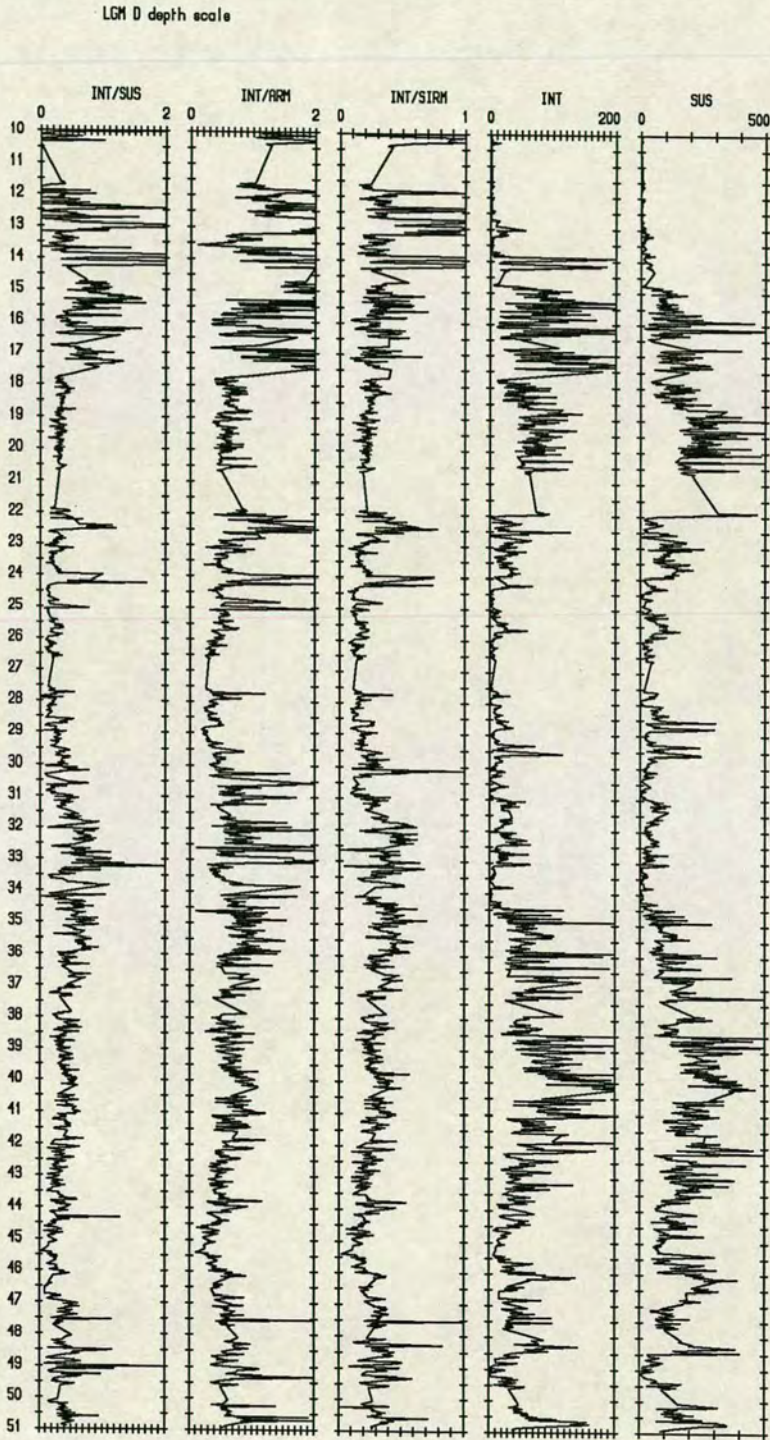


Figure 5.15. Normalized palaeointensity curves for core D, with the unnormalized NRM intensity and susceptibility shown for comparison. Intensity is in mA/m and susceptibility is in SI units.

susceptibility). They all appear to be offset by about 6 metres.

If these normalized values of intensity are really indicating the intensity of the geomagnetic field then it appears that the geodynamo also shows the Milankovitch periodicities but that they are lagging the climatic effects which seems to indicate that there must be a direct linkage between the geodynamo and the astronomical phenomena and that this linkage can not be through the climate.

5.4 Initial Dating of the Core

The conversion of the depth scale to time scale is always a difficult part of any palaeo-secular variation study. In the case of these cores the age of the sediment makes the use of radiocarbon dating impractical except in the upper sections, where the palaeo-magnetic signal is poor. Also Watts (1985) comments that there were problems with the conventional radiocarbon dates that he obtained from a core from this lake. He indicates that there may be inclusion of old carbon in the sediments of the lake. No radiocarbon age determinations have yet been made on the cores taken in 1990.

A second common method for the age determination of cores is the use of pollen analysis to indicate periods of warming and cooling, which can be correlated to similar occurrences at other sites which have been dated.

Therefore in an initial attempt to date the long cores from Monticchio the down-core susceptibility profiles were used (figure 5.7). Previous work from Lac du Bouchet (Creer 1991) has shown that % non-arboreal pollen can be correlated well with susceptibility, showing that susceptibility is a good proxy climate indicator. This is advantageous since magnetic susceptibility is a very simple measurement to make and can be carried out on a core relatively quickly.

In the case of the Monticchio cores the magnetic susceptibility was compared to the SPECMAP $\delta^{18}\text{O}$ record derived from marine cores by Imbrie *et al.* (1984) (figure 5.17). There is evidence from geochemical analysis of the cores that the base of the Holocene is at about 7.5 metres down (Robinson, *Pers. Com.*). This is indicated by the change in values of the carbon/nitrogen ratio (figure 5.18). This can be interpreted as a change in organic input coming from aquatic plants to terrestrial plants, which would accompany the climatic change at the end of the Weichselian glacial period.

The remainder of the correlation was completed by comparison of the smoothed susceptibility record with the SPECMAP $\delta^{18}\text{O}$ record. Several possible correlations were tried, assuming that the long period variations seen in the susceptibility record were ~ 40 Kyr and ~ 100 Kyr. Figure 5.19 shows the two initial estimates of the depth to time transform that were derived. The final line shown on figure 5.19 is a depth

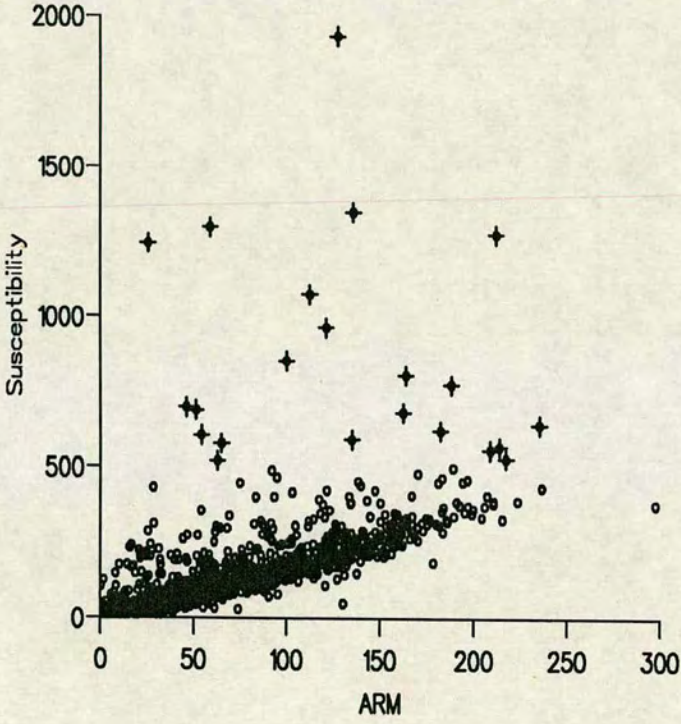


Figure 5.16. Intensity of Susceptibility (SI units) vs. ARM (mA/m) of Core D. Crosses indicate tephra layers which were removed from later analysis (see text for more details)

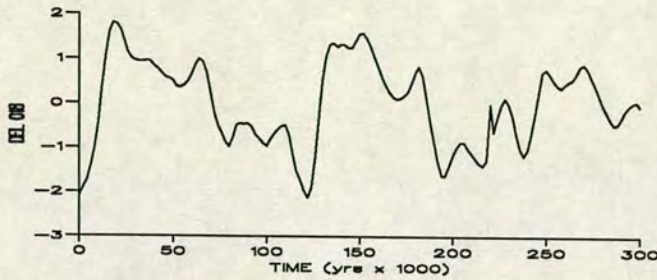


Figure 5.17. The SPECMAP $\delta^{18}\text{O}$ Isotope Curve, Imbrie *et al.* 1984

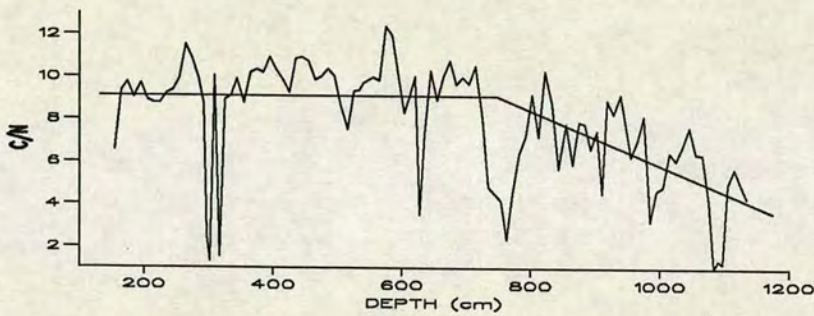


Figure 5.18. Carbon to Nitrogen Ratio, Core C

to time transform derived from preliminary pollen analysis. As can be seen this line agrees with the older estimate of age except for the location of the end of oxygen isotope stage 2. This depth time transform was selected for the final conversion of core D to a time scale after initial spectral analysis on the time series created (figure 5.22) showed that this time series produced the best fit to the expected frequencies.

5.5 Spectral Analysis of Core D

Once the cores had been transformed to the time scale it became possible to investigate the periodicities found in section 5.3.2. As can be seen in figure 5.20 and 5.21 the periodicities can still be seen clearly by eye when the data are plotted against a time scale adding further credence to their reality.



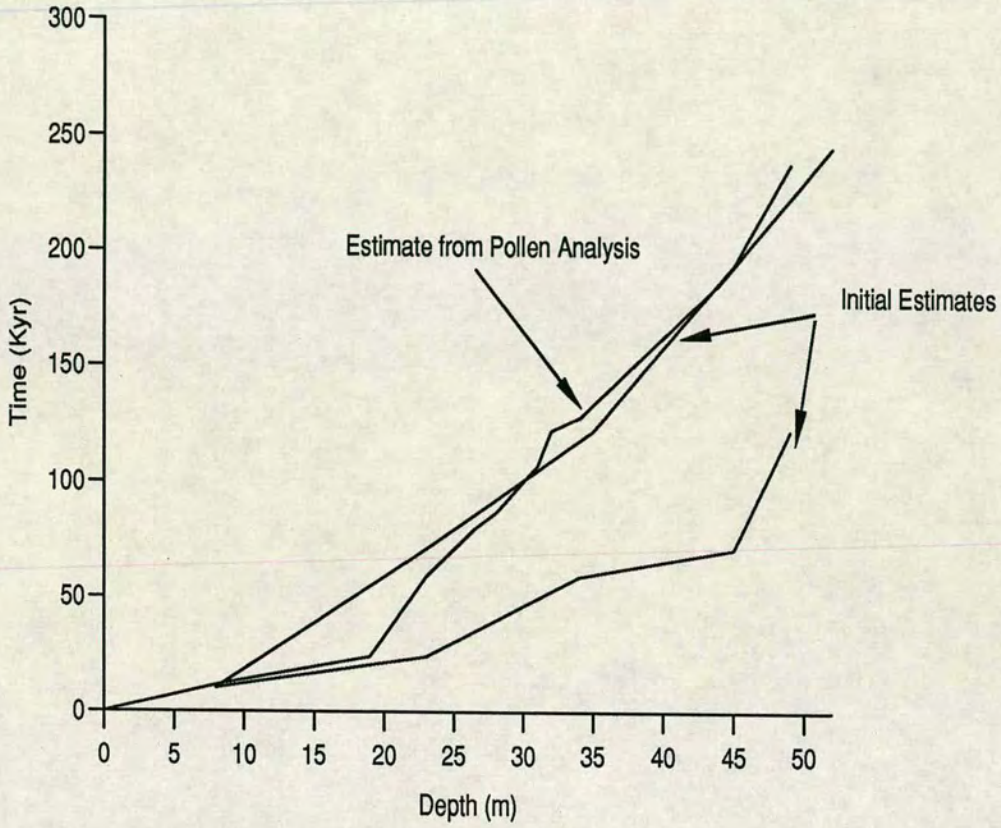


Figure 5.19. A comparison of the depth to time transforms used

Method

As is discussed in chapter 4 the Lomb-Scargle (Lomb 1976, Scargle, 1982) is superior to both the conventional FFT and MEM methods of spectral analysis especially when applied to unevenly sampled data sets, or when searching for periods of the same order as the length of the record.

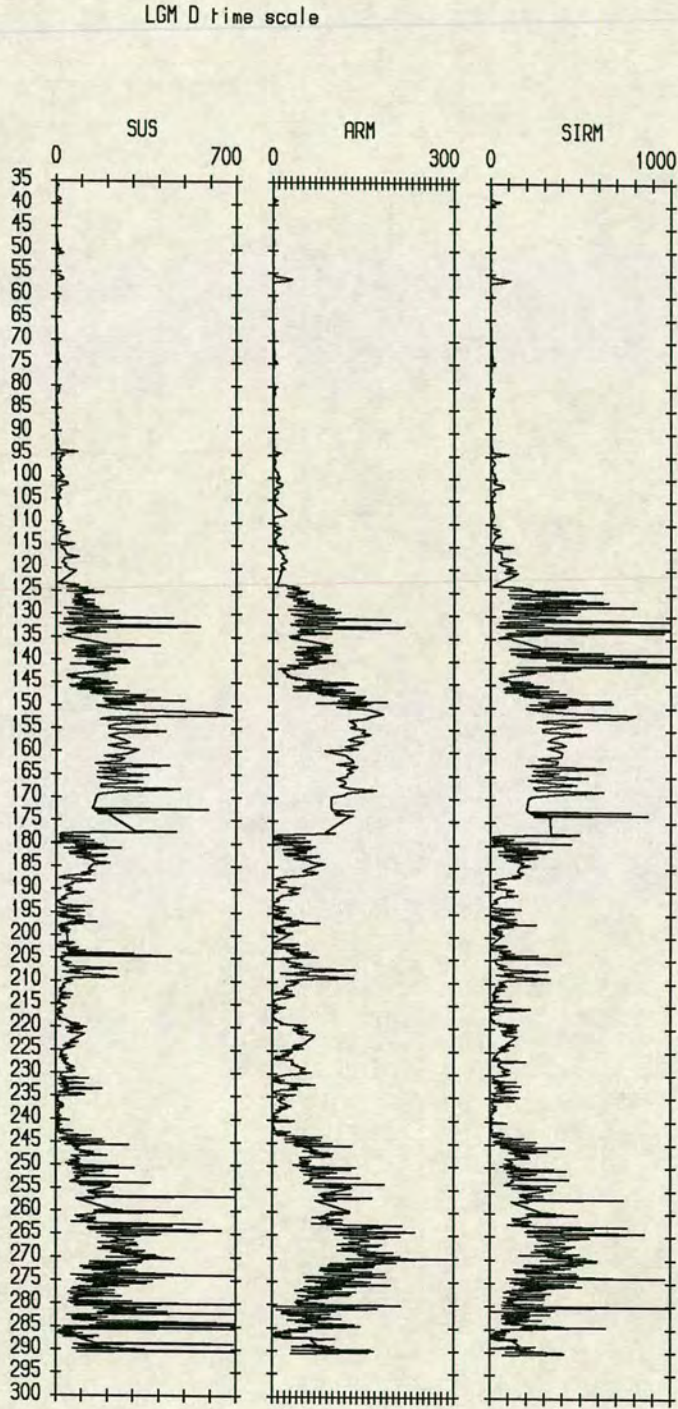


Figure 5.20. The magnetic parameters which are controlled by magnetic grain size and type, after transformation to a time scale. Susceptibility is in SI units, ARM and SIRM are in mA/m.

LGM D time scale

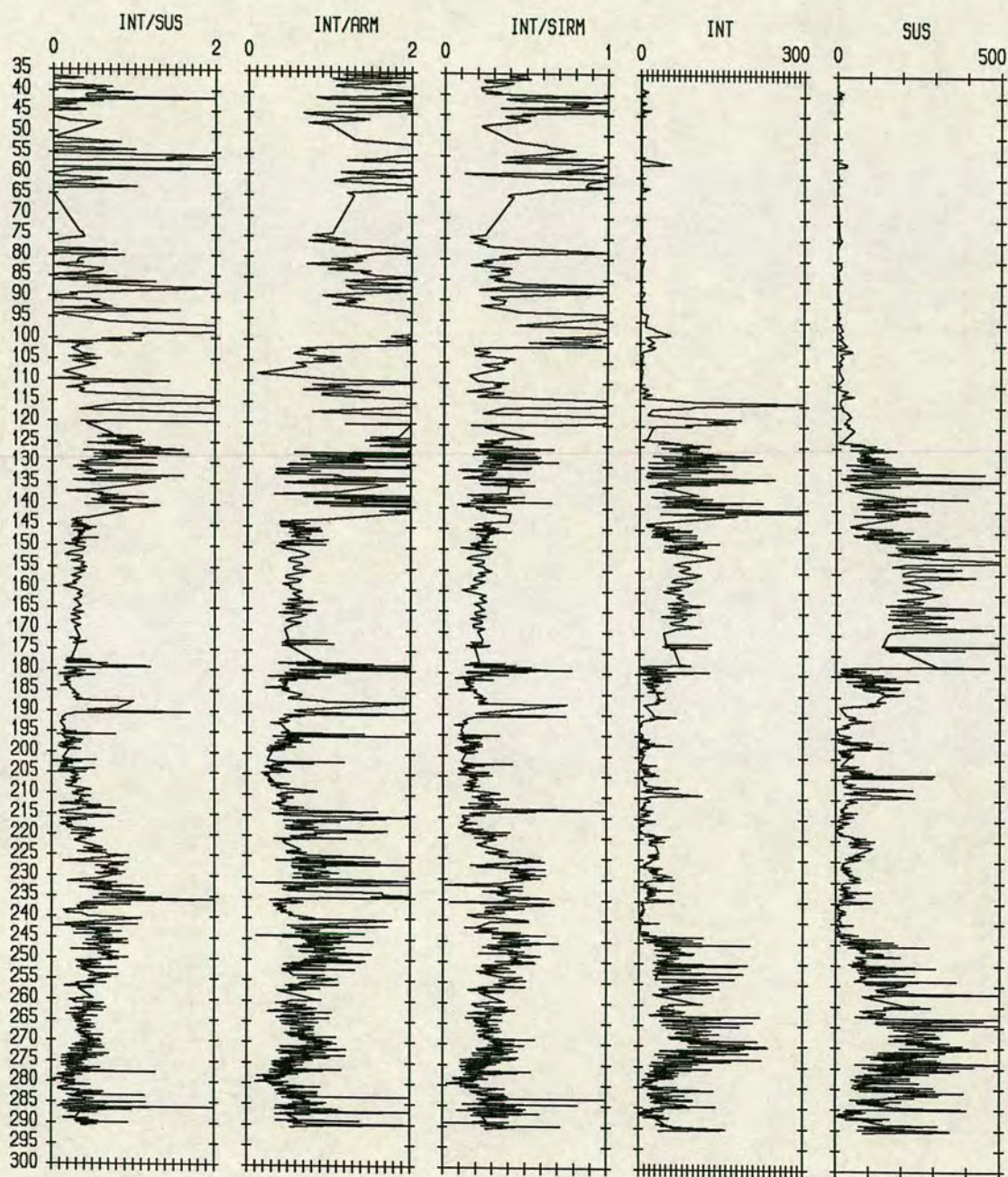


Figure 5.21. The normalized palaeointensity parameters transformed to a time scale, NRM intensity and susceptibility are included for reference. Intensity is in mA/m and susceptibility is in SI units.

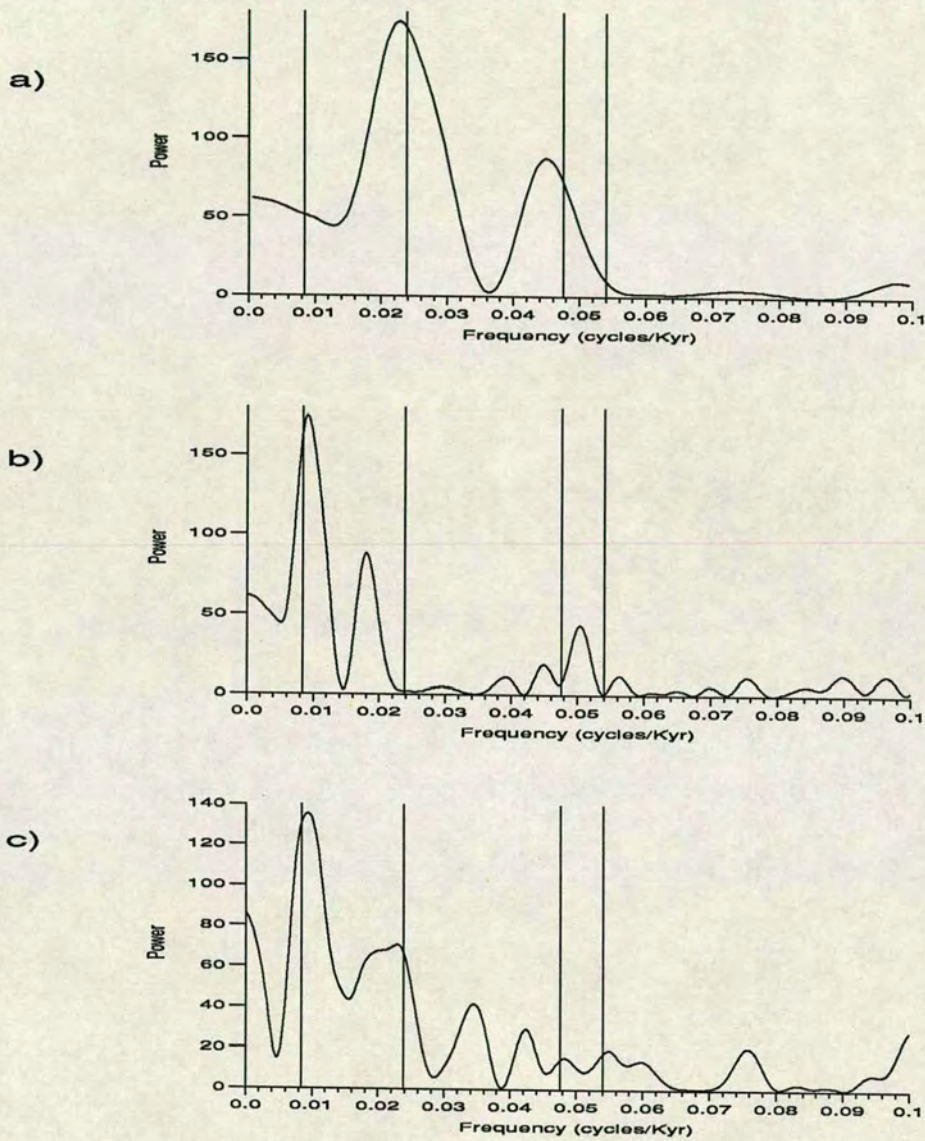


Figure 5.22. Lomb-Scargle analysis of the susceptibility record for core D, using the three depth to time conversions shown in figure 5.19. a) is the lower of the two initial estimates, b) is the higher of the initial estimates and c) is the time scale derived from pollen analysis.

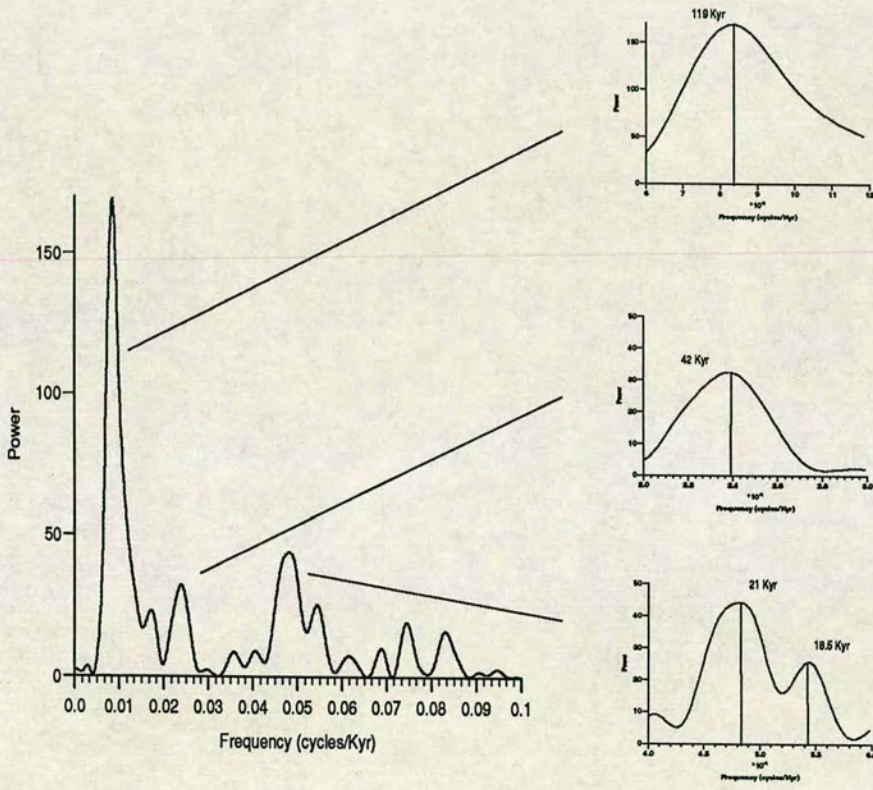


Figure 5.23. Lomb-Scargle analysis of palaeointensity (normalized by susceptibility) for core D

5.6 Discussion

Milankovitch Cycles and Astronomical Periods

Milankovitch suggested there are three astronomical cycles that can affect the climate by varying the insolation:

- Changes in the eccentricity of the Earth's orbit (e) which varies with a period of between 92,000 years and 100,000 years.
- Changes in the obliquity of the ecliptic (the tilt of the Earth's axis) ($\Delta\xi$) which varies with a period of 41,000 years.
- Precession of the equinoxes (P) which varies with periods of 23,000 years and 19,000 years.

These factors are known to effect global temperatures as recorded in the marine $\delta^{18}\text{O}$ record.

Figure 5.22c clearly shows two of the main astronomical periods as calculated by Milankovitch suggesting that changes in climate do control the susceptibility variations. Figure 5.23 also shows the main astronomical periods. Some discussion needs to be given to a consideration as to whether these periods in the palaeointensity of the geodynamo have been induced via climate or directly by forces acting on the core-mantle interface.

The first possible explanation of these periods is that NRM intensity normalized by susceptibility is not a true recorder of the intensity of the geodynamo. A second possibility is that there is a link between climate and the efficiency of the geodynamo. Or finally that the geodynamo is forced by the astronomical cycles.

The first question raised above has been considered by King *et al.* (1983) who conclude that providing the magnetic grain type, size and concentration are roughly constant down core then normalization of the NRM intensity by ARM or susceptibility is valid. As was shown in section 5.3.2 it appears that these criteria are fulfilled by core D, so it seems possible to conclude that the NRM normalizations by susceptibility, ARM and SIRM are a reliable representation of the intensity of the geodynamo.

The second point seems unlikely since the normalized curves are about 35 Kyr out of phase from the climate as recorded in the susceptibility, ARM and SIRM records. Therefore it seems hard to invoke the direct influence of climate on the geodynamo to explain these results.

Therefore I must conclude that there appears to be a link between the astronomical cycles and the efficiency of the geodynamo. This was first suggested by Malkus (1963,

1968), though he considered that precessional torques produced by the difference in flattening between the core and mantle could provide sufficient energy to drive the geodynamo. This theory has been doubted by Loper (1975) and Rochester *et al* (1975), there has been support from Stacey (1969) and Vernekar (1972) though it now seems likely that thermal convection is the main energy source of the geodynamo, it is still possible that changes in the precession and in the eccentricity of the Earth's orbit could modulate the geodynamo. Wollin *et al* (1978) propose that the precession of the core is more pronounced when the the eccentricity is at a maximum. They conclude that the intensity of the geomagnetic field is in phase with the climate for the deep sea core they studied. A closer look at their data seems to show a slight lag between the two though it is difficult to determine it's size on the resolution of their data. Similar results have also been reported by Kent and Opdyke (1977), though again the resolution of this record is too poor to allow a study of the exact phase relationship between the intensity record and the climatic record to be made.

5.7 Evidence for Seismicity in Lago di Monticchio

The surrounding area of southern Italy is still seismically active, as a result of motion between structural fault blocks formed in the sedimentary basins. There have been several large earthquakes in recent times. The Sele Valley was the centre of two large earthquakes (near source intensity X) in 1694 and 1980, and Santa Arcangelo to the south west had a similarly large earthquake in 1857. Westaway and Jackson (1987) studied another large earthquake in the Ariano basin in 1962. All of these earthquakes are large enough to have caused slumping and liquefaction in the sediments at Lago di Monticchio, and there is no reason to doubt that such large earthquakes have been occurring locally since the lake's formation.

Liquefaction Features

It is necessary to distinguish between features caused by normal sedimentary processes (autokinetic) and those caused by earthquake processes (allokinetic) (Leeder, 1987). Liquefaction of sediments occurs when the pore pressure \mathbf{P} in the body of the sediment approaches the solid stress σ , this is defined in equation 5.1 where σ' is the effective stress.

$$\sigma' = \sigma - \mathbf{P} \quad (5.1)$$

Under normal (autokinetic) conditions this will not occur. However during a seismic event a cyclic stress is applied causing a transfer of stress to the pore fluid. This will

result in the loss of strength within the body of the sediment and it will behave like a liquid. This process is enhanced by

1. high initial porosity/void ratio,
2. low confining pressures, i.e; shallow burial,
3. high values of applied shear stress,
4. large numbers of applied stress cycles,
5. low initial shear stress,
6. fine and medium grain size which prevents rapid drainage and therefore pore fluid dissipation.

The passage of a liquefaction front through the sediment depends on the vertical homogeneity of that sediment body, but of the above factors the most important are the magnitude and duration of the applied stress.

Youd and Perkins (1978) showed that events below magnitude 5 and at a distance of greater than 150 km away are unlikely to cause liquefaction. But all the earthquakes mentioned above are within in this range and could have affected the sediments at Monticchio.

The best evidence for seismically induced effects in the sediments are layers of intra-folial deformation overlain by an undisturbed layer. This features are termed "seismites" by Seilacher (1984). Simms (1975) listed a number of factors important in the correlation of seismic events with seismites:

- proximity to presently active seismic zones,
- presence of potentially liquifiable sediments,
- similarity to structures formed experimentally,
- small scale internal structures with in deformed zones indicating liquefaction,
- structures restricted to single stratigraphic intervals,
- zone of structures and similar facies correlatable over large areas,
- absence of detectable influence by slope failure or other sedimentary, biological or deformational process.

The sediments of Monticchio fulfill all of these requirements with the possible exception of correlation over a wide area as only two cores were studied for these effects. Examples of such structures are well documented. The Alaskan earthquake of 1964 (US Geol. Survey Papers 543 & 544) shows ground impressions of sand and water escape structures. The 1979 Imperial Valley event provides evidence of liquefaction in sedimentary layers (US Geol. Survey Paper 1254).

Cores 3 and 4 were examined for seismites, core 4 showed several signs of shearing and slumping. While core 3 seemed generally less disturbed but showed several seismites. The effects of disturbance could also be seen in the generally scattered palaeomagnetic results from both cores.

Microsedimentary examination of the second series of cores taken is underway at the University of Trier, though it is expected to be some years before this painstaking work is complete. However initial investigations do not show any evidence of disturbance in these cores.

It is possible that "seismitic-like" features could be caused during the coring process, but this seems unlikely in the first series of cores since the Mackereth corer is a relatively "gentle" coring method with low penetration velocities. However the use of a vibro-hammer to penetrate tough layers during the second coring campaign may have caused damage to some sections of these cores.

The differences between the two sets of cores is mostly likely to have been caused by the differences in coring sites (see figure 5.2). Reflection seismic studies on the lake show that there is a region in the centre of the lake which shows considerable slumping and possible fault structures. The Mackereth corers were taken from this region, due to the need for deep water to operate this corer. Whereas the second series of cores were taken from shallower water nearer the edge of the lake in a flat and, apparently, undisturbed section of the lake.

Chapter 6

Results from Lago di Martignano

6.1 Introduction

Lago di Martignano is a small maar lake (~ 2 km by 1.5 km) situated just north of Rome, Italy, ($42^{\circ}7'$ N, $12^{\circ}20'$ E) at a height of approximately 200 m (see figure 6.1). A series of cores were taken in the summer of 1989. The cores were returned to Edinburgh unopened and then subsampled for palaeomagnetic measurement and also for pollen studies.

6.2 Setting and Geology

Lago di Martignano was formed during the Pleistocene. This crater is one of a large number which formed in the region in a quaternary phase of igneous emplacement along a line moving southward from Tuscany, at the same time when Lago di Monticchio was formed (see section 5.2).

The volcanos in the region are typically multi-centred; the volcanism produced complexes of explosion centres. Lago di Martignano occupies a crater in the Sabatini group, which is centred on Lago di Bracciano. It is one of a few lakes in the complex which has not been completely infilled over time, though some of the local lakes are reported to have been drained artificially during Roman times (Bonatti 1970). Stella *et al* (1972) studied the limnology of the lake and published a bathymetric map (see figure 6.2). The catchment area surrounding the lake is small, extending only to approximately 250m from the edge of the lake and to a height of about 50m above the

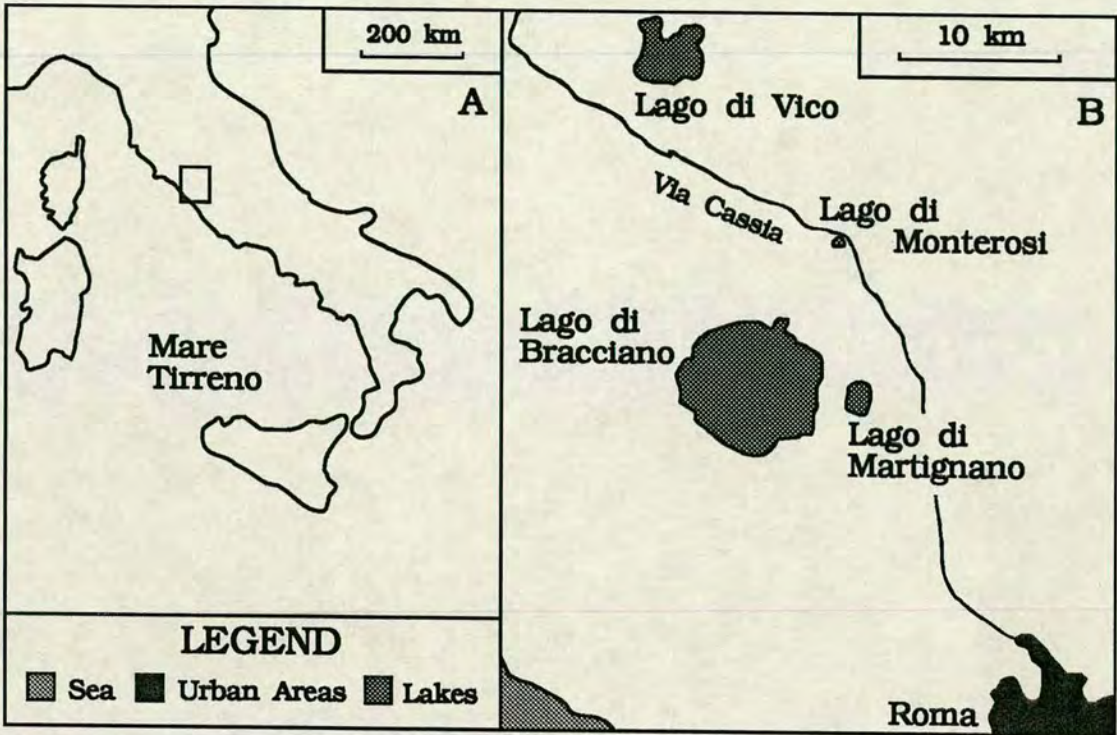


Figure 6.1. Location of Lago di Martignano, after Kelly and Huntley, 1991.

lake surface. There are signs of two raised shore lines within the catchment area indicating the lake level has at some time in the past been higher than at present. Also an attempt to core near the edge of the lake under about 10m of water recovered only a few cm of sediment, which resembled the present shore line sediment, indicating a period when lake levels were lower than today. As can be seen in figure 6.2, about half of the catchment area is used for agriculture, with this being a mixture between arable and pastoral farming.

Figure 6.2 shows the locations from which the four cores were taken.

6.3 Description of Palaeomagnetic Results

The cores from Martignano were subsampled as described in section 3.2.1 and the magnetic remanence was measured on a three axis superconducting cryogenic magnetometer. A series of pilot samples were stepwise demagnetized revealing median destructive fields (MDF) of around 20mT. The samples from each of the three cores were bulk demagnetized in an alternating field of 10mT to remove viscous components.

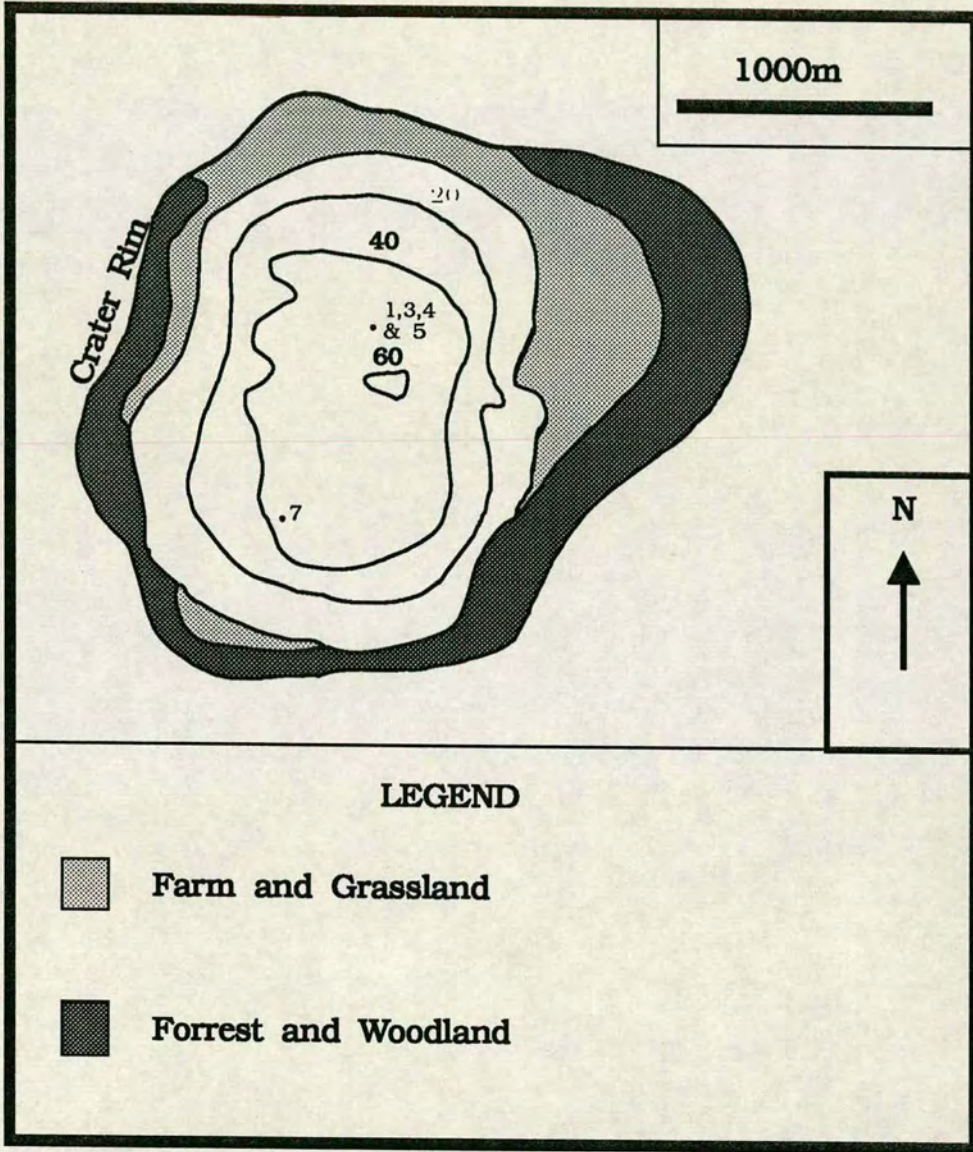


Figure 6.2. Bathymetry of Lago di Martignano, after Kelly and Huntley, 1991.

Martignano Stack Depth Scale

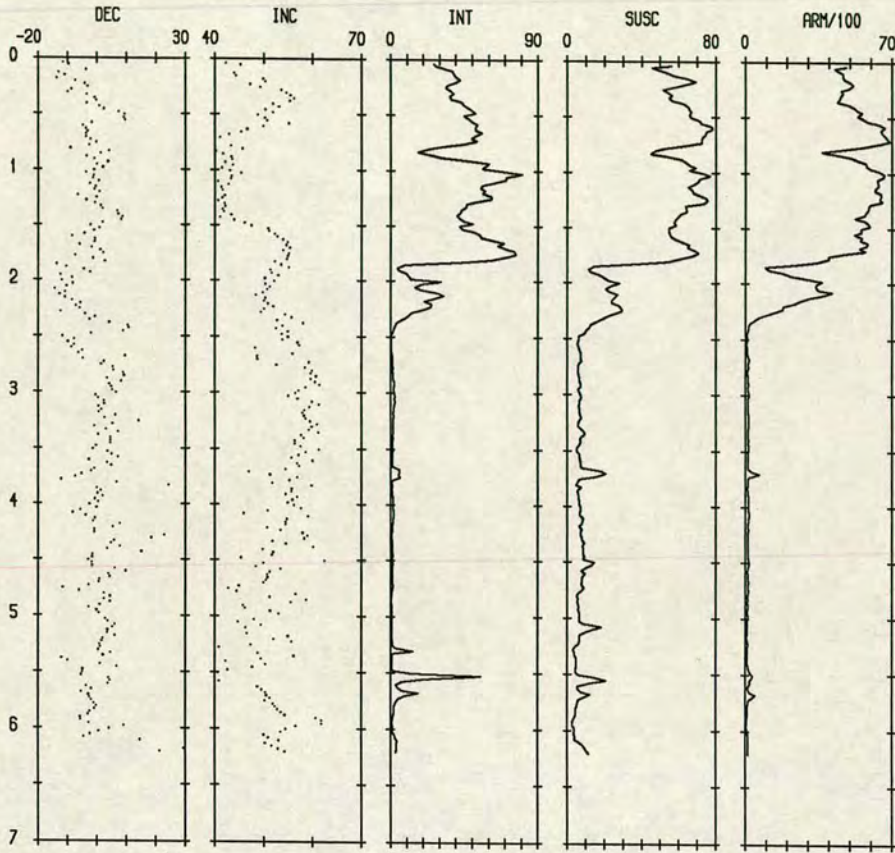


Figure 6.3. Martignano Merged Record on MART 1 Depth Scale. Declination and intensity are in degrees, intensity and ARM are in mA/m and susceptibility is in SI units.

Next the susceptibility of each sample was measured. The samples were then demagnetized and given an ARM in an alternating peak field of 100mT biased with a steady field of 0.1mT (the Earth's field is ~ 0.05 mT).

Depths down the three cores were converted to a common depth scale, defined by core 1 since it was the longest. Depth time transform functions were constructed by correlation of the susceptibility logs of the three cores. The measured data from the cores were merged to improve the signal to noise ratio, by merging the results of the three cores and averaging all samples which differed in depth by less than 1.5cm on the common depth scale, using the FORTRAN program MERGE (Smith, 1985). Figure 6.3 shows the merged results from the three cores after AF cleaning.

The first feature of figure 6.3 to note is the large increase in intensity at a depth of 1.8m, which is interpreted as a change in proportion of magnetic minerals effect rather than a reflection of changes in the geomagnetic field since the susceptibility and ARM logs show a similar increase at this depth. The cause of this change is investigated further in section 6.6.

The directional data from the cores shows a well-defined pattern of secular variation especially in the upper part of the core where intensity is strong. There is slightly more scatter in the lower part of the core.

The series of narrow intensity spikes at the base of the core are identified with tephtras which were easily visible to the naked eye on inspection of the opened cores. These points were removed from the directional stack as they were unlikely to hold a stable DRM.

6.4 Construction of a Time scale

To convert the down-core depths to a time scale, 8 samples were taken for radiocarbon analysis. The results are shown in figure 6.4, and clearly there is a problem in determining how best to interpret and use them. The lower most three samples give a Late Glacial age for the base of the core, and this is consistent with the lithostatigraphy and the pollen analysis (Kelly and Huntley, 1991). The upper-most age is also consistent with the expected age of the top of the core which should be close to the present.

But the middle four dates are statistically almost identical. There is no evidence from the palaeomagnetic results, from the lithostatigraphy or from pollen analyses to indicate that there was an instantaneous deposition of 2.5m of sediment and there is no significant reworking of the sediment. This could be attributed to the very low carbon content of the samples (0.2 – 0.9g), which required the use of extended counting times, leading to experimental errors in the age determination.

In order to obtain a usable time scale a series of regression analyses were performed and a linear regression of age against the square root of depth was found to provide the best empirical fit to the data. This regression avoided the need for negative sedimentation rates and relied less on the poorer data. Therefore all ages used below have been obtained using the regression:

$$A = 253.2 + (421 \times \sqrt{D}) \quad (6.1)$$

where A is the age in ^{14}C yr BP and D is the depth in cm. The curve shown on figure 6.4 represents this regression for the length of the stacked record.

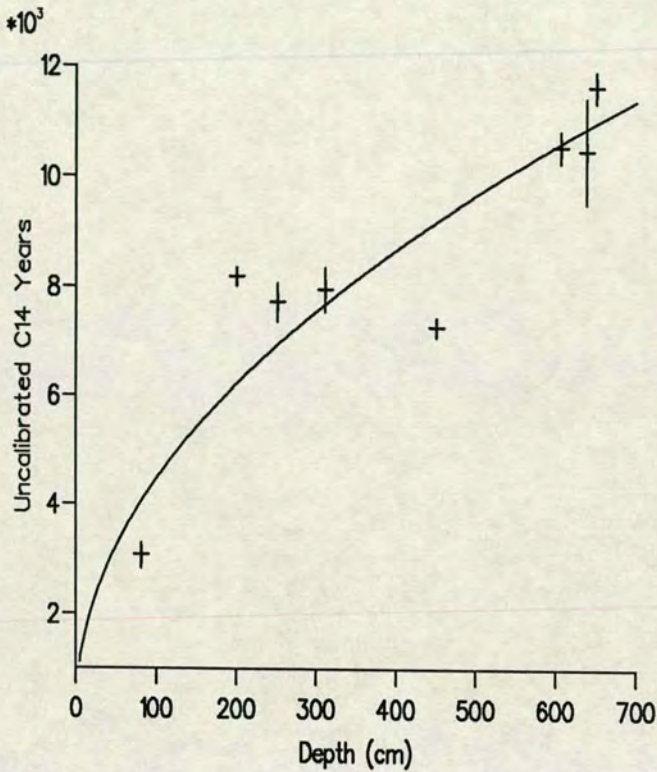


Figure 6.4. Lago di Martignano Depth to Time Transform, after Kelly and Huntley, 1991

6.5 Description of the Secular Variation

Figure 6.5 shows the stacked record from Lago di Martignano after transformation to the time scale using the depth to time transform developed in section 6.4. It can be seen that the large increase in intensity occurs at ~ 6000 years BP and that the palaeosecular variations (PSV) seen in the directional data are still clearly visible. The top of the core is dated at ~ 1000 years BP, while the base extends to $\sim 11,000$ years BP.

The directional PSV curves for Lago di Martignano will now be compared with other secular variation curves which have been published for Europe. Figure 6.6 shows the comparison with Lake Windermere (Turner and Thompson, 1981). The Windermere record shows the largest amplitude variations in the lower 5,000 years of the record, especially in the inclination record. Creer (1983) gave the maxima and minima of

Martignano Stack Time Scale

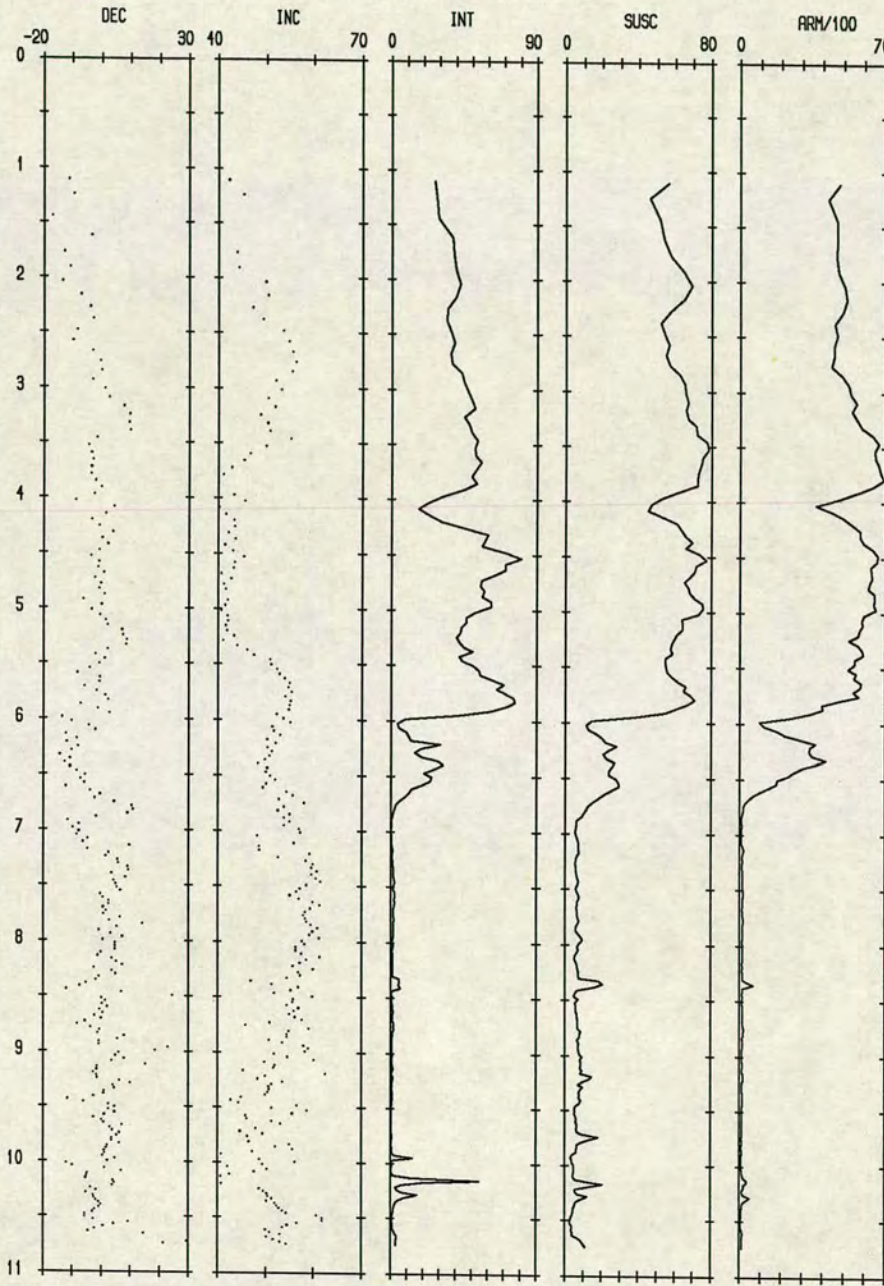


Figure 6.5. Martignano Stacked Record on a Time Scale. Declination and intensity are in degrees, intensity and ARM are in mA/m and susceptibility is in SI units.

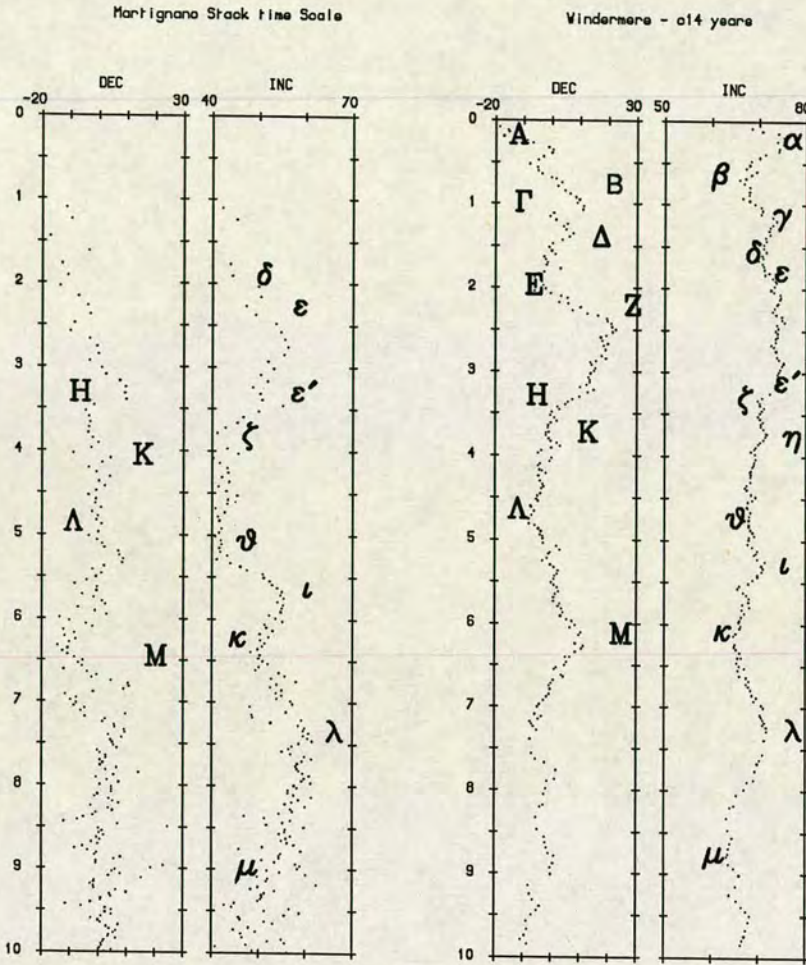


Figure 6.6. Comparison of Lago di Martignano and Lake Windermere (Turner and Thompson, 1981). All units are degrees.

declination capital greek letters ($A - M$) as labels and lower case greek letters ($\alpha - \mu$) for the inclination record.

As can be seen in figure 6.6, correlation of the declination features $H - M$ was possible for the Martignano record. Inclination features δ to μ can also be correlated, but feature η can not be resolved in the Martignano record which has a very small amplitude in the Windermere record.

Figure 6.7 shows the same comparison with Smith's (1985) Mackereth core stack for Lac du Bouchet. The Holocene record for Lac du Bouchet is poor since it is contained within only 1.5m of highly organic and weakly magnetized sediment. However Smith succeed in correlating declination features Γ to M , and inclination features ν to μ with the Windermere record.

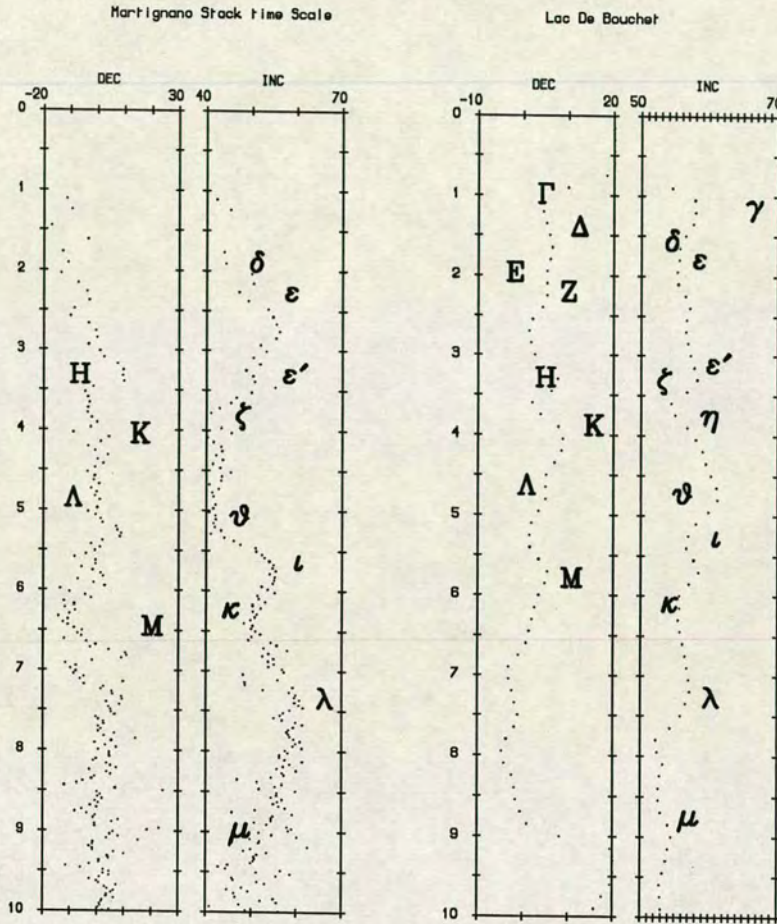


Figure 6.7. Comparison of Lago di Martignano and Lac du Bouchet (Smith, 1985). All units are degrees.

Comparison of the Lac du Bouchet record with the Lago di Martignano record allows the identification of the same maxima and minima in declination and inclination as were seen above in the Windermere record.

Both of these comparisons provide support for the regression chosen to fit the C¹⁴ dates as discussed in section 6.4.

6.6 Magnetic Mineral Studies on the Sediments of Lago di Martignano

To determine the cause of the major intensity increase recorded in the cores from Martignano a series of mineral magnetic studies were carried out.

SIRM's and Coercivity Measurements

A number of samples were given an isothermal remanent magnetization in a field of 2T which was sufficient for saturation. The SIRM's were measured on a Molspin fluxgate magnetometer. The samples were then given stepwise increasing reverse isothermal remanent magnetizations (IRM). The coercivity of remanence was then measured. Some of the results of these experiments are shown in figure 6.8 where it can be seen the samples fall into two distinct groups. In the first group (A), from the upper part of the sequence, the SIRM is reduced to zero by back fields of $\sim 30\text{mT}$ and these samples are saturated in the reverse direction by a field of about 100mT. The second group (B) are not reduced to zero intensity until a much larger field ($\sim 90\text{mT}$) is applied and are not completely saturated in a reversed direction with a 2T field. The saturated intensities (M_{ST}) of group B are much lower than those of group A.

The coercivity of remanence (H_{cr}) is the strength of the steady (dc) field required to remove the saturation magnetization completely when applied in the opposite direction. Dankers (1981) determined values for H_{cr} for synthetic samples of magnetites, titanomagnetites and haematites and showed that magnetites and titanomagnetites have high SIRM's (M_{ST}) and H_{cr} 's of less than 40mT. While haematites have lower SIRM's but H_{cr} 's of between 60mT to $>3000\text{mT}$.

Comparison of figure 6.8 with Dankers' results should allow the dominant magnetic carrier of the samples to be identified. Therefore it is possible to conclude that the samples in group A are magnetite and group B are haematite. Some possible reasons for this change are discussed in section 6.7.

To confirm that the changes in mineral type coincide with the intensity changes, the following experiment was carried out. A set of samples ($\sim 20\%$) were given an SIRM in 1T and were then given a reverse IRM in 10mT. Figure 6.9 shows a graph of $[(SIRM - IRM_{10})/SIRM] \times 100\%$ against depth for core MART1 showing that the coercivity of the samples coincides with the sharp changes in intensity.

A magnetic extraction was carried out on samples from each part of the core. The samples were placed in a large volume of water and then stirred in a beaker, a permanent magnet covered in latex rubber was placed in the beaker to attract the magnetic minerals from within the suspension. This procedure was successful for the samples from the upper part of the core but failed in the lower part due to the low concentration of magnetic minerals in these samples.

Thermomagnetic studies were carried out on the extract recovered from the upper part of the core. Figure 6.10 illustrates that the mineral is magnetite because its Curie Temperature (θ_c) is $\sim 580^\circ\text{C}$. The cooling curve does not match the heating curve

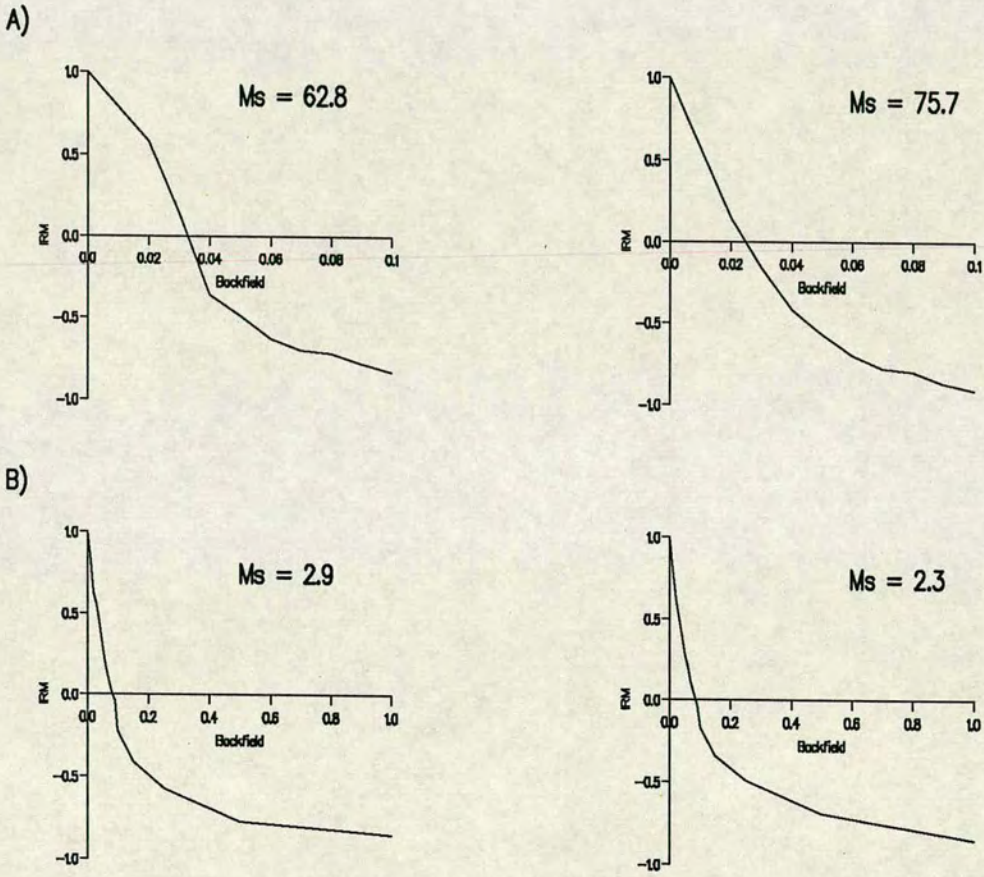


Figure 6.8. SIRM investigations of samples from Lago di Martignano. IRM measured in mA/m and backfield in Telsas.

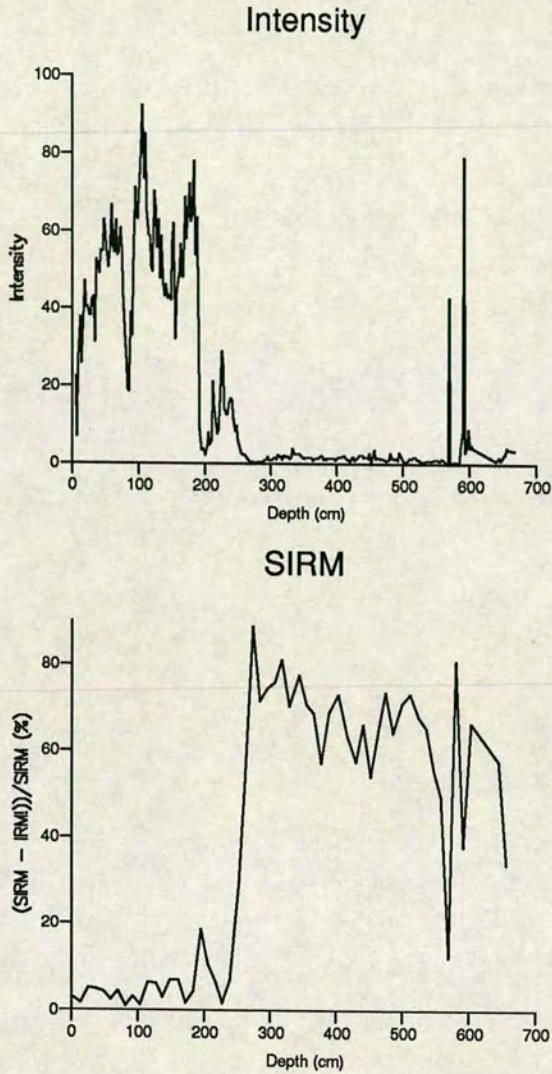


Figure 6.9. Magnetic Hardness of the Magnetic Carrier (low % are softest)

which indicates that some oxidation of the sample occurred during heating, though there is remarkably little change. Unfortunately technical difficulties prevented the experiment being repeated with an inert atmosphere to avoid this.

This indicates that the primary magnetic carrier in the samples from this section of the core is magnetite.

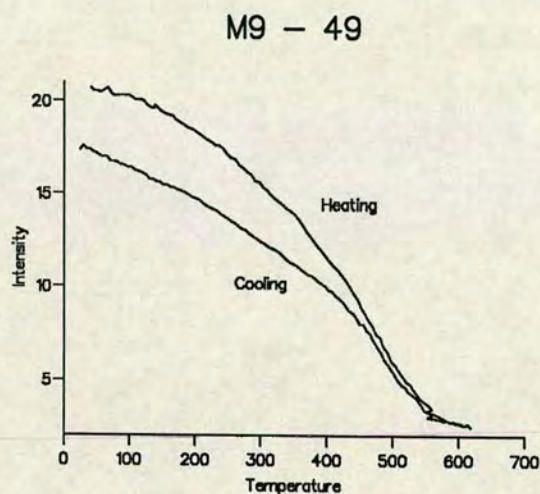


Figure 6.10. Thermomagnetic measurement of a sample from the upper part of the core

6.7 Human Impact on the Palaeomagnetic Record and the Pollen Record

Human impact on the pollen record is twofold — agricultural usage will lead to an increase in the pollens of cereals and other cultivated plants in the record, and will also show as a decrease in tree pollens, particularly in mesophylous trees which make good building materials and firewood. This decrease in tree pollen will also result from the need to clear areas of woodland for arable and pastoral usage.

The palaeomagnetic record is also likely to be affected by these activities as increased run-off will result from the clearance of the catchment, which will in turn lead to an increased mineralogenic input into the lake sediments. If the forest in the catchment was cleared by burning rather than felling — as seems more likely in a primitive culture, then this burning would convert haematite to magnetite (Thompson and Oldfield, 1986).

The earliest evidence of Neolithic settlements in Italy is dated at between 7000 - 6000 years BP (Ammerman and Cavalli-Sforza, 1984), a date which coincides well with the

first peak in palaeomagnetic intensity at Martignano, and also with an increase in olive (*Olea europaea*) pollen in the record (at 2.37m see figures 6.3 & 6.11). There is a gradual increase in all sclerophyllous taxa before this time, but along with *Phillyrea*, olive forms a majority of the sclerophyllous pollen peak. However this peak occurs well before any archeological evidence of olive cultivation in Europe. The first recorded cultivation of olives in Palestine, is dated at approximately 5500 - 5700 years BP (Zohari, 1986). Therefore it seems that these changes must be interpreted as environmental change not human impact.

The most striking feature of the palaeomagnetic record is the "step-like" increase in intensity at a depth of 1.8 m (\sim 6000 yrs BP), at a slightly deeper depth than the first occurrences of *Secale cereale* (rye) pollen (1.73 m). This is the only cereal pollen which first occurs after the arrival of Neolithic man in Italy. All other cereal pollens (*Triticum* Spp. (wheat), *Avena* Spp. (oats) and *Hordeum* Spp. (barley)) occur sporadically throughout the pollen record and seem to be indicative of parkland conditions with a discontinuous tree cover from the Late Glacial, and continuing to survive in the increased tree cover of the Holocene (Kelly and Huntley, 1991).

Therefore it seems reasonable that Neolithic man arrived in the vicinity of Lago di Martignano at approximately 6000 years BP. The pollen record shows a general decline in mesophyllous trees and a corresponding increase in grasses and arable crops from this time onwards. The increase in palaeomagnetic intensity recorded at this point is due to a change in magnetic hardness (see figure 6.9) of the magnetic carrier as well as an increase in the magnetic mineral content of the sediment. This is probably due to increased soil erosion following the initial tree clearance in the catchment area. The increased magnetic hardness can be interpreted as magnetite becoming the dominant magnetic carrier in the sediment. Thompson *et al* (1975) conclude from their studies of Lough Neagh, Northern Ireland that magnetic susceptibility is an erosion indicator, though in this case the main factor determining the susceptibility appears to be changes in the input of titanomagnetites due to the increased soil erosion within the catchment.

In Martignano magnetic mineral studies (see section 6.6) indicate that there is a change of magnetic mineral associated with the change in intensity. This can be interpreted as the result of fire in the catchment area. Rummery *et al* (1979) found enhanced susceptibility in lake sediment samples from Llyn Bychan, North Wales, sixteen weeks after a large fire in the catchment area. Thus it seems possible that a single large fire in the catchment area of Martignano, quite possibly caused by man, could account for the major increase in magnetic intensity. The subsequent high values of intensity represent the increased erosion due to the removal of tree cover. The fire also converted the haematite to maghaematites and magnetites, both of which have

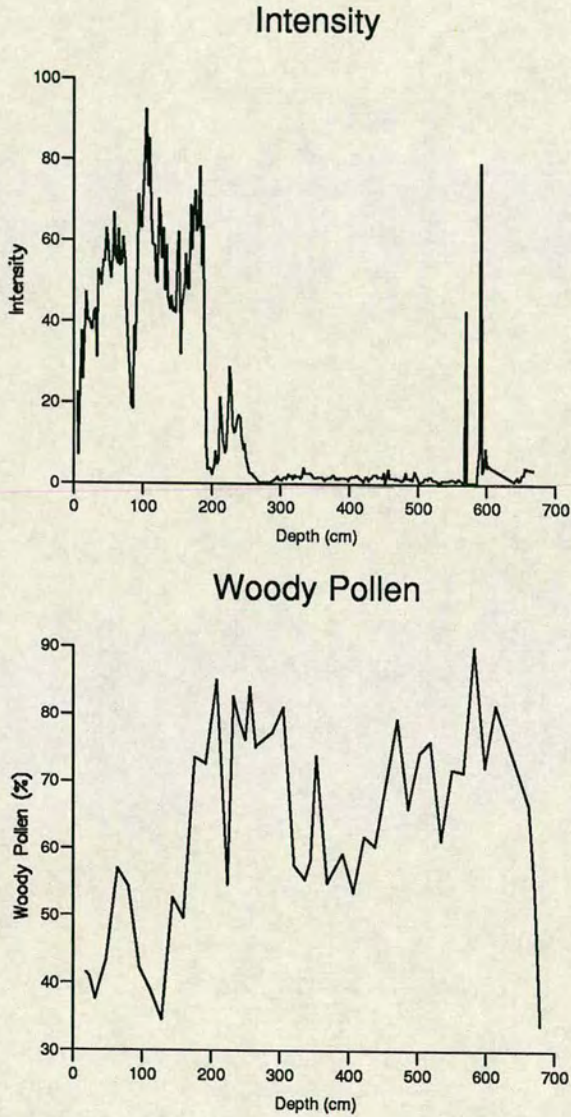


Figure 6.11. Comparison of the % woody pollen and NRM intensity of core 1, Martignano. It can be seen that the main intensity increases occur at the same depths as declines in the % of woody pollen.

much higher spontaneous magnetizations than haematite.

6.8 Conclusions

The sediments from Lago di Martignano carry a stable NRM. The results have been converted to a time scale and the PSV curve has been correlated with other West European records and can be considered as a preliminary Italian type curve. Future acquisition of more data from this lake and from other lakes in the region, and improving the timescale with more age control points are however desirable. Never the less in its present form it seems possible that the curve described here could be used to date other cores from the region, quickly and easily.

The major increase in intensity of the DRM is caused by mineral changes which appear to be related to a major burning event in the catchment area. This caused the conversion of haematite to magnetite and also increased the erosion of the top soils into the lake, as the tree cover in the catchment never recovered to the density that existed prior to 6000 years BP. It is very likely that this burning, which must have been continued over a number of years, which effected the palaeomagnetic and pollen records, is linked to the arrival of Neolithic man in Northern Italy.

This conclusion agrees well with Zohari's (1986) date of 6000 – 7000 years BP for the arrival of Neolithic man at coastal sites nearby.

Chapter 7

Modeling of the Palaeo-Geomagnetic Field

7.1 Introduction

The study of PSV from lake sediments allows the investigation of variations of the geomagnetic field with a period of a few thousands of years. However there are problems with the quality of lake sediment records such as the lack of spatial distribution of the records, the lack of time control on the sediments and possibly undetected systematic errors in the records derived.

Therefore it is not possible to apply methods of global analyses of the geomagnetic field that have been developed for observatory measurements, and historic measurements for the last century. But it should be possible to investigate some simple questions about the nature of the past magnetic field. Creer and Tucholka (1983a) consider a number of these problems such as:

- Are the spatial and temporal variations of the present geomagnetic field representative of the past field?
- What has been the relative importance of the dipole and non-dipole fields as sources of long period secular variation?
- It has been noted that it is convenient to separate the present non-dipole field into “standing” and “drifting” parts. Is it possible to carry out a similar separation for the past field?
- What is the typical lifetime for a non-dipole focus? Have any of these foci lasted long enough to pass under the same point several times as they have drifted?

One way to answer these questions is to examine the “PSV” curves generated by simple computer models. As was noted above it is possible to separate the non-dipole field into “standing” and “drifting” parts, the standing foci tend to wax and wane and the drifting foci tend to move westward through time (Creer, 1983). There is no unique way to model the distribution within the core of the sources of the Earth’s field. But one class of models which has been developed to model the field at various epochs consists of a set of dipoles situated in the core (e.g., Allredge and Hurwitz, 1964). Other types of model include the use of current loops on the inner/outer core boundary and the core/mantle boundary (e.g., Roy and Wagner, 1982), but mathematically there is little difference between the field produced by a dipole and a current loop (Allredge, 1980).

7.2 Modeling Theory

The simplest models discussed below superimpose a non-dipole field represented by assemblages of dipoles or current loops located at different latitudes and longitudes within the outer core, on the main field represented by the time-averaged geomagnetic dipole which is supposed to be axial and hence equated to g_1^0 (see appendix B). If necessary this representation of the dipole can be altered by adding an equatorial dipole (g_1^1 and h_1^1 the geocentric equatorial dipole, GED). The intensity of the GED relative to g_1^0 may also be varied.

7.2.1 Simple Drifting and Oscillating Dipole Models

Allredge and Hurwitz (1964) modeled the geomagnetic field for epochs 1945 and 1955 fields with eight deep seated ($r=1,750$ km) radial dipoles plus a central dipole. They achieved a very good fit. These radial dipoles are located below the fluid outer core, within the solid inner core, but could be taken to represent current loops located very much closer to the core-mantle boundary (Allredge, 1980). Creer and Tucholka (1982) studied the phase relationships of the declination and inclination SV which would be recorded at observation points located at different geographical positions around the latitude and longitude of these radial dipole locations.

The programs that I have developed for the dipole modeling (see Appendix A) are in general based upon the equations developed by Hurwitz (1960). Consider an eccentric dipole located at a distance r_0 from the centre of a spherical earth of radius a , with a colatitude θ_0 and an east longitude λ_0 . Let the components of its magnetic moment be M_r, M_θ and M_λ at a point (r, θ, λ) . Hurwitz calculated both closed and open formulae to describe the potential W_r, W_θ and W_λ at a point $P(r, \theta, \lambda)$. For the

closed form of the potential, the distance ρ from the dipole to P is:

$$\rho^2 = r^2 + r_0^2 - 2rr_0 [\cos \theta_0 \cos \theta + \sin \theta_0 \sin \theta \cos(\lambda - \lambda_0)] \quad (7.1)$$

The closed potentials can then be given as

$$W_r = M_r r [\cos \theta_0 \cos \theta + \sin \theta_0 \sin \theta \cos(\lambda - \lambda_0) - r_0/r] / \rho^3 \quad (7.2)$$

$$W_\theta = M_\theta r [-\sin \theta_0 \cos \theta + \cos \theta_0 \sin \theta \cos(\lambda - \lambda_0)] / \rho^3 \quad (7.3)$$

$$W_\lambda = M_\lambda r \sin \theta \sin(\lambda - \lambda_0) / \rho^3 \quad (7.4)$$

If $r > r_0$ these equations can be expressed in a more general form:-

$$a \sum_{n=0}^{\infty} \sum_{m=0}^{\infty} \left(\frac{a}{r}\right)^{n-1} (A_n^m \cos m\lambda + B_n^m \sin m\lambda) P_n^m(\cos \theta) \quad (7.5)$$

Hurwitz goes on to show that A_n^m and B_n^m for the three components are W_r :

$$A_n^m = \left(\frac{M_r}{a^3}\right) \left(\frac{r_0}{a}\right)^{n-1} n P_n^m(\cos \theta_0) \cos m\lambda_0 \quad (7.6)$$

$$B_n^m = A_n^m \tan m\lambda_0 \quad (7.7)$$

W_θ :

$$A_n^m = \left(\frac{M_\theta}{a^3}\right) \left(\frac{r_0}{a}\right)^{n-1} \left(\frac{dP_n^m(\cos \theta_0)}{d\theta_0}\right) \cos m\lambda_0 \quad (7.8)$$

$$B_n^m = A_n^m \tan m\lambda_0 \quad (7.9)$$

W_λ :

$$A_n^m = -\left(\frac{M_\lambda}{a^3}\right) \left(\frac{r_0}{a}\right)^{n-1} \left(\frac{m}{\sin \theta_0}\right) P_n^m(\cos \theta_0) \sin m\lambda_0 \quad (7.10)$$

$$B_n^m = -A_n^m \cot m\lambda_0 \quad (7.11)$$

These formulae allow the calculation of a series of spherical harmonic coefficients from a set of radial dipoles. Then maps of the geomagnetic field can be drawn for different moments of time, for specific positions and/or strengths of the radial dipoles. The

model has been tested using Model G of McFadden *et al* (1988) (see Section 7.2.4). The evolution of the directions of the field vector produced by the model at any observation point through time can be calculated to produce a synthetic SV curve.

7.2.2 Current Loop Models

A magnetic dipole is equivalent to an electric current loop with infinitesimal radius located at the same point. A circular current loop with finite radius located closer to the observer may be a more realistic type of elementary source for the geomagnetic field. Zidarov and Petrova (1974) fitted the annual mean data from 61 geomagnetic observatories with a model using a single current loop. Obviously this model was far too coarse to allow any study of secular variation on the same scale as this study. However they did note that whilst the magnetic moment of the loop remained constant over a period of time the current intensity and radius of the loop did not. Peddie (1979) derived eleven models using between one and seven current loops in each one. Using the assumption that the electrical conductivity of the Earth's outer core is believed to be extremely high ($\sim 5 \times 10^8 \text{ } \Omega\text{m}^{-1}$), skin effects in such a highly conductive material are often supposed to cause the secular variation of the geomagnetic field, due to the movement of electrical currents in this layer. Secular variations are also thought to be produced in this region of the outer core because if they occurred any deeper they would be screened by the outer layers of the core.

A comparison of current loop models and dipole models may be carried out by using a spherical harmonic analysis. Allredge (1980) developed the equations shown below for this analysis. A current loop maybe considered to be equivalent to a radially magnetized spherical cap bounded by the loop (Chapman and Bartels, 1940, p.15). A loop of radius R_0 located a distance r_0 from the centre of the Earth, would be equivalent to a cap centred at a distance $r_1 = (R_0^2 + r_0^2)^{1/2}$ (see figure 7.1). Each differential area dA is equivalent to a radial magnetic dipole of moment:

$$dM_r = I r_1^2 \sin \theta_1 d\theta_1 d\lambda_1 \quad (7.12)$$

where λ_1 is the longitude of the areal element (dA) of the spherical cap and the other terms are shown in Figure 7.1.

Hurwitz (1960) (c.f. Equation 7.5, Section 7.2.1) showed that this moment will produce a potential at P of

$$dW_r(r, \theta, \lambda) = a \sum_{n=0}^{\infty} \sum_{m=0}^{\infty} \left(\frac{a}{r}\right)^{n-1} (dg_n^m \cos m\lambda + dh_n^m \sin m\lambda) P_n^m(\cos \theta) \quad (7.13)$$

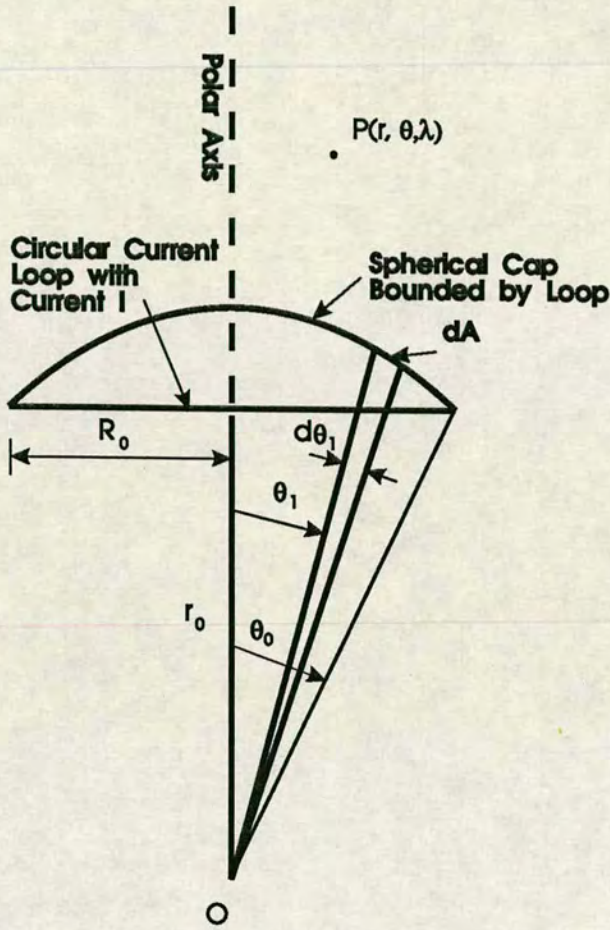


Figure 7.1. Projection of loop on a plane passing through the coordinate axis and its equivalent radially magnetized spherical cap, after Allredge 1980.

where a is the radius of the Earth and $r > a$,

$$dg_n^m = \frac{dM_r}{a^3} \left(\frac{r_1}{a}\right)^{n-1} n P_n^m(\cos \theta_1) \cos m \lambda_1 \quad (7.14)$$

$$dh_n^m = dg_n^m \tan m \lambda_1 \quad (7.15)$$

P_n^m are Schmidt-normalized associated Legendre functions (see Section 7.2.1) and dg_n^m and dh_n^m are differential spherical harmonic coefficients.

The total potential at $P(r, \theta, \lambda)$ is obtained by integrating equations 7.14 and 7.15

to give

$$g_n^m = \iint dg_n^m = I r_1^2 \frac{n}{a^3} \left(\frac{r_1}{a}\right)^{n-1} \int_{\theta_1=0}^{\theta_0} \int_{\lambda_1=0}^{2\pi} \cos m \lambda_1 d\lambda_1 P_n^m(\cos \theta_1) \sin \theta_1 d\theta_1 \quad (7.16)$$

The first term involving λ_1 is zero for $m > 0$ so that only zonal terms remain (again, see Section 7.2.1). From symmetry considerations it follows that $h_n^m = 0$. For $m = 0$ equation 7.16 becomes

$$g_n^0 = I \frac{n r_1^2}{a^3} \left(\frac{r_1}{a}\right)^{n-1} 2\pi \int_{\theta_1=0}^{\theta_0} P_n^0(\cos \theta_1) \sin \theta_1 d\theta_1 \quad (7.17)$$

Allredge (1980) shows that this can be solved as

$$[g_n^0]_l = \frac{2n}{\sin \theta_0} \left(\frac{r_1}{a}\right)^{n-1} \left(\frac{P_n^1(\cos \theta_0)}{\sqrt{2n(n+1)}}\right) \frac{M_r}{a^3} \quad (7.18)$$

where from equation 7.12

$$M_r = \pi r_1^2 \sin^2 \theta_0 I$$

Equation 7.18 can be compared with the same expression for a dipole from Hurwitz (1960) (c.f. Section 7.2.1)

$$[g_n^0]_d = n \left(\frac{r_0}{a}\right)^n - 1 \frac{M_r}{a^3} \quad (7.19)$$

7.2.3 Spherical Harmonic Models

Yukutake and Tachinaka (1968) developed a model separating the non-dipole field (NDF) into standing and drifting parts by analyzing the Gaussian coefficients of the field back to the 17th century. They defined the magnetic potential U as:

$$U = a \sum_{n=1}^{\infty} \sum_{m=0}^n U_n^m P_n^m(\cos \theta) \quad (7.20)$$

where U_n^m is given by:

$$U_n^m = F_n^m \cos(m\lambda + \varphi_n^m) + K_n^m \cos m\{\lambda + V_n^m(t - \tau_n^m)\} \quad (7.21)$$

where $P_n^m(\cos \theta)$ is Schmidt's semi-normalized spherical function (see Appendix B), and a is the mean radius of the Earth.

θ and λ are the colatitude and east longitude. F_n^m and φ_n^m are the amplitude and phase angle of the standing part of the field, and K_n^m and τ_n^m represent the amplitude

of the drifting part and its phase measured in the unit of time. V_n^m is the drift velocity measured in $0.01^\circ/\text{year}$ and t is time with its origin at 1800AD, defined by:

$$t = (T - 1800)/100 \quad (7.22)$$

where T is the epoch in the year AD.

Combining equation 7.20 with the standard representation of the potential (U) (equation B.7) in terms of the Gauss coefficients (g_n^m and h_n^m) gives:

$$g_n^m(t) = F_n^m \cos \varphi_n^m + K_n^m \cos mV_n^m(t - T_n^m) \quad (7.23)$$

$$-h_n^m(t) = F_n^m \sin \varphi_n^m + K_n^m \sin mV_n^m(t - T_n^m) \quad (7.24)$$

This allowed them to minimise the functions using a least squares fit to the available Gauss coefficients from historical studies. This then allowed the study of the relationship between the drifting and standing parts of the NDF through time. Unfortunately this approach requires that a spherical harmonic representation of the field is available. This can be achieved for epochs since the 17th century. But the paucity and non-uniform geographic distribution of palaeosecular variation (PSV) records for the period from 10,000 years BP does not allow a spherical harmonic analysis to be performed for earlier epochs through the Holocene. But if a much larger set of records, perhaps about 50, were recovered it would be possible to apply this method to them, so permitting a more secure division between drifting and standing sources in the NDF.

7.2.4 The McFadden, Merrill and McElhinny Model

Ideally, secular variation may be understood by observing sequential records for which the pattern of directions and intensities as they evolve through time may be seen. However circumstances arise where the order in time of a body of observations may not be known e.g. those originating from lava flows. Such bodies of data may however be usefully studied by calculations of the scatter of populations at locations.

McFadden *et al.* (1988) developed a model (Model G) which gives a good fit to both the present Earth field and also to palaeosecular variation data from lava flows over the past 5 million years. This model is based upon the angular dispersion of the palaeomagnetic field. Cox (1962) and Creer (1962a,b) showed that this dispersion is a function of (palaeo)latitude. The dispersion (or scatter) of the field can be calculated using

$$S^2 = (N - 1)^{-1} \sum_{i=1}^N (\Delta_i)^2 \quad (7.25)$$

where Δ_i is the angle between the i th virtual geomagnetic pole (VGP) position and the spin axis (which is given by Equation 7.26), and N is the number of VGP values used.

$$\tan \Delta = \frac{\sqrt{(-z \cdot \cos \lambda + 2 \cdot x \cdot \sin \lambda)^2 + (2 \cdot y)^2}}{-z \cdot \sin \lambda - 2 \cdot x \cdot \cos \lambda} \quad (7.26)$$

where x, y and z are the components of the magnetic field and $\lambda = (\pi - \theta)$.

For their analysis of the present (IGRF65) field the VGP was calculated at 10° longitude intervals around each line of latitude used. The results of this analysis (Figure 7.2) show an obvious asymmetry in S between the northern and southern hemispheres. McFadden *et al.* (1988) discuss how rotations of the spherical harmonics would

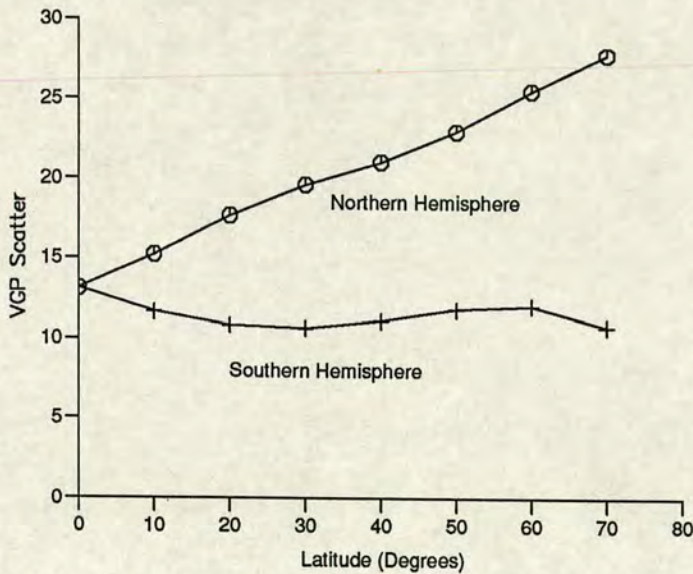


Figure 7.2. Latitudinal variation of VGP scatter calculated from IGRF65, after McFadden *et al.* (1988)

affect this asymmetry and conclude that over time an average of the two hemispheres would be a reasonable first-order approximation. They also show that palaeomagnetic data from the last 5 Myr gives a good fit to the present day field scatter.

Roberts and Stix (1972) have shown that it is possible to separate the magnetic field solutions for a spherical dynamo into two independent families, which they refer to as dipole and quadrupole. Under conditions of a mean velocity field symmetric about the equator together with the α -effect of dynamo theory which is antisymmetric with

respect to the equator. Spherical harmonic terms of degree n and order m belong to the dipole family if $(n - m)$ is odd and to the quadrupole family if $(n - m)$ is even. This separation can be seen for some of the low degree Gauss coefficients in Table 7.1

Table 7.1. Dipole and Quadrupole Families

	Dipole Family	Quadrupole Family
Dipole	g_1^0	g_1^1, h_1^1
Quadrupole	g_2^1, h_2^1	g_2^0 g_2^2, h_2^2
Octupole	g_3^0 g_3^2, h_3^2	g_3^1, h_3^1 g_3^3, h_3^3

Model G was developed by making use of this separation. Two synthetic fields, one created by taking g_1^0 and the remainder of the dipole family to give S_d , and the other by taking g_1^0 and the quadrupole family to give S_q , were analyzed. It was necessary to include g_1^0 in both families as the concept of a VGP requires a strong g_1^0 term. McFadden *et al.* (1988) showed that this method of analysis gives two independent components of the scatter (S), such that S is approximately the quadrature sum of S_d and S_q , i.e.

$$S^2 \approx S_d^2 + S_q^2 \tag{7.27}$$

Figure 7.3 shows the scatter from the two families. It is quite clear that the latitude dependence of scatter comes from the dipole family, while the scatter from the quadrupole family is latitude independent, with the entire scatter at the equator coming from the quadrupole family. Merrill and McFadden (1988) showed that these features appear to be a real property of the geomagnetic field rather than an artifact of the analysis technique. McFadden *et al.* (1988) used a least-squares technique to fit straight lines to this data, so that

$$S_d = A\lambda \tag{7.28}$$

where A is a constant and λ is latitude ($\lambda = \pi - \theta$) and

$$S_q = B \tag{7.29}$$

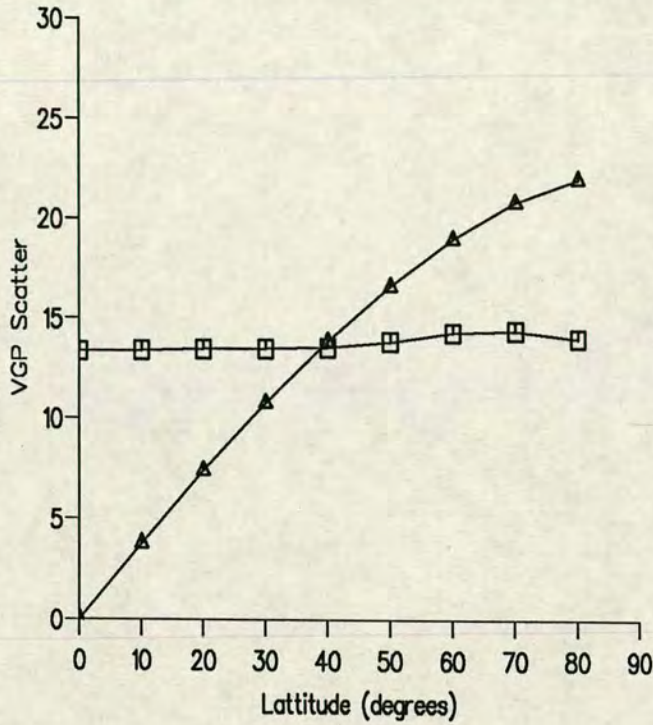


Figure 7.3. VGP scatter for IGRF65 separated into the contributions from the quadrupole and dipole families. The Quadrupole family scatter is shown by squares and the Dipole family is marked by triangles. After McFadden *et al.* (1988)

where B is simply a constant.

Thus from Equations 7.27, 7.28 and 7.29 model G can be expressed simply as:

$$S = \sqrt{A^2 \lambda^2 + B^2} \quad (7.30)$$

McFadden *et al.*'s analysis of IGRF65 gives $A = 0.21 \pm 0.01$ and $B = 13.6^\circ \pm 0.3^\circ$. They also carried out a similar analysis on PSV data from lava flows and hence determined $A = 0.23 \pm 0.6$ and $B = 12.8^\circ \pm 0.6^\circ$. They therefore concluded that there is no significant difference between the present field and that of the past 5 Myr.

Although McFadden *et al* analyze the magnetic field only for the present epoch and for the average over the last 5 Myr, the same method can be applied over periods of thousands of years. Once a dipole model has been constructed and tuned to fit a PSV curve from a particular lake or lakes, a series of spherical harmonics may be constructed from the dipole model, using the equations of Hurwitz (1960). These harmonics could

Preparation of the Data

Palaeosecular variation records from five lakes (see figure 7.4 for locations) were used as basis for this modeling work. The object was to deal only with the larger scale features of the palaeosecular variation record so it was decided to smooth all the records using an eight knot cubic spline, so removing any shorter period variations. These processed records are illustrated in figures 7.5 to 7.9.

The next stage in the construction of a model was to examine each record to distinguish the characteristics of its PSV record. This was done by comparison with Creer's (1983) models of the shapes of secular variation recorded at a site for various types of dipole. Creer noted three types of dipole variation:

1. Precession of the main dipole. This he simulated by allowing the equatorial dipole component to rotate with a uniform angular velocity. The characteristics of this type of SV are that the declination and inclination oscillations are out of phase by $T/4$. (Creer defined T as the period of the dipole motions).
2. Drifting radial dipoles of fixed moment. Yukutake and Tachinaka (1969) showed that their calculations of the drifting part of the NDF had a quadrupolar symmetry. This can be modeled by four radial dipoles located in the mid latitudes and separated by roughly 180° of longitude. The main features of this SV record were that the shape of the declination features is flat topped and that the shapes of the inclination features are pointed with larger amplitude minima than maxima.
3. Oscillating or pulsating dipoles fixed in position. These two types of dipole differ only in that an oscillating source will produce an anomaly that changes sign periodically while a pulsating source will merely grow and decay in magnitude. This can be simply modeled as a radial dipole with an oscillating part of intensity m_1 and a steady bias intensity m_2 , where $m_1 < m_2$. The SV curve for an oscillating dipole exhibits the following characteristics: the declination anomalies are rounded and the inclination maxima are flattened but the minima are of larger amplitude and are pointed.

The Models

Each of the five records was studied and a comparison was made to the example curves Creer (1983) produced.

The first thing noted was that in most of the lakes the declination record was more detailed than the inclination record. Therefore more effort was made to match the declination record with the model at each site. It was also noted that the change in



Figure 7.4. Location of the five sites used for the world modeling of the palaeosecular variations

then be split into dipole and quadrupole families and an analysis of the scatter of the field at periods through time carried out. This has been done here, and a test of Model G has been made using synthetic data which fits the behavior of the Earth's magnetic field over the last 10,000 years.

7.3 Results of Modeling

Introduction

Five lake records (figure 7.4) were available for use as the basis of the modeling, three from the northern hemisphere, one from the southern and one from close to the equator. For most types of modeling this would be too small a data set to allow any useful models to be obtained. For this reason it was decided to make use of the Allredge and Hurwitz (1964) equations for a series of eccentric dipoles (see section 7.2.1). The use of this style of model allows the time series nature of the records to be utilised, as the time varying part of the field is modeled at each site. If the assumption is made that the secular variations at each site are correlated in some way to those at other sites then the variation through time can be modeled from a set of dipoles which either oscillate or drift.

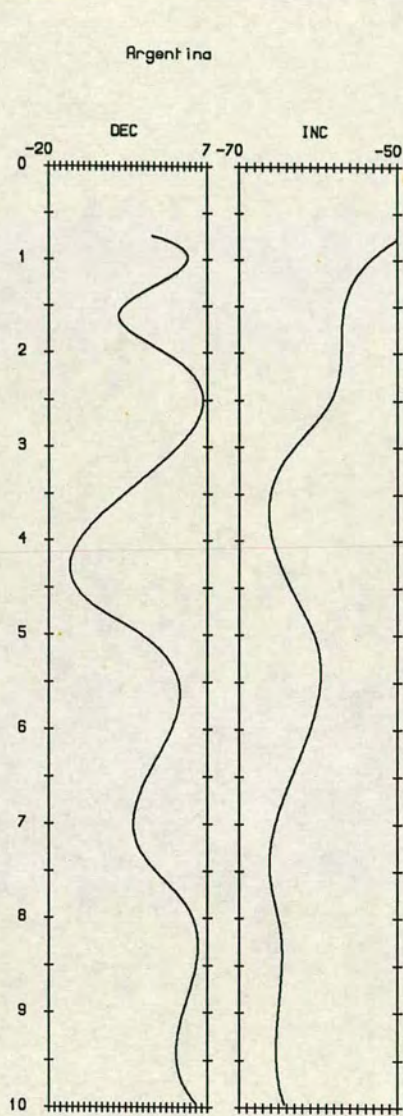


Figure 7.5. PSV record from Lake Moreno, Argentina, after smoothing using an eight knot cubic spline (Creer *et al* 1983). Declination and inclination are measured in degrees.

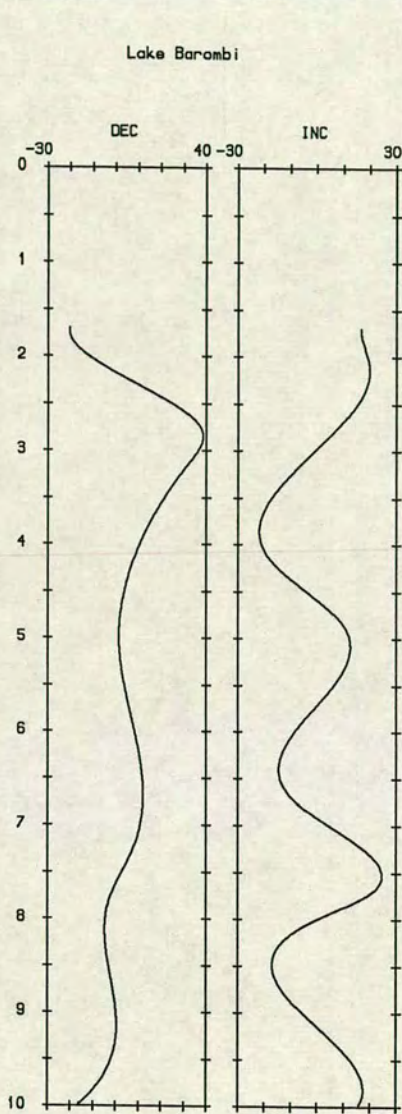


Figure 7.6. PSV record from Lake Barombi, Cameron, after smoothing using an eight knot cubic spline (Thouveny and Williamson, 1988). Declination and inclination are measured in degrees.

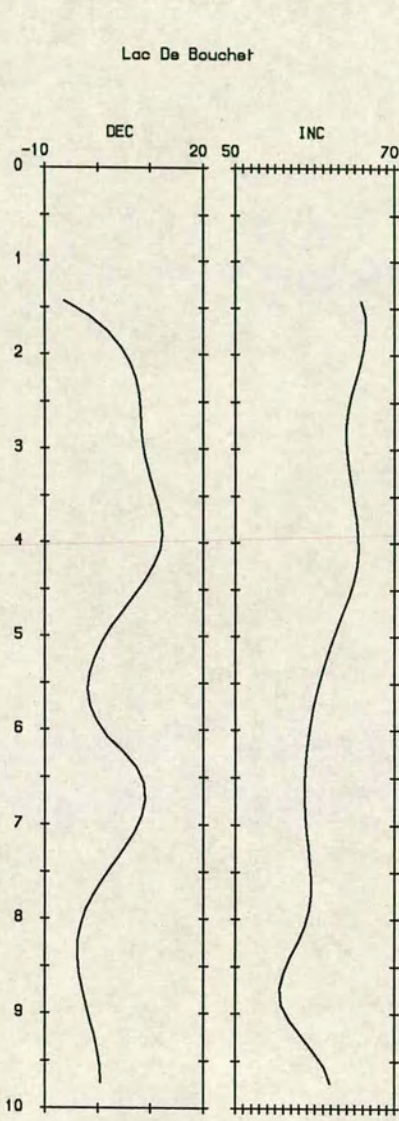


Figure 7.7. PSV record from Lac du Bouchet, France, after smoothing using an eight knot cubic spline (Smith, 1985). Declination and inclination are measured in degrees.

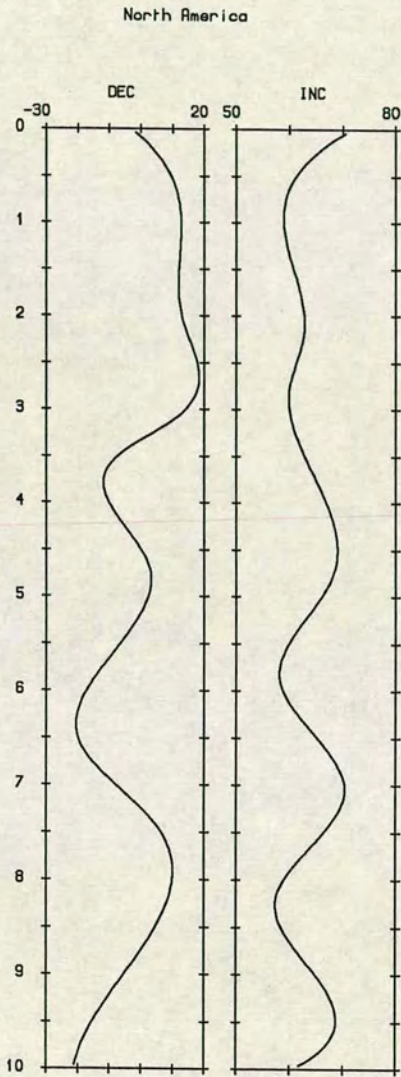


Figure 7.8. PSV record from the Great Lakes Region, North America, after smoothing using an eight knot cubic spline (Creer and Tucholka, 1982). Declination and inclination are measured in degrees.

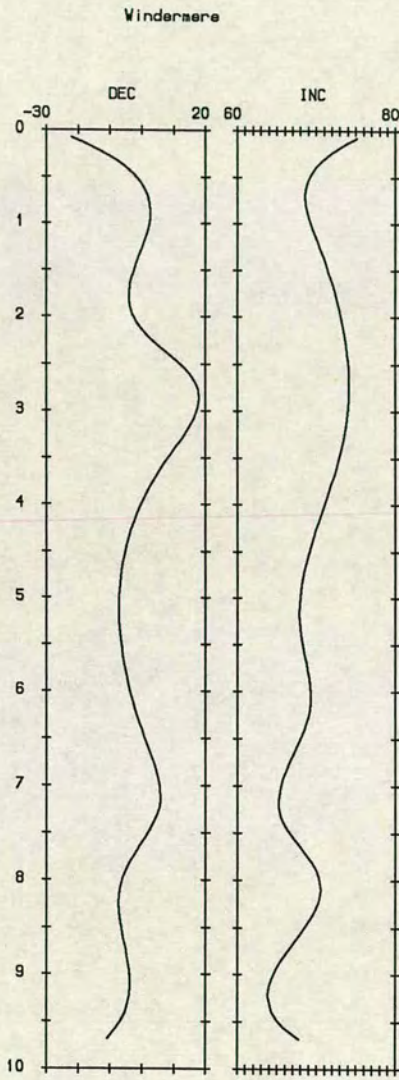


Figure 7.9. PSV record from Lake Windermere, Britain, after smoothing using an eight knot cubic spline (Turner and Thompson, 1981). Declination and inclination are measured in degrees.

secular variation which occurred at about 4,500 years BP, which was first noted by Creer and Tucholka (1982), appears to be present in all five of the records. Hence two separate models were developed, one for the upper part of the record and a second for the lower part.

One obvious feature of this study was the presence of the characteristic declination feature associated with two drifting radial dipoles, which can be seen in the upper parts of the Lac du Bouchet (figure 7.7) and the North American (figure 7.8) records. The onset of this feature occurs ~ 1200 years later in the North American record, indicating a westward drift of $\sim 0.08^\circ/\text{yr}$; however the length of the feature indicates a speed of $\sim 0.05^\circ/\text{yr}$.

Table 7.2 summarises the other features seen in the two parts of the five records.

Table 7.2. The main features seen in the five lake records studied

Upper Part		
Lake	Type of Feature	Period (years)
Argentina	oscillating	~ 2000
Barombi	GED	~ 3000
Bouchet	2RD	~ 3500
N.America	2RD	~ 3500
Windermere	2RD (?)	~ 3500
Lower Part		
Argentina	oscillating	~ 2500
Barombi	oscillating	~ 2500
Bouchet	oscillating	~ 2500
N.America	oscillating	~ 3500
Windermere	oscillating	~ 2000

The model was developed on a lake by lake basis, with an acceptable model being developed for first one lake and then another, and constant reference being made to the earlier lakes to check that modifications to the model had not effected the previous fit too much.

For the upper part of the model, the two drifting radial dipoles ($45^\circ\text{N}, 90^\circ\text{E}$ and $45^\circ\text{N}, 270^\circ\text{E}$) were fitted to the Lac du Bouchet and North American records first with a drift speed of $0.05^\circ/\text{yr}$ westward. Then an oscillating dipole located at $45^\circ\text{N}, 105^\circ\text{E}$, was added, possibly corresponding to the Mongolian anomaly identified by Yukutake and Tachinaka (1968) in their study of the foci of the non-dipole field. The addition of this dipole was necessary to improve the model at Windermere.

A drifting dipole was added to fit the record at Barombi, with an initial position of

Table 7.3. Drifting part of model for last 5,000 years

Colatitude (°)	Longitude (°)	Drift Speed (°/yr)	Radius (Km)	Intensity (m/M)
45.0	90.0	-0.05	2000	0.09
45.0	270.0	-0.05	2000	-0.09
90.0	40.0	-0.10	1750	0.16

Table 7.4. Oscillating part of model for last 5,000 years

Colatitude (°)	Longitude (°)	Period (years)	Phase (years)	Radius (Km)	Intensity (m/M)
45.0	105.0	2000	-1000	1750	0.16
131.0	0.0	3000	1000	2000	0.16

0°N, 40°E, with a westward drift of 0.10°/yr. This corresponds to the African anomaly noted by Yukutake and Tachinaka.

Finally an oscillating source was added for Argentina at 41°S, 0°E. This does not correspond to any of the sources identified by Yukutake and Tachinaka. But as it is the only record in the southern hemisphere the model is less well constrained here, and Yukutake and Tachinaka's data set for the southern hemisphere was also of poorer quality than in the north.

The final model for the upper part of the records is summarised in tables 7.3 and 7.4.

The lower parts of the records were modeled in the same manner though there was less direct interaction between the model at different sites because no drifting sources were identified. The second part of the model is shown in table 7.5.

In the northern hemisphere the two drifting dipoles have been replaced by a pair of oscillating sources in the same position and three more oscillating sources have been added in the mid-latitudes. A single oscillating source replaces the drifting equatorial dipole, again in a similar position. The oscillating source in the southern hemisphere has moved slightly east (5°) from the previous model.

To produce the final models shown in figures 7.10 to 7.14 the secular variation pattern at each location was calculated for each model and the two models were joined together at 4,500 years BP. The directional logs resulting from this process were then smoothed using an eight knot cubic spline to remove the discontinuities between the two sections, and to make the resultant record directly more comparable to the original data.

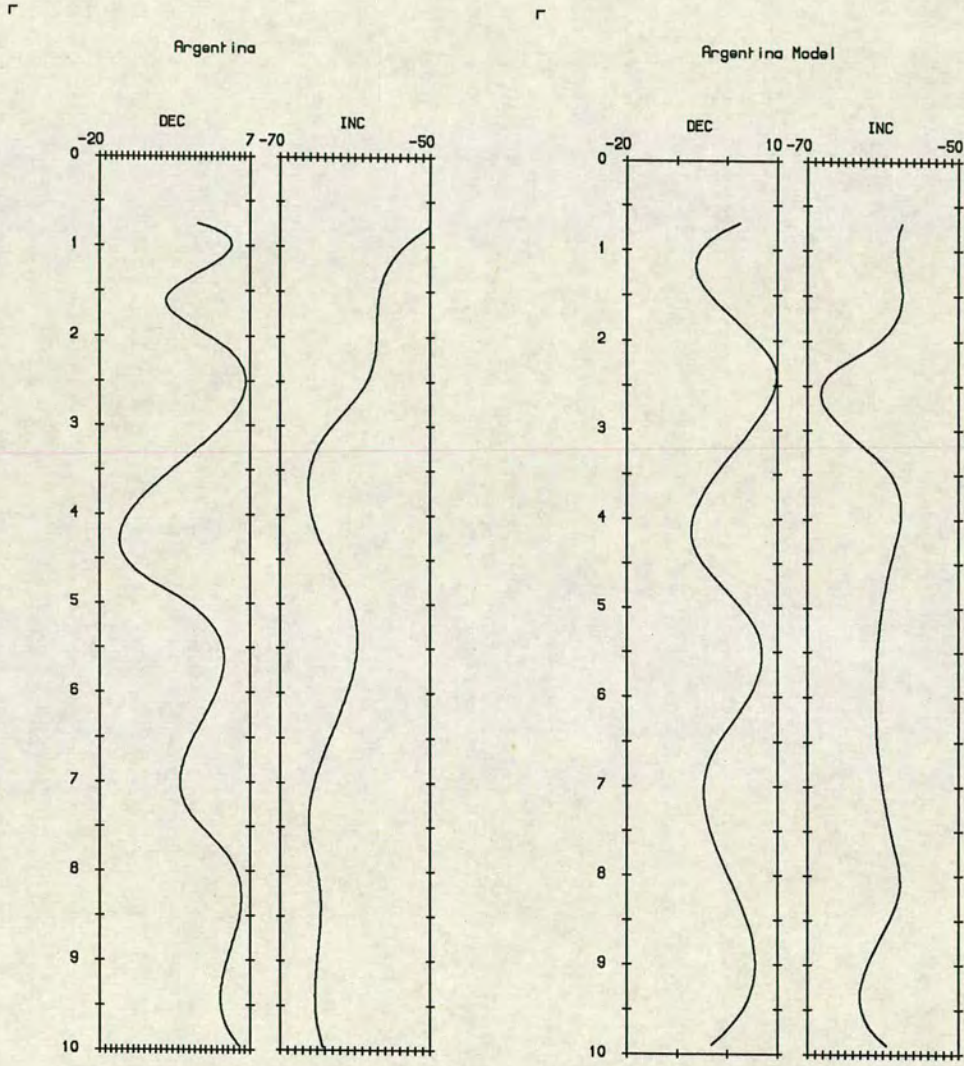


Figure 7.10. The final dipole source model for Lake Moreno. Declination and inclination are measured in degrees.

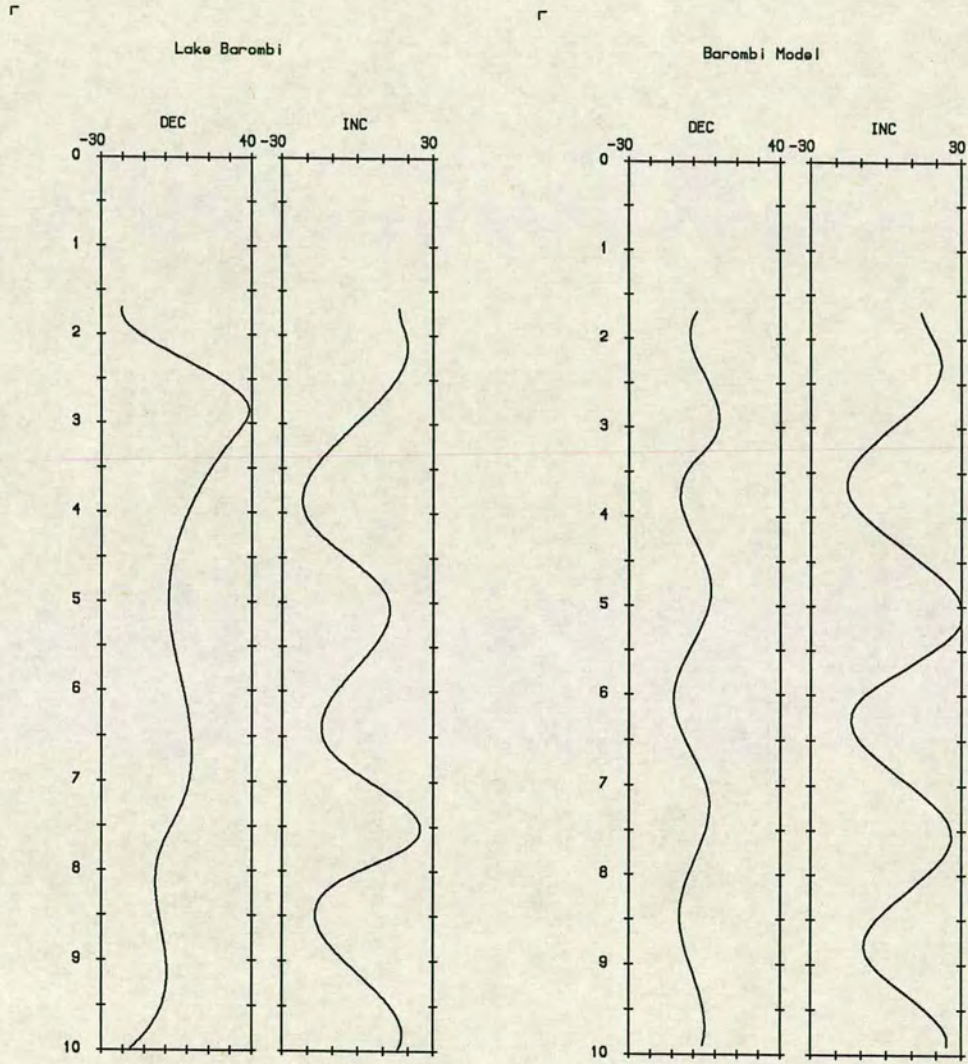


Figure 7.11. The final dipole source model for Lake Barombi. Declination and inclination are measured in degrees.

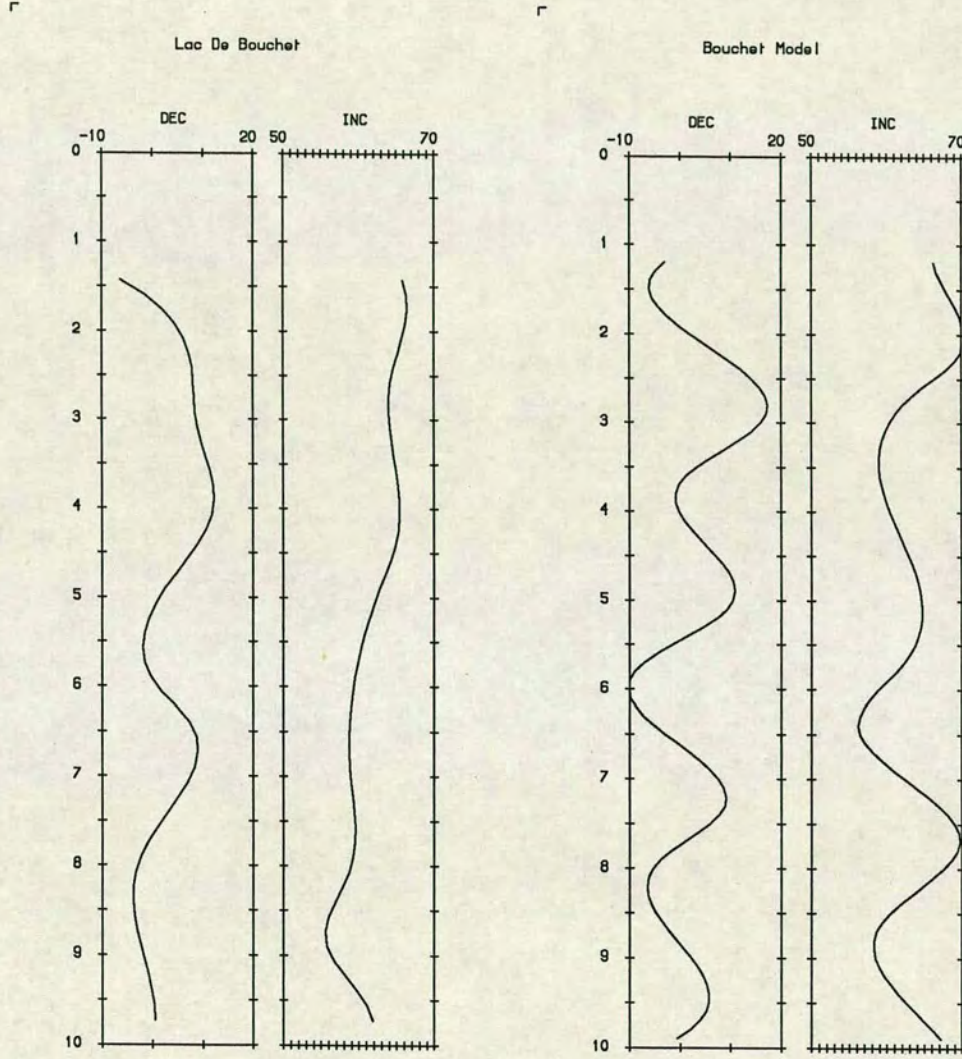


Figure 7.12. The final dipole source model for Lac du Bouchet. Declination and inclination are measured in degrees.

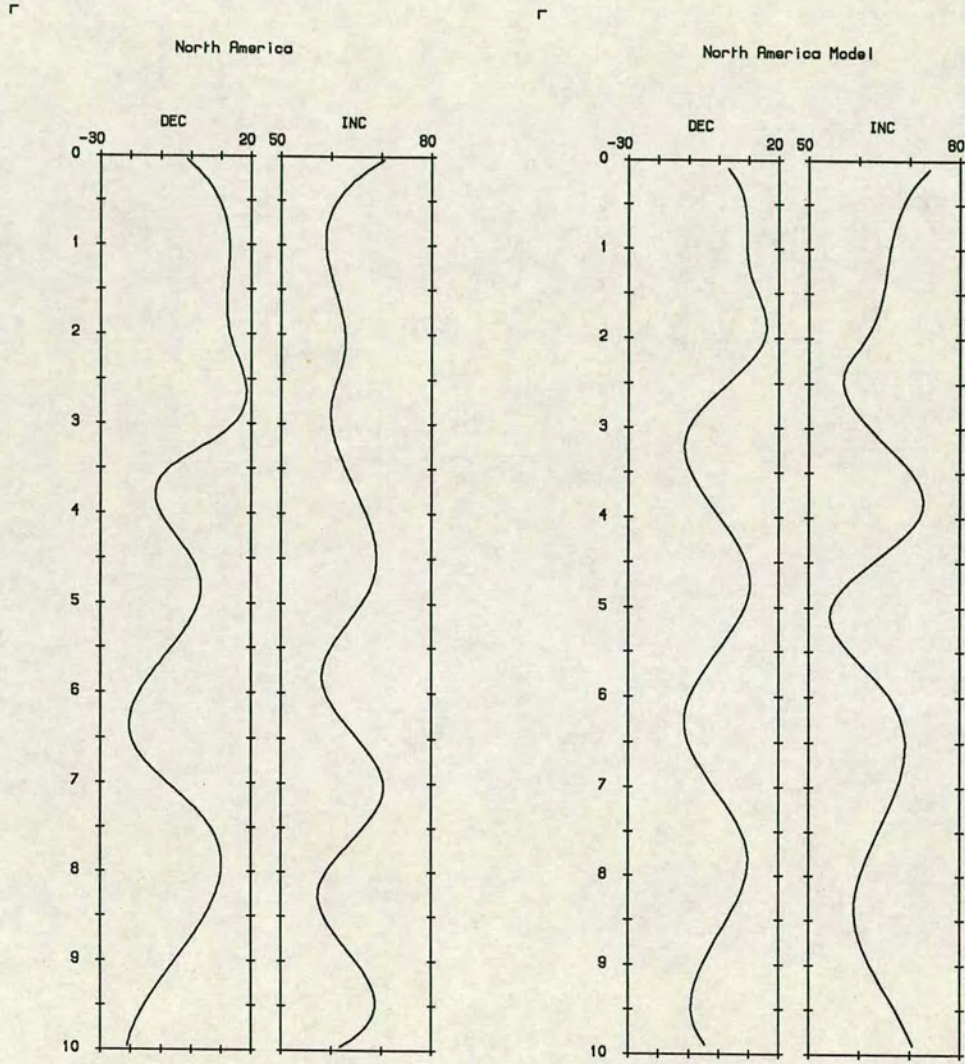


Figure 7.13. The final dipole source model for North America. Declination and inclination are measured in degrees.

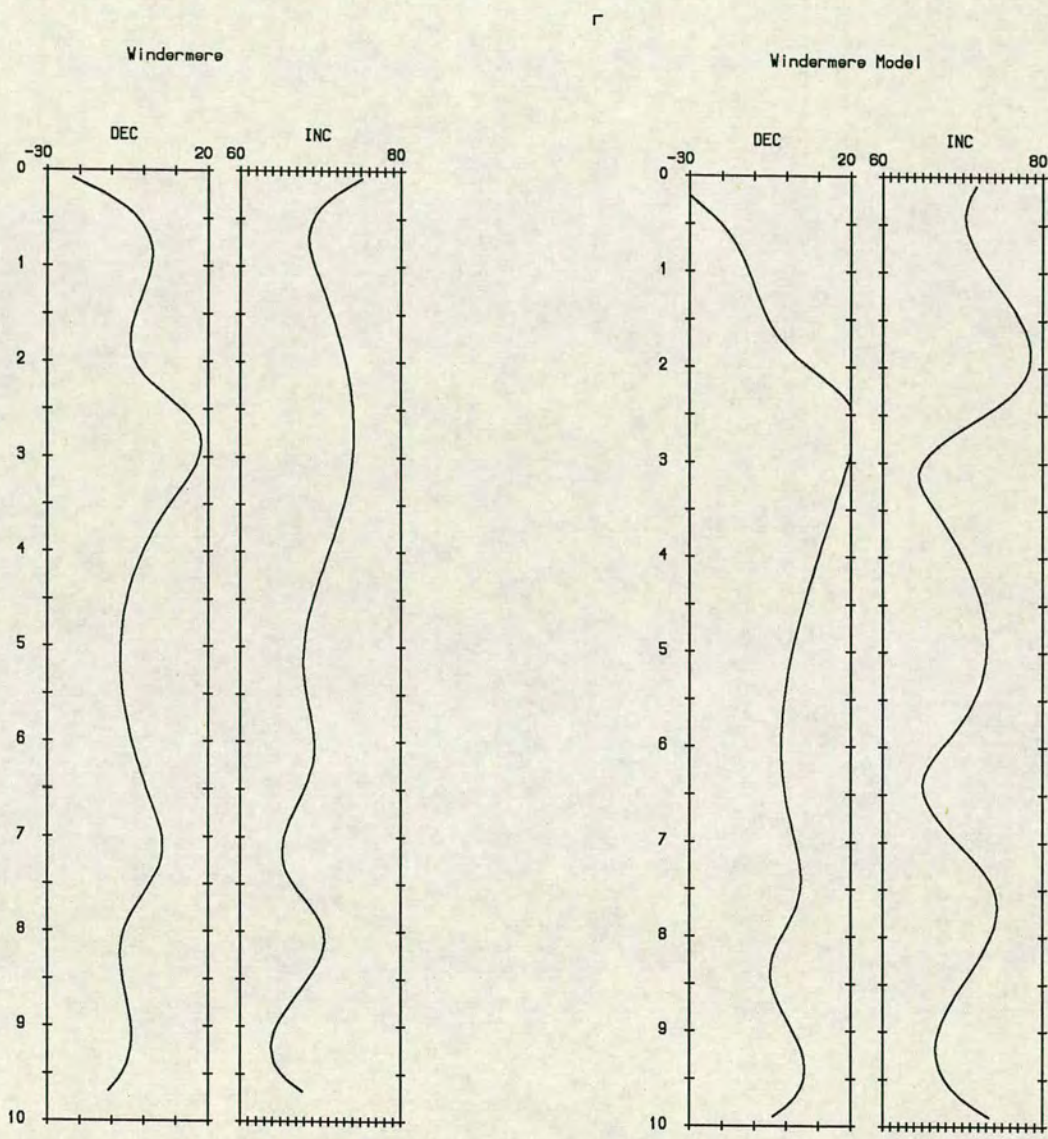


Figure 7.14. The final dipole source model for Lake Windermere. Declination and inclination are measured in degrees.

Table 7.5. Oscillating part of model for 10,000 to 5,000 years BP

Colatitude (°)	Longitude (°)	Period (years)	Phase (years)	Radius (Km)	Intensity (m/M)
45.0	105.0	2000	-1000	1000	0.09
45.0	265.0	3000	0	1000	0.09
50.0	80.0	2500	0	1750	0.09
65.0	200.0	3200	1000	2000	0.16
55.0	270.0	3000	900	2000	0.14
90.0	20.0	2500	1000	2000	0.14
131.0	5.0	3000	1000	2000	0.16

The final step was to compare the model results to the original data sets. A correlation coefficient (ρ) was calculated for the declination and inclination record at each site, with the results of the model. These coefficients are shown in table 7.6.

Correlation coefficients were calculated using the standard formula:

$$\rho = \frac{\sum_{i=1}^N (\Delta X_i \Delta Y_i)}{\sqrt{\sum_{i=1}^N (\Delta X_i)^2 \sum_{i=1}^N (\Delta Y_i)^2}} \quad (7.31)$$

where $\Delta X_i = X_i - \bar{X}$ and $\Delta Y_i = Y_i - \bar{Y}$. ρ can vary from -1 for an exact negative correlation to $+1$ for an exact correlation. The significance of ρ can be tested against Student's t -distribution. To determine the significance of the correlation coefficients it was necessary to estimate the number of degrees of freedom. Each dipole in the model has 5 or 6 degrees of freedom (colatitude, longitude, drift speed or period and phase, distance from the centre of the Earth and intensity) and each of the original records has ~ 7 degrees of freedom, giving an average of 40 degrees of freedom for these correlation calculations. Hence for a 95% significance level at 40 degrees of freedom ρ must be ≥ 0.3044 (Fisher, 1990).

In all the lakes, except Barombi, the correlation of the declination record to the model is better than the inclination record. As was discussed above the declination record in general has better definition than the inclination record, with the exception of Barombi.

Therefore it can be seen from table 7.6 that all of the declination records are significantly correlated, and all of the inclination records except Argentina and Windermere are significantly correlated. The only really poor correlation is the inclination record of Argentina. This is mostly a result of the fact that there is only one record from the southern hemisphere, to reflect this I have used only one source in the southern

Table 7.6. Correlation coefficients of the model and the lake data

Lake		Correlation Coefficient (ρ)
Argentina	dec	0.698
Argentina	inc	-0.045
Barombi	dec	0.321
Barombi	inc	0.890
Bouchet	dec	0.461
Bouchet	inc	0.335
North America	dec	0.693
North America	inc	0.310
Windermere	dec	0.650
Windermere	inc	0.218
Average		0.45

hemisphere. It would have been quite possible to have placed more dipoles around the southern hemisphere to improve the fit of the model at Argentina, however there would have been no physical justification for these dipoles.

7.4 Test of Model G

Once the final model had been completed the spherical harmonic coefficients that described the field were calculated at 1000 year intervals going back in time. Then for each of these data sets the scatter of the field at sites around the globe were calculated for the total field and for the dipole and quadrupole families discussed in section 7.2.4.

Sample results of this analysis can be seen in figure 7.15. Comparison of this figure with figure 7.3 shows that it appears that Model G does fit the magnetic field as recorded in lake sediments over the last 10,000 years. The average values for $A = .24 \pm .7$ and $B = 11^\circ \pm 1.1^\circ$, which agree with the values found by McFadden *et al* (1988).

7.5 Conclusions and Discussion

The first conclusion drawn from this modeling is that non-dipole field (NDF) features do appear to be long lived, certainly on the order of 4500 years. It can also be noted that the secular variation records from at least the northern hemisphere, indicate that there is a definite change in the nature of the NDF approximately 4500 years ago, this is supported by the results of the modeling.

This model also shows that it is valid to describe the NDF in terms of “standing”

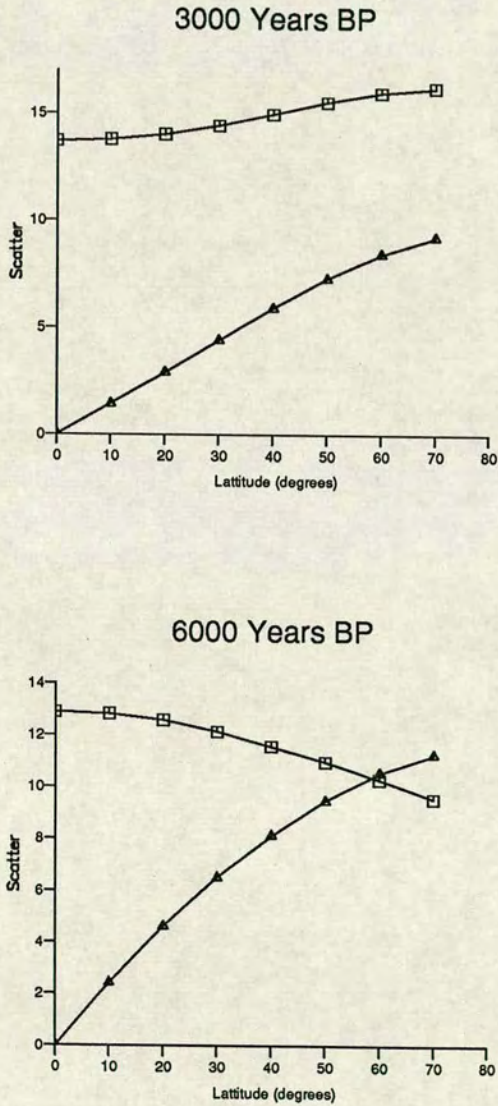


Figure 7.15. Sample results of applying Model G to the synthetic data produced by the model

and “drifting” sources, in the past 4500 years, but it seems that in the preceding 5500 years that this division is less important.

Chapter 8

Conclusions

8.1 Introduction

The results of the research described in this thesis are summarised under two headings:-

1. the acquisition of new data, viz the palaeosecular variation records recovered from Lago di Monticchio and Lago di Martignano, Italy, and their comparison with other records from Europe;
2. the modeling of palaeosecular variations of the Holocene geomagnetic field, with a collection of eccentric radial dipoles.

8.2 Palaeosecular Variations in Italy and Europe

The stable NRM present in the sediments recovered from both of the Italian lakes has been studied to give a secular variation curve for Lago di Martignano which relates well with other secular variation curves from northern Europe so that the features found are a regional feature of the geomagnetic field during the Holocene rather than from effects particular to the local catchment area resulting from, for instance, sedimentation.

The records for Lago di Monticchio have not yet been used to construct a PSV curve because there are as yet no reliable age controls.

Palaeointensities have been calculated for all the samples from core D, by normalizing with susceptibility, ARM and SIRM to correct for variations in the quantities of magnetic minerals down-core, and a long wavelength signal is visually apparent.

A first attempt to date core D from Lago di Monticchio was made by correlating the variation of susceptibility taken to provide a proxy climate indicator with the marine oxygen isotope record (Imbrie *et al.*, 1984). This method has great potential

for application to work on long sediment cores because susceptibility can be measured much more rapidly than direct dating by conventional methods such as palynology. The base of core D is thus tentatively dated as at 250 Kyr.

Spectral analysis of the palaeointensities shows that energy is concentrated at four periods, 119 Kyr, 42 Kyr, 21 Kyr and 19 Kyr. All of these periods are associated with astronomical frequencies, namely the eccentricity of the Earth's orbit (e), obliquity of the ecliptic ($\Delta\xi$) and precession of the equinoxes (P). Milankovitch argued that these cycles affect the climate of the earth by modulating the incoming solar insolation. Berger (1988) has recently calculated these periods more precisely. Previous workers (e.g. Wollin *et al*, 1978, Kent and Opdyke, 1977) suggested that these periods appear to be present in the geodynamo, though others have dismissed these reports as being solely due to ineffective normalization of climatic effects on the intensity record (e.g. Kent, 1982).

It has been shown that the the extremes of the climatic variations in the core studied, as recorded by susceptibility, are ~ 35 Kyr out of phase with the maxima and minima of the palaeointensity record, so it seems possible that the geodynamo is directly modulated by the astronomical frequencies. Wollin *et al* (1978) proposed that changes in the eccentricity and precession of the equinoxes could effect the efficiency of the dynamo by increasing turbulence in the core as a result of the difference in ellipticity of the core and the mantle, as first suggested by Malkus (1963,1968).

Investigation of the large increase in intensity of magnetization found in the sediments of Lago di Martignano has lead to the conclusion that the catchment area of the lake was cleared for agriculture by Neolithic man approximately 6000 yr BP. The burning of the forest in the catchment has effected both the palaeomagnetic record and shows as a depletion of tree pollen in the pollen record.

8.3 Geomagnetic Field Modeling, from Palaeosecular variations

In Chapter 7 a method of modeling the geomagnetic field over the last 10 Kyr was developed using the very limited dataset of available palaeosecular variation curves from around the world. Radial dipoles either free to drift along lines of longitude, or to oscillate in intensity were fitted to a secular variation curve observed for each site, potentially allowing a spherical harmonic analysis to be performed on the resultant field at any time covered by the model.

The model can be judged to be successful by the high correlations at 95% significance found with the original data. Though the results for the southern hemisphere

where only one data set was available for study are less certain.

The spherical harmonic coefficients so generated from the model were used to test Model G of McFadden *et al* (1988), it was found that the modeled results fitted Model G well. Therefore it can be concluded that Model G is valid for the past 10 Kyr.

Appendix A

Computer Programs

A.1 Palaeomagnetic Data Handling

A.1.1 Introduction

A number of programs were written to simplify the data handling required by a project of this size, using a UNIX system, which has influenced the style of the programs, most having been designed to read from the standard input (usually the keyboard, but quite possibly a file) and to write to standard output (again usually the screen, but sometimes a file). The programs are able to act as “filters” so that the data can be placed in a “pipeline” passing the output of one program to the input of the next program.

A.1.2 Data Entry

Some data have to be entered into the computer from the keyboard, e.g. the depths and weights of the cubes and any measurements made on the Molspin magnetometer such as the ARM's and SIRM's. The following programs were written to make this task easier.

DEPTHS prompts the user for the first cube number and depth and then "guesses" how deep the next cube is, if this guess is correct then the user need only type "return" or they can type the correct depth of the next sample.

DEPTHS

```

/* depth to stdout (this should be redirected to a file). Guesses the */
/* depth of the next cube to save time                               */

#include<stdio.h>
#include<math.h>

main(){

    int last_cube,this_cube;
    float this_depth, last_depth;
    char depth[8];

    fprintf(stderr,"first cube no: "); /* write to stderr since stdout */
    fflush(stderr);                    /* will be a file                */
    gets(depth);                       /* read the cube number */
    this_cube=atoi(depth);
    fprintf(stderr,"depth of first cube");
    fflush(stderr);
    gets(depth);
    this_depth=atof(depth);

    while(this_depth != -1.0){
        /* repeat this loop until the depth is -1 */
        last_cube=this_cube;
        last_depth=this_depth;
        printf("%d\t%f\n",last_cube,last_depth);
        /* write the last sample number */
        /* and cube number to the file */
        fflush(stdout);
        this_depth += 2.25;
        /* guess the depth of the next cube, this depth+2.25 */
        this_cube++; /* increment the cube number */
        fprintf(stderr,"cube %d ( %6.2f) ",this_cube,this_depth);
        fflush(stderr); /* prompt the user with the guess */
        gets(depth);
    }
}

```

```

        if(strlen(depth)!=0) this_depth=atof(depth);
        /* check if the guess is right, ie is depth 0 char long? */
    }
    return(0);
}

```

The next program **WEIGHTS**, deals with all other data entered from the keyboard, such as weights, susceptibilities etc. It is basically a simplified version of **DEPTHS** which does not guess the next value to be input.

WEIGHTS

```

/* weights.c - read from stdin a list of data prompting by sample number  */
/* output is written to stdout which should almost certainly be a file  */

#include<stdio.h>
#include<math.h>

main(){

    int last_cube,this_cube;
    float this_weight, last_weight;
    char weight[8];

    fprintf(stderr,"first cube no: ");
    /* write to stderr, since stdout is a file */
    fflush(stderr);
    gets(weight);
    this_cube=atoi(weight);
    fprintf(stderr,"weight of first cube");
    fflush(stderr);
    gets(weight);
    this_weight=atof(weight);

    while(this_weight != -1.0){
        /* read data until the value given is -1 */
        last_cube=this_cube;
        last_weight=this_weight;
        printf("%d\t%f\n",last_cube,last_weight);
        /* write output to stdout */
    }
}

```

```

        fflush(stdout);
        this_cube++; /* increment sample number */
        fprintf(stderr,"cube %d ",this_cube);
        /* prompt with next sample number */
        fflush(stderr);
        gets(weight);
        this_weight=atof(weight);
    }
    return(0);
}

```

The next program deals with data obtained in files from the cryogenic magnetometer which contain a lot of information which is unnecessary for lake sediment palaeomagnetism, such as geographic and sedimentary corrections to the declination and inclination. A sample of such a file is shown below:

```

[identifier - sample lake]
rock 11790.000A lgmd30          .00   .00   .0   .0   .0 7.3   .0
90.0   2.25   alternate
[
      geographic stratigraphic
]
[ sample number   dec   inc dec   inc   vgp   intensity error]
rock 1790.000A   2.3 233.7 -51.6 233.7 -51.6 -30.1 -128.1 1.57E-05 .05
[demag date   time   ]
10 04/09/91 10:22:16
rock 1790.000A   2.3 232.7 -50.4 232.7 -50.4 -31.3 -127.2 1.13E-05 .04
20 04/09/91 10:24:01
rock 1790.000A   2.3 232.2 -51.5 232.2 -51.5 -31.2 -128.5 8.20E-06 .03
30 04/09/91 10:26:16

```

Therefore the following **AWK** program was written to split the raw data files down into a file for each demagnetization step. **AWK** is a pattern matching language, written by Aho, Kernigan and Weinberger (1988), which has a similar syntax to the C programming language.

The program is normally run on a PC to reduce the amount of data transferred to the mainframe computer for later processing. During this project it was run using **GNU AWK**, an implementation for the PC carried out by the Free Software Foundation, however **AWK** is a standard part of any UNIX distribution so this program could be run under any UNIX operating system.

The program is run by typing

AWK -F GET.AWK FILENAME.DAT

GET.AWK

```

BEGIN{ n=split(ARGV[1],file,".") # get the base of the input file name
#
#           ie d30 if the input file is d30.dat
    outf=file[1]".0";printf("") > outf;
    outf=file[1]".5";printf("") > outf;
    outf=file[1]".10";printf("") > outf;
    outf=file[1]".20";printf("") > outf;
    outf=file[1]".30";printf("") > outf; }
#
# the above lines create or truncate the files required
# for output
#
{if(($12==0)||($12==10)||($12==20)||($12==30)||($12==5))\
# check the demag step is one required $12 indicates the 12th column
  {outf = file[1]".$12
    n1=split($2,samp,".") # remove .000a from the sample number
    printf("%s\t%7.3f\t%7.3f\t%10.5f\n"
      ,samp[1],360-$4,-$5,$10*1000000)>>outf}}
#
# the final line outputs the data: samp[1] is the sample number, $4 is the
# declination, moved into the correct coordinate system, $5 is the inclination
# similarly corrected, $10 is the intensity (times a 10e6 to convert from
# emu/cm3 to mA/m ) this is written to the relevant output file for that demag
# step

```

A.1.3 Data Processing

To ease the processing of the cores the data were stored in a simple file for each section in a different directory depending on the contents of the file. Figure A.1 shows the structure which is assumed by several of the following programs.

To automate the processing of the data as much as possible the UNIX utility **MAKE** was used. This utility takes a set of rules describing how a file is created and applies them. These rules are held in a file (**makefile**), once this file is correctly constructed the data can be processed by simply typing **make**. A sample **makefile** is shown here:

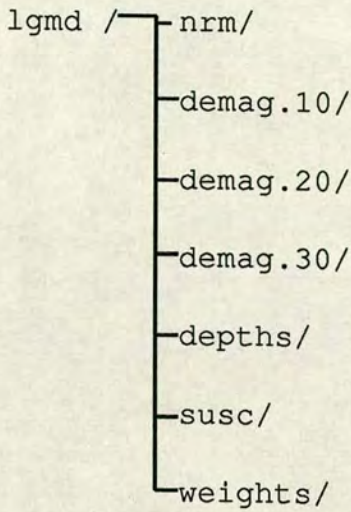


Figure A.1. The Directory Structure used to hold the Data Files for a Core

```

.SUFFIXES: .0 .tot .weit .cor .logi .susc .arm
.0.tot: ; joint ../depths/$.dep $.0 > $.tot
.tot.weit: ; wjoin $*
.weit.cor: ; mean <$.weit >$.cor
.cor.logi: ; logit <$.cor >$.logi
.cor.susc: ; suscit $*
.susc.arm: ; ajoin $*

```

```

all:d01o.cor d01u.cor d02o.cor d02u.cor d03o.cor d03u.cor d04o.cor d04u.cor
d05o.cor d06o.cor d06u.cor d07o.cor d07u.cor d08o.cor d08u.cor d09o.cor
d09u.cor d10o.cor d10u.cor d11u.cor d12o.cor d12u.cor d13o.cor d13u.cor
d14o.cor d14u.cor d15o.cor d15u.cor d16o.cor d16u.cor d17o.cor d17u.cor
d18.cor d19.cor d20.cor d21.cor d22.cor d23o.cor d23u.cor d24o.cor d24u.cor
d25o.cor d25u.cor d26o.cor d26u.cor d27.cor d28.cor d29o.cor d29u.cor d30.cor

```

Since the makefile for each core will be similar the program **MAKEMAKE** was written, this program creates a makefile based on the files found in the directory and then creates the necessary intermediary files.

MAKEMAKE

```

#!/bin/sh

#file for creating makefiles for data preparation
#
#usage makemake suffix > makefile
#
#first of all the headers needed

name=$1
cat << END
.SUFFIXES: .$name .tot .weit .cor .logi .susc
.$name.tot: ; joint ../depths/\$*.dep \$*.$name > \$*.tot
.tot.weit: ; wjoin \$*
.weit.cor: ; mean <\$*.weit >\$*.cor
.cor.logi: ; logit <\$*.cor >\$*.logi
.cor.susc: ; suscit \$*
.susc.arm: ; ajoin \$*
END

echo
#then set up all: for all .dat files in the dir
m='/bin/ls *.$name | sed 's/\.'$name'/.cor/'
echo 'all:$m'
#and finally the rules for the directory
echo
/bin/ls *.$name | sed 's/\(.*\.)'$name'/\1cor:\1'$name'/'

m='/bin/ls *.$name '
set $m
for i in $*
do
i='basename $i $name'
cat > ${i}cor </dev/null
cat > ${i}tot </dev/null
cat > ${i}weit </dev/null
cat > ${i}logi </dev/null
cat > ${i}susc </dev/null
cat > ${i}arm </dev/null

```

```
touch ${i}$name
done
# feed all of this in to makefile,
# you may need to edit it a little but not much
```

MAKE calls certain programs for each file that it needs to make. A file is recreated if it is older than a file that it depends on, for example in the above **makefile** if **d30.0** had been modified since **d30.cor** then **MAKE** would run **JOINT** to make **d30.tot**, then **WJOIN** to give **d30.weit**, then **MEAN** to produce **d30.cor**.

All the programs called are simple shell scripts, which use either the Bourne shell or C shell to run in.

JOINT

```
#!/bin/sh
#$1 is depth file $2 nrm file
sort +0 $1 >/tmp/tmp1.$$
sort +0 $2 >/tmp/tmp2.$$

#use the Unix utility SORT to order the 2 input files $1 and $2

join /tmp/tmp1.$$ /tmp/tmp2.$$ |sort -n

# use the Unix utility JOIN to join the 2 sorted files, and then numerically
# sort the output

/bin/rm /tmp/tmp1.$$ /tmp/tmp2.$$

#remove the temporary files when finished
```

WJOIN

```
#!/bin/csh

if ( -r ../weights/$1.wei ) then

# check that a weights file exists to match the .tot file
```

```
joint $1.tot ../weights/$1.wei >! $1.weit

# call joint to join the two files

else

# otherwise just copy the .tot file to .cor

cp $1.tot $1.weit
endif
```

MEAN

```
#!/bin/sh

cat > /tmp/mean1.$$
#read the stinput to a temporary file

m='awk '{s += $3} END {print s/NR}' /tmp/mean1.$$'
#
# call awk to calculate the mean of the declination ($3) and store the
# result in m

# then call awk to subtract the mean from each sample's declination

awk '{s=$3-$m'      # subtract the mean declination from the dec
  if ($6) w=$5/$6   # if there is a weight or susceptibility in column 6
    else w = $6     # divide the intensity by it
printf "%d %7.2f\t%7.2f\t%5.2f\t%f\t%f\t%f\t%f\n"
  ,$1,$2,s,$4,$5,w,$6}' /tmp/mean1.$$

/bin/rm /tmp/mean1.$$
# remove the temporary file
```

LOGIT

```
#!/bin/sh
```

```
awk '{$5=log($5);print($0)}'
# simply call awk to calculate the log of the intensity ($5)
# for each line of the input and print the entire input ($0)
```

SUSCIT

```
#!/bin/csh
if ( -r ../susc/$1.sus ) then
# check there is a susceptibility file
# and then call JOINT to join the 2 files
joint $1.cor ../susc/$1.sus >! $1.susc
else
cp $1.cor $1.susc
# otherwise just copy .cor to .susc
endif
```

AJJOIN

```
#!/bin/csh

if ( -r ../arm/$1.arm ) then
# if an arm file exists then join it to the susc file
# using JOINT
joint $1.susc ../arm/$1.arm >! $1.arm
endif
```

Once make has been run all that remains is to concatenate the individual sections together, this can be done using the UNIX utility **CAT**, for example

```
cat *.cor > lgmd.dat
```

This file can then be passed through a the filter **LINUP** to produce formatted output suitable for G. Smith's (1985) program **COREPLOT**, once a header and format line have been inserted with an editor.

LINEUP

```

        program lineup

20    read (*,*,end=30) i,f1,f2,f3,f4,f5
c     read stdin until end of file is reached
        write (*,10) i,f1,f2,f3,f4,f5
c     write to stdout with a fixed format
        goto 20
10    format (i4,' ',5(f15.4,1x))
30    end

```

One final program is included in this suite of data processing utilities **SCALE** which reads a file and produces the scale file needed in **COREPLOT**. The usage is `scale [-h] [up to five column names]`.

```

SCALE
#!/bin/sh

# make analysis of cores automatic and create scale file for coreplot

#copy file from stdin
cat >/tmp/scale.$$

i=$1
if test "$i" = "-h"
then
    shift
fi
# is the file an alltype? ie -h set
(case $i in
-h) tail +4 /tmp/scale.$$ ;; # yes so ignore the first 3 lines
*) cat /tmp/scale.$$ ;;
# now call awk to calculate the max and min of each column
esac) awk ' BEGIN{ decmin=incmin=intmin=susmin=weimin=9999999;
    decmax=incmax=intmax=susmax=weimax=-999999;}
    {if(decmin>$2) decmin=$2;
    if(decmax<$2) decmax=$2;
    if(incmin>$3) incmin=$3;
    if(incmax<$3) incmax=$3;
    if(intmin>$4) intmin=$4;
    if(intmax<$4) intmax=$4;

```

```

    if(susmin>$5) susmin=$5;
    if(susmax<$5) susmax=$5;
    if(weimin>$6) weimin=$6;
    if(weimax<$6) weimax=$6;}
END { # finally round the limits up and down
if (decmin<0)
{
    if(decmin < -100) SCMIN=100;
    if(decmin < -10 && decmin >= -100) SCMIN = 10;
    if(decmin < 0 && decmin >= -10) SCMIN =1;
}
else
{
    if(decmin > 100) SCMIN=100;
    if(decmin > 10 && decmin <= 100) SCMIN = 10;
    if(decmin > 0 && decmin <= 10) SCMIN =1;
}

    if(decmax > 100) SCMAX=100;
    if(decmax > 10 && decmax <= 100) SCMAX = 10;
    if(decmax > 0 && decmax <= 10) SCMAX =1;

    decmin=int((decmin-SCMIN)/SCMIN)*SCMIN;
    decmax=int((decmax+SCMAX)/SCMAX)*SCMAX;

    if(incmin > 100) SCMIN=100;
    if(incmin > 10 && incmin<= 100) SCMIN = 10;
    if(incmin > 0 && incmin <= 10) SCMIN =1;

    if(incmax > 100) SCMAX=100;
    if(incmax > 10 && incmax <= 100) SCMAX = 10;
    if(incmax > 0 && incmax <= 10) SCMAX =1;

    incmin=int((incmin-SCMIN)/SCMIN)*SCMIN;
    incmax=int((incmax+SCMAX)/SCMAX)*SCMAX;

    if(intmin > 100) SCMIN=100;
    if(intmin > 10 && intmin <= 100) SCMIN = 10;
    if(intmin > 0 && intmin <= 10) SCMIN =1;

    if(intmax > 100) SCMAX=100;

```

```

if(intmax > 10 && intmax <= 100) SCMAX = 10;
if(intmax > 0 && intmax <= 10) SCMAX =1;

intmin=int((intmin-SCMIN)/SCMIN)*SCMIN;
intmax=int((intmax+SCMAX)/SCMAX)*SCMAX;

if(susmin > 100) SCMIN=100;
if(susmin > 10 && susmin<= 100) SCMIN = 10;
if(susmin > 0 && susmin <= 10) SCMIN =1;

if(susmax > 100) SCMAX=100;
if(susmax > 10 && susmax <= 100) SCMAX = 10;
if(susmax > 0 && susmax <= 10) SCMAX =1;

susmin=int((susmin-SCMIN)/SCMIN)*SCMIN;
susmax=int((susmax+SCMAX)/SCMAX)*SCMAX;

if(weimin > 100) SCMIN=100;
if(weimin > 10 && weimin<= 100) SCMIN = 10;
if(weimin > 0 && weimin <= 10) SCMIN =1;

if(weimax > 100) SCMAX=100;
if(weimax > 10 && weimax <= 100) SCMAX = 10;
if(weimax > 0 && weimax <= 10) SCMAX =1;

weimin=int((weimin-SCMIN)/SCMIN)*SCMIN;
weimax=int((weimax+SCMAX)/SCMAX)*SCMAX;

if(susmax==susmin) susmax++;
if(weimax==weimin) weimax++;

# and then print the output to stdout

print ("3rd floorJCMB");
print ("3.0 5.0 1");
printf("%6.1f%6.1f 'echo ${1-DEC}' '\n",decmin,decmax);
printf("%6.1f%6.1f 'echo ${2-INC}' '\n",incmin,incmax);
printf("%6.1f%6.1f 'echo ${3-INT}' '\n",intmin,intmax);
printf("%6.1f%6.1f 'echo ${4-WEI}' '\n",susmin,susmax);
printf("%6.1f%6.1f 'echo ${5-SUS}' '\n",weimin,weimax);
}'

```

```
/bin/rm /tmp/scale.$$  
# tidy up after ourselves
```

A.2 Modeling Programs

A.2.1 Introduction

As with the data processing programs above these modeling programs were written to run on a UNIX system. Hence a majority are written in C, making use of the easy of modular program design and command line handling abilities of this language. These features combined with the UNIX shell language and tool philosophy allow the construction of simple programs to carry out repetitive programming tasks quickly and efficiently.

A.2.2 Dipole Models

The dipole models can be split into two groups the drifting and the oscillating models, the programs to handle these two groups are very similar.

A.2.3 Single Site Models

To model secular variation at a single site for a set of oscillating or drifting dipoles two programs were written **OSCIDIPOLE** and **DRIFT**. These programs are essentially the same, the differences being in the output routines. They read a series of dipole parameters from the standard input and output declination, inclination and intensity from the present to 10,000 years BP. These functions are calculated using simple arithmetic formulae.

All the programs dealing with dipole modeling use the same format to handle the data associated with each dipole which is declared in a header file **DIPOLE.H** This file is included in each program and defines a structure **DIPOLE** which contains the individual values for each dipole and a pointer to the next element in the structure, or a null pointer if it is the last in the list.

```
DIPLES.H
```

```
struct dipole {int no;  
               double lat;  
               double dlong;  
               double mom;
```

```

double radius;
double phase;
double period;
double x,y,z;
struct dipole *next=0;};

```

```

#define ERAD 6370.0 /* earth radius */
#define sqr(x) ((x)*(x))
#define driftspeed phase

```

The dipoles are read one to a line by the subroutine `read_d.c` which allocates memory to the structure as required for each new dipole and moves the pointer to the end of the list each time.

READ_D.C

```

#include <stdio.h>
#include "dipole.h"

read_d(head,tail)
struct dipole **head,**tail;
{
    struct dipole *new;
    new = (struct dipole *)malloc(sizeof(struct dipole));
    if (!new) {
        printf("NO SPACE FOR MORE DIPOLES");
        return;
    }
    if (!*tail) {
        new->no=1; /* its the first dipole */
        *head=new;
    } /* set head of list to first dipole */
    else
    {
        new->no=(*tail)->no +1;
        (*tail)->next= new;
    } /* join the list */
    new->next=0; /* mark end of list */
    *tail = new; /* move pointer to end of list */
    scanf("%lf%lf%lf%lf%lf%lf",&new->lat,&new->dlong,&new->period,
        &new->phase,&new->mom,&new->radius);
        /* read variables from stdin */

```

```

    return;
}

```

DRIFT then calls **DRIFTOUT.C** which calculates the declination, inclination and intensity at the site latitude and longitude (slat & slong) through time, and then prints the output on the standard output.

DRIFTOUT.C

```

#include <math.h>
#include <stdio.h>
#include "dipole.h"

driftout(head,cx,cz,slong,slat)
/* write list of dec,inc,int thru time to stdout */
float cx,cz,slat,slong;
struct dipole *head;
{
    float xx,yy,zz,inc,ynt,dec;
    float pi;
    int j,t;
    struct dipole *ptr;

    pi=4*atan(1.);
    ptr=head;

    for(j=1;j<=200;j++){ /*time in hundreds of years */
        t=j*100; /* time in years */
        xx=yy=zz=0.;
        head=ptr; /* reset start of list */
        drifting(head,t);
        calc(head,slong,slat);
        while (head){
            xx += head->x;
            yy += head->y;
            zz += head->z;

            head=head->next;
        }
        ynt = sqrt(sqrt(cx+xx)+sqrt(yy)+sqrt(cz+zz));
        dec = (atan2(yy,(cx+xx)))/pi*180;
        inc = (atan2((cz+zz),sqrt(sqrt(yy)+sqrt(xx+cx))))/pi*180;
    }
}

```

```

        printf (" %5d %10.3f %10.3f %10.4f\n",t/10,dec,inc,ynt);
    }

    return;
}

```

This calls the subroutine **DRIFTING.C** to perform the calculation of the movement of the dipoles. There is no variable assigned to store the drift speed but a define statement in **DIPOLE.H** assigns this to phase, since a dipole can not drift and oscillate.

DRIFTING.C

```

#include <math.h>
#include "dipole.h"

void drifting(head,time)
struct dipole *head;
int time;
{
    float pi=4*atan(1.0);
    while (head){
        head->dlong -= (100*(head->driftspeed));
        /* positive drift is westward but dlong is eastward */
        if( head->dlong > 2*pi ) head->dlong -= 2*pi;
        if( head->dlong < -2*pi ) head->dlong += 2*pi;
        /* check if dipole has passed 0 in either direction */
        head=head->next; /* next dipole in list */
    }
    return;
}

```

OUTPUT.C performs an identical function in **OSCDIPOLE.C** the only difference being that the phase and frequency of the dipoles is used to calculate the changes through time within the subroutine.

OUTPUT.C

```

#include <math.h>
#include <stdio.h>

```

```

#include "dipole.h"

output(head,cx,cz) /* write list of dec,inc,int thru time to stdout */
float cx,cz;
struct dipole * head;
{
    float xx,yy,zz,inc,ynt,dec;
    float pi;
    int j,t;
    struct dipole * ptr;

    pi=4*atan(1.);
    ptr=head;

    for(j=1;j<=100;j++){ /*time in hundreds of years */
        t=j*100; /* time in years */
        xx=yy=zz=0.;
        head=ptr; /* reset start of list */
        while (head){
            xx += head->x*sin(pi*2*t/head->period+head->phase);
            yy += head->y*sin(pi*2*t/head->period+head->phase);
            zz += head->z*sin(pi*2*t/head->period+head->phase);

            head=head->next;
        }
        ynt = sqrt(sqr(cx+xx)+sqr(yy)+sqr(cz+zz));
        dec = (atan2(yy,(cx+xx)))/pi*180;
        inc = (atan2((cz+zz),sqrt(sqr(yy)+sqr(xx+cx))))/pi*180;

        printf (" %5d %10.3f %10.3f %10.4f\n",t/10,dec,inc,ynt);
    }

    return;
}

```

Finally the output of these two programs could be passed through **COREPREP.C** which writes a header and format statement on to the top of the file to make it compatible with G. Smith's (1985) program **COREPLOT**.

COREPREP.C

```

#include <stdio.h>

/* This program converts simple time,dec,inc,int files into the 6 column
   files required by coreplot, It takes an optional header at the command line
   which results in a header, FORTRAN format statement and integer number
   being appended to the file's head, this is for compatibility with the
   existing version of coreplot on emas. */

main(argc,argv)
int argc;
char **argv;
{
    float f,f1,f2,f3;

    if (argc>1) { /* is there a header line? */

        printf("%s\n",argv[1]);
        printf("(f8.1,2(1x,f10.3),1x,f12.8,2(1x,f3.1))\n");
        printf("1000\n");
    }

    while (scanf("%f %f %f %f",&f,&f1,&f2,&f3) != EOF){
        printf (" %8.1f %10.3f %10.3f %12.8f 0.0 0.0\n",f,f1,f2,f3);
    } /* simply echo the input lines to the output with a format */

    return;
}

```

To allow the calculation of site curves for groups of both drifting and oscillating dipoles the shell script **OSCDRIFT** was written. This requires that the oscillating and drifting dipoles be stored in files with the same basename and the suffixes .osc and .dri.

```

OSCDRIFT

#!/bin/sh

# take two input files $1.osc and $1.dri and produce their output

```

```

# through time ready for coreprep

o='wc -l $1.osc| awk '{print $1}'' # find the length of the input files
o='expr $o - 2'
d='wc -l $1.dri| awk '{print $1}''
d='expr $d - 2'

driftxyz $d < $1.dri >/tmp/drift.dat & # calculate x,y & z components
oscxyz $o <$1.osc >/tmp/osc.dat & # for the drifting and oscillating dipoles
wait # wait for both the above to finish
joint /tmp/drift.dat /tmp/osc.dat |odsum

/bin/rm /tmp/drift.dat /tmp/osc.dat
# clean up the tmp files

```

The two programs called to calculate the components **DRIFTXYZ** and **OSCXZY** are identical to **DRIFT** and **OSCDIPOLE** described above except that x,y & z are output instead of declination, inclination and intensity. The program **JOINT** is described on page 115 (section A.1.3). **ODSUM** simply sums the x,y & z values for each time horizon and outputs them to the standard output.

ODSUM.C

```

#include<stdio.h>
#include<math.h>

main(){

    float x,y,z;
    float t,x1,x2,y1,y2,z1,z2,dec,inc,ynt;
    float pi=4*atan(1.);
    char line[80];

    while(gets(line)!=NULL){ /* until the end of the file */
        sscanf (line,"%f %f %f %f %f %f %f",
                &t,&x1,&y1,&z1,&x2,&y2,&z2);
/* read the input lines */
        x= (x1+x2)/2;
        y=(y1+y2)/2;

```

```

        z=(z1+z2)/2;
/* average the x,y & z values from each group */
        dec= (atan2(y,x))/pi*180;
        inc= (atan2(z,sqrt(x*x+y*y)))/pi*180;
        ynt= sqrt(x*x+y*y+z*z);
/* calculate the dec,inc & int for each time */
        printf("%5.0f %f %f %f \n",t,dec,inc,ynt);
    }

    return(0);
}

```

A.2.4 World Models

These programs are designed to expand a group of dipoles into a spherical harmonic description of the magnetic field for the whole of the Earth's surface. This is achieved by using Hurwitz's (1960) equations for eccentric dipoles. The centre of the analysis is the program **HARMONICS.C** which reads a series of dipoles (using **READ_D.C**) and then calls **HARMOUT.C** which calculates the spherical harmonics from the dipoles given.

HARMOUT.C

```

#include <stdio.h>
#include <math.h>
#include "dipole.h"
#define NPOLY 120

conv();
schmidt();

harmout(head)
struct dipole *head;
{
    int i,j,l=180,k,np=NPOLY,n,m;
    double slat=0,slong=0,p[NPOLY],q[NPOLY],pi,v;
    double colat,a[NPOLY],b[NPOLY],power,tmp;

    pi=4*atan(1.0);
    conv(&slat,&slong,head); /* convert degrees to radians */
    while(head){ /* for each dipole */

```

```

schmidt(head->lat,p,q,np); /* get schmidt normalized
                                coefficients */
n=m=0;
for (k=1;k<NPOLY;k++){
    if (m>n) {
        m=0;
        n++;
    }
    if ((n-1)==0) power=1;
        /* work around bug in c pow function */
    else power= pow((double)(head->radius),(double)
                                (n-1));
    tmp= (head->mom)*power* n * p[k] *
                                cos((double)m*(head->dlong));
    a[k] += tmp;
    b[k] += tmp * tan((double)m* (head->dlong));
    m++;
}
head = head->next; /* get next dipole */
}
n=0;
m=1;
for(k=2;k<np;k++){
    a[k] *=100000;
    b[k] *=100000;
    if(m>n){
        m=0;
        n++;
    }
    printf ("%d %d %10.4lf %10.4lf\n",n,m,a[k],b[k]);
    m++; /* increment m */
}
return;
}

```

The subroutine SCHMIDT.C calculates the Schmidt normalized coefficients P and Q for a coordinate system based on the direction of the dipole.

SCHMIDT.C

```
#include <stdio.h>
```

```

#include <math.h>
#include "dipole.h"

/* Based on a fortran program written by R.Hipkin */

schmidt(colat,p,q,np) /*colat in rad,arrays p and q, number of
                      polynomials to be calculated */
float colat;
int np;
double p[],q[];
{
    int m=1,n=0,k,nsub1,m2,index,index1,index2;
    double fact,fact1,fact2;
    double costheta,sintheta;

    p[1]= 1.0;
    sintheta=p[3]= sin(colat);
    q[1]=0.0;
    costheta=q[3]= cos(colat);

    for(k=2;k<np;k++){
        if (m>n) {
            m=0; /* begin new degree */
            nsub1=n;
            n=n+1;
        }
        if (k!=3){ /* sectorial harmonics */
            if (m==n){ /* sectorial harmonics */
                fact=sqrt((double)(1.0-0.5/n));
                index=k-n-1;
                p[k]=fact*sintheta*p[index];
                q[k]=fact*(sintheta*q[index]+
                           costheta*p[index]);
            }
            else
            { /*non sectorial harmonics */
                m2= sqr(m);
                fact = sqrt((double)(n*n-m2));
                fact1 =(n+nsub1)/fact;
                fact2= sqrt((double) (nsub1*nsub1 - m2))/fact;
                index1=k-n;
                index2=index1-n+1;
            }
        }
    }
}

```

```

        p[k] = fact1 * costheta *p[index1]
                -fact2*p[index2];
        q[k]= fact1*(costheta* q[index1]
                -sintheta*p[index1]) -fact2*q[index2];
    }
}
    m=m+1;
}
return;
}

```

It should be noted that **HARMONICS** does not alter the dipoles input in any way and no attempt is made to provide for changes through time. This is achieved by using **OSCTIME.C** and **DRIFTTIME.C** which are versions of **OSCDIPOLE.c** and **DRIFT.C** which call a different output routines **COEFFOUT.C** and **COEFFOUTD.C** which are very similar, and just calculate the new state of a group of dipoles after a period of time.

COEFFOUT.C

```

#include <stdio.h>
#include <math.h>
#include "dipole.h"

coeffout(head,y)
float y; /* number of years ago for output position */
struct dipole * head;
{
    float pi;
    int j;
    double moment;

    pi= 4*atan(1.);

    while (head){ /* for each dipole */
        if (head->no!=1) /* it's not the central dipole */
            moment= head->mom*sin(pi*2*y
                /head->period+head->phase);
        else
            moment=head->mom;
        head->lat *= 180/pi;
    }
}

```

```

        head->dlong *= 180/pi;
        printf(" %lf %lf %lf %lf %lf %lf\n",
                head->lat,head->dlong,head->period,
                head->phase,moment,head->radius);
        head=head->next; /* get the next dipole */
    }
    return;
}

```

The output of **HARMONICS** can be used in several ways depending on the type of analysis required. Two filters are available **DIPOLE** and **QUAD** which reduce the harmonic coefficients to either the dipole or quadrupole families of McFadden *et al* (1988).

DIPOLE.F

```

        program dipole
c     filters quadrupole family members from harmonics produced by
c     harmonics.c

        real*8 a,b,tmp,tmp2
        integer n,m

10     read(*,*,end=20) n,m,a,b
        tmp=(n-m)/2.0
        tmp2= tmp-dble(int(tmp))
        if (tmp2.lt..1)then
            write(*,*) n,m,' 0.0 0.0'
            goto 10
        endif
        write(*,*)n,m,a,b
        goto 10
20     continue
        end

```

QUAD.F

```

        program quad

```

```
c filters dipole family members from harmonics produced by
c harmonics.c
```

```

      real*8 a,b,tmp,tmp2
      integer n,m

10    read(*,*,end=20) n,m,a,b
      if(n.eq.1) goto 30
      tmp=(n-m)/2.0
      tmp2= tmp-dble(int(tmp))
      if (tmp2.gt..1)then
        write(*,*) n,m,' 0.0 0.0'
        goto 10
      endif
30    write(*,*)n,m,a,b
      goto 10
20    continue
      end
```

The output from **HARMONICS**, either filtered or not, can then be piped into **COMPS.F** which converts the harmonic coefficients into x,y & z components for display or further analysis.

COMPS.F

```

program comps

      IMPLICIT REAL*8(A-H,O-Z)
      DIMENSION GH(600),G1(120),G2(120),G3(120),G4(120),G5(120),
1      P(66),Q(66),CL(10),SL(10)
      EQUIVALENCE (G1,GH( 1)),(G2,GH(121)),(G3,GH(241)),(G4,GH(361)),
1      (G5,GH(481))

C
C
      date=1965.0
      itype=1
      i=1
910  read (*,*,end=900) n,m,gh(i),gh(i+1)
      if (m.eq.0) then
        i=i+1
        goto 910
```

```
        endif
        i=i+2
        goto 910
900    continue
C
        do 920 jloop=170,10,-10
        do 920 iloop=0,361,10

        colat = dble(jloop)
        elong = dble(iloop)
        alt=0.0
C    SET INITIAL VALUES
C
        X      = 0.0
        Y      = 0.0
        Z      = 0.0
        IF (DATE.LE.1960.0.OR.DATE.GE.1990.0) GO TO 9
        T      = 0.2*(DATE - 1965.0)
        LL     = T
        ONE    = LL
        T      = T - ONE
        LL     = 120*LL
        TC     = 1.0 - T
        IF (DATE.LE.1985.0) GO TO 10
        LL = LL - 120
        TC = TC - 1.0
        T  = T + 1.0
10 R    = ALT
        ONE = COLAT*0.0174533
        CT  = DCOS(ONE)
        ST  = DSIN(ONE)
        ONE = ELONG*0.0174533
        CL(1) = DCOS(ONE)
        SL(1) = DSIN(ONE)
        CD   = 1.0
        SD   = 0.0
        L    = 1
        M    = 1
        N    = 0
        IF (ITYPE.EQ.2) GO TO 1
C
C    CONVERSION FROM GEODETIC TO GEOCENTRIC COORDINATES
```

C

```

A2   = 40680925.
B2   = 40408585.
ONE  = A2*ST*ST
TWO  = B2*CT*CT
THREE = ONE + TWO
RHO  = DSQRT(THREE)
R    = DSQRT(ALT*(ALT + 2.0*RHO) + (A2*ONE + B2*TWO)/THREE)
CD   = (ALT + RHO)/R
SD   = (A2 - B2)/RHO*CT*ST/R
ONE  = CT
CT   = CT*CD - ST*SD
ST   = ST*CD + ONE*SD

```

C

```

1  RATIO = 6371.2/R
   RR    = RATIO*RATIO

```

C

C COMPUTATION OF SCHMIDT QUASI-NORMAL COEFFICIENTS P AND X(=Q)

C

```

P(1) = 1.0
P(3) = ST
Q(1) = 0.0
Q(3) = CT
DO 8 K=2,66
IF (N.GE.M) GO TO 2
M    = 0
N    = N + 1
RR   = RR*RATIO
FN   = N
GN   = N - 1
2  FM = M
IF (M.NE.N) GO TO 3
IF (K.EQ.3) GO TO 4
ONE  = DSQRT(1.0 - 0.5/FM)
J    = K - N - 1
P(K) = ONE*ST*P(J)
Q(K) = ONE*(ST*Q(J) + CT*P(J))
CL(M) = CL(M-1)*CL(1) - SL(M-1)*SL(1)
SL(M) = SL(M-1)*CL(1) + CL(M-1)*SL(1)
GO TO 4
3  GM = M*M
ONE  = DSQRT(FN*FN - GM)

```

```

TWO = DSQRT(GN*GN - GM)/ONE
THREE = (FN + GN)/ONE
I = K - N
J = I - N + 1
P(K) = THREE*CT*P(I) - TWO*P(J)
Q(K) = THREE*(CT*Q(I) - ST*P(I)) - TWO*Q(J)
C
C SYNTHESIS OF X, Y AND Z IN GEOCENTRIC COORDINATES
C
4 LM = LL + L
ONE = (TC*GH(LM) + T*GH(LM+120))*RR
IF (M.EQ.0) GO TO 7
TWO = (TC*GH(LM+1) + T*GH(LM+121))*RR
THREE = ONE*CL(M) + TWO*SL(M)
X = X + THREE*Q(K)
Z = Z - (FN + 1.0)*THREE*P(K)
IF (ST.EQ.0.0) GO TO 5
Y = Y + (ONE*SL(M) - TWO*CL(M))*FM*P(K)/ST
GO TO 6
5 Y = Y + (ONE*SL(M) - TWO*CL(M))*Q(K)*CT
6 L = L + 2
GO TO 8
7 X = X + ONE*Q(K)
Z = Z - (FN + 1.0)*ONE*P(K)
L = L + 1
8 M = M + 1
C
C CONVERSION TO COORDINATE SYSTEM SPECIFIED BY ITYPE
C
ONE = X
X = X*CD + Z*SD
Z = Z*CD - ONE*SD
F = DSQRT(X*X + Y*Y + Z*Z)
C
itmp=iloop
if (iloop .gt. 180) itmp=itmp-360
write (*,'(2(i4,x),3g14.4)') itmp,180-jloop-90,x,y,z
920 continue
C
C
9 CONTINUE
END

```

These components can be passed directly to a mapping package or piped into SCATTER which will carry out an analysis of the VGP scatter in ten degree latitude bands, as suggested by McFadden *et al* (1988).

SCATTER.C

```

#include <stdio.h>
#include <math.h>

main(){
    double dlat,t,s,top1,top,bot,x,y,z,pi;
    int i,j,lat,elong;

    pi=4.*atan(1.);
    for (j=0;j<17;j++){
        t=0.0;
        for (i= -180;i<180;i +=10){
            scanf("%d %d %lf %lf %lf",&elong,&lat,&x,&y,&z);
            dlat=((double)lat)*pi/180.0;
            top1=(-z*cos(dlat)+2.0* x *sin(dlat))*(-z*cos(dlat)
                +2.0* x* sin(dlat));
            top = sqrt(top1+(4*y*y));
            bot= -z*sin(dlat)-2*x*cos(dlat);
            s= (atan2(top,bot))*180/pi;
            if((top>0 && bot <0) || (top <0 && bot >0))
                s -= 180.0;
            t += s*s;
        }
        scanf("%d %d %lf %lf %lf",&elong,&lat,&x,&y,&z);
        /* don't read 0 degrees and 360 degrees */
        printf("%d %lf\n",lat,sqrt(t/35));
    }
    return;
}

```

Appendix B

Spherical Harmonics

If measurements are made in the atmosphere just above the Earth's surface which can be assumed to be insulating and non-magnetic, then the magnetic potential (U) satisfies:

$$\nabla^2 U = 0 \quad (\text{B.1})$$

and the magnetic induction of the field is

$$B = -\nabla U \quad (\text{B.2})$$

so that U obeys Laplace's equation:

$$\nabla^2 U = \frac{\partial^2 U}{\partial x^2} + \frac{\partial^2 U}{\partial y^2} + \frac{\partial^2 U}{\partial z^2} = 0 \quad (\text{B.3})$$

Solving equation B.3 in spherical coordinates (r, θ, λ) with the origin at the centre of the Earth with r increasing upwards, θ increasing southward and λ increasing eastward, gives solutions of the form:

$$r^k P_n^m(\cos \theta) \frac{\cos}{\sin} (m\lambda) \quad (\text{B.4})$$

where k is either n or $-(n-1)$, $m \leq n$ and $P_n^m(\cos \theta)$ is a Legendre function and is related to Legendre polynomials by:

$$P_n^m(\cos \theta) = N \sin^m \theta \frac{\partial^m}{\partial (\cos \theta)^m} P_n(\cos \theta) \quad (\text{B.5})$$

where N is a normalizing factor, which can be chosen for convenience. In the analysis of the geomagnetic field it is convenient to ensure that the average value of the square of $P_n^m(\cos \theta)$ over the surface of a sphere has the same value for all values of m . To

achieve this Schmidt introduced the value of N given by:

$$N^2 = 2 \frac{(n-m)!}{(n+m)!} \quad (\text{B.6})$$

(Parkinson, 1983). This normalization is generally used through out geomagnetic analysis.

The solution of equation B.3 for U on the surface of the Earth is:

$$U(r, \theta, \lambda) = \sum_{n=1}^{\infty} \sum_{m=0}^n \left(\frac{r^n}{a^{n-1}} \right) (b_n^m \cos m\lambda + c_n^m \sin m\lambda) \quad (\text{B.7})$$

$$P_n^m(\cos \theta) \sum_{n=1}^{\infty} \sum_{m=0}^n \left(\frac{a^{n+2}}{r^{n+1}} \right) (g_n^m \cos m\lambda + h_n^m \sin m\lambda) P_n^m(\cos \theta)$$

where a is the Earth's radius.

The summations start with $n = 1$ as $n = 0$ corresponds to $U =$ a constant or a zero field in the first summation and a magnetic monopole, which violates Maxwell's equations in the second; Legendre functions of the second kind ($Q_n^m(\cos \theta)$) are also excluded since these lead to a singular point at the pole ($\theta = 0$).

The coefficients b_n^m and c_n^m are related to the external field and can be ignored in a study of the internal field (g_n^m and h_n^m) since they are approximately the same size as the errors in the determination of g_n^m and h_n^m (Lowes, 1974).

Since the potential U is not a directly observable quantity, the three components of the magnetic field must be measured. X, Y and Z as north, east and vertically down these are related to U by:

$$X = -B_\theta = \left(\frac{1}{r} \right) \frac{\partial U}{\partial \theta} \quad (\text{B.8})$$

$$Y = B_\lambda = -(r \sin \theta)^{-1} \frac{\partial U}{\partial \lambda} \quad (\text{B.9})$$

$$Z = -B_r = \frac{\partial U}{\partial r} \quad (\text{B.10})$$

which allows the differentiation of equation B.7 giving:

$$X = \sum_{n=1}^{\infty} \sum_{m=0}^n [g_n^m \cos m\lambda + h_n^m \sin m\lambda] \frac{\partial}{\partial \theta} (P_n^m(\cos \theta)) \quad (\text{B.11})$$

$$Y = \sum_{n=1}^{\infty} \sum_{m=0}^n [g_n^m \sin m\lambda - h_n^m \cos m\lambda] \frac{m}{\sin \theta} P_n^m(\cos \theta) \quad (\text{B.12})$$

$$Z = \sum_{n=1}^{\infty} \sum_{m=0}^n [g_n^m \cos m\lambda + h_n^m \sin m\lambda] - n + 1 P_n^m(\cos \theta) \quad (\text{B.13})$$

The coefficients g_n^m and h_n^m in equations B.11 to B.13 are known as the Gauss coefficients and have units of Tesla (T). It should be noted that when $m = 0$ h_n^m is 0.

Expressing equation B.7 (without b_n^m and c_n^m) with only the g_1^0 term represents the field of a dipole with its axis coincident to the axis of rotation of the Earth, this is known as a geoaial dipole (GAD). If the terms g_1^1 and h_1^1 are used then the equation represents a dipole in the equatorial plane, a geoequatorial dipole (GED), with a longitude of $\tan^{-1}(h_1^1/g_1^1)$.

Combining these two terms gives the field of an eccentric dipole with inclination to the axis of rotation:

$$I = \tan^{-1} \left[\left\{ (g_1^1)^2 + (h_1^1)^2 \right\}^{1/2} / g_1^0 \right] \quad (\text{B.14})$$

The next coefficients in the expansion of equation B.7 ($g_2^0, g_2^1, h_2^1, g_2^2, h_2^2$) contribute a quadrupole field, with g_2^0 representing an axi-symmetric quadrupole, i.e. two opposite axial dipoles displaced along the axis, g_2^1 and h_2^1 represent axial dipoles displaced in the equatorial plane and g_2^2 and h_2^2 are equatorial dipoles displaced in the equatorial plane.

Higher order coefficients represent higher order multipoles at the centre of the Earth, which allow greater detail to be added to the representation of the geomagnetic field.

References

- Aho, A., Kernighan, B.W. and Weinberger, P., *AWK - A Pattern Scanning and Processing Language*, Bell Laboratories, Murray Hill, New Jersey, 1988
- Allredge, L.R. and Hurwitz, L., Radial Dipoles as Sources of the Earth's Main Magnetic Field, *J. Geophys. Res.*, **69:12**, 2631 - 2640, 1964.
- Allredge, L.R., Circular Current Loops, Magnetic Dipoles and Spherical Harmonic Analyses, *J. Geomag. Geoelectr.*, **32**, 357 - 364, 1980.
- Ammerman, A.J. and Cavalli-Sforza, L.L., *The Neolithic Transition and the Genetics of Populations in Europe*, Princeton Univ. Press, Princeton, New Jersey, 1983
- Berger, A., Milankovitch Theory and Climate, *Revs. of Geoph.* **36:4**, 624-657, 1988
- Berryman, J., Choice of Operator Length for Maximum Entropy Method Spectral Analysis, *Geophysics*, **43**, 1384-1391, 1978
- Bonatti, E., Pollen Sequence in the Lake Sediments, in Hutchinson, G., (ed) *Lanula: an Account of the History and Development of the Lago di Monterosi, Latinum, Italy. Transactions of the American Philisophical Soc*, **60**, 26-31, 1970
- Brigham, E., *The Fast Fourier Transform*, (Englewood Cliffs, NJ; Prentice Hall), 1974
- Bullard, E., Freedman, C., Gellman, H. and Nixon, J., The Westward Drift of the Earth's Magnetic Field, *Phil. Trans. Roy. Soc. A*, **243**, 67, 1950
- Bullard, E., Edmund Halley (1656-1742) *Endeavour* **15**, 189, 1956
- Burg, J., Maximum Entrophy Spectral Analysis, *37th Ann. Int. Meeting Soc. Explor. Geophys. Oklahoma City.*, 1967
- Chapman, S. and Bartels, J., *Geomagnetism* (2 vols.) Claredon Press, 1940

- Clark, R. Statistical Analysis of Palaeomagnetic Data, 249–261, *Geomagnetism of Baked Clays and Recent Sediments* eds. Creer, K.M., Tucholka, P. and Barton, C.E., Elsevier 1983.
- Colinson, D.W. Depositional Remanent Magnetization in Sediments. *J. Geophys. Res.* **70**, 4663 – 4668, 1965
- Cox, A., Analysis of Present Geomagnetic Field for Comparison with Palaeomagnetic Results, *J. Geomag. Geoelectr.*, **13**, 101 – 112, 1962.
- Creer, K.M., The Dispersion of the Geomagnetic Field due to Secular Variation and its Determination for Remote Times from Palaeomagnetic Data, *J. Geophys. Res.*, **67**, 3461 – 3476, 1962a.
- Creer, K.M., An Analysis of the Geomagnetic Field using Palaeomagnetic Methods, *J. Geomag. Geoelectr.*, **13**, 113 – 119, 1962b.
- Creer, K.M., Computer Synthesis of Geomagnetic Palaeosecular Variations, *Nature*, **304**, 695 – 699, 25th Aug 1983.
- Creer, K.M., Review of Lake Sediment Palaeomagnetic Data, *Geophys. Surv.*, **7**, 125 – 160, 1985.
- Creer, K.M., Thouveny, N. and Blunk, I., Climatic and Geomagnetic Influences on the Lac du Bouchet Palaeomagnetic SV Record through the last 110, 000 years, *P.E.P.I.*, **64**, 314–341, 1990.
- Creer, K., Dating of a Maar Lake Sediment Sequence Covering the Last Glacial Cycle, *Quat. Procs.* **1**, 75–87, 1991
- Creer, K.M. and Tucholka, P., Secular Variation as Recorded in Lake Sediments: a Discussion of North American and European Results. *Phil. Trans. R. Soc. Lond.* **74**, 199–221, 1982.
- Creer, K.M. and Tucholka, P., Geomagnetic Objectives of Palaeomagnetic and Archeomagnetic Research, 276 – 289, *Geomagnetism of Baked Clays and Recent Sediments*, eds. Creer, K.M., Tucholka, P. and Barton, C.E., Elsevier 1983a.
- Creer, K.M. and Tucholka, P., Epilogue, 276 – 289, *Geomagnetism of Baked Clays and Recent Sediments*, eds. Creer, K.M., Tucholka, P. and Barton, C.E., Elsevier 1983b.

- Creer, K.M., Valencio, D., Sinito, A., Tucholka, P. and Vilas, J., Geomagnetic Secular Variation 0–14000 Years Before Present as Recorded by Lake Sediments from Argentina. *Geophys. J. R. Astro. Soc.* 1983.
- Dankers, P., Relationship between Median Destructive Field and Remanent Coercive Forces for Dispersed Natural Magnetite, Titanomagnetite and Hematite, *Geophys. J. R. Astro. Soc.*, **64**, 447–461, 1981
- du Riche Preller, Italian Mountain Geology Part 3, Central and Southern Italy, *pubs. Wheldon and Wesley Ltd, London*, 1923
- Fisher, R.A., *Statistical Methods, Experimental Design and Scientific Inference*. Oxford University Press, Oxford, 1990.
- Gilberte, W., *De Magnete*, (1600), reprinted by Dover, New York, 1958
- Halley, E. A Theory of the Variation of the Magnetical Compass. *Phil. Trans.*, **13**, 208–221, 1683.
- Hamanno, Y. An Experiment on the Post-Depositional Remanent Magnetization in Artificial and Natural Sediments. *Earth Planet Sci. Let.*, **51**, 221 – 232 1980.
- Horne, J.H. and Baliunas, S.L., A Prescription for Period Analysis of Unevenly Sampled Time Series, *Ap. J.* **302**, 757, 1986
- Hurwitz, L., Eccentric Dipoles and Spherical Harmonic Analysis, *J. Geophys. Res.* **65**, 2555 – 2556, 1960.
- Imbrie, J., Hays, J., Martinson, D., McIntyre, A., Mix, A., Morley, J., Pisias, N., Prell, W. and Shackleton, N., The Orbital Theory of Pleistocene Climate: Support from a revised Chronology of the Marine ¹⁸O Record, in *Milankovitch and Climate*, ed. by A. Berger et al., 269–305, D. Reidel, Hingham, Mass. 1984
- Kelly, M.G. and Huntley, B., An 11,000-year record of vegetation and environment from Lago di Martignano, Latium, Italy, *J. Quat. Sci.* **6(3)**, 209–224, 1991.
- Kent, D., Apparent Correlation of Palaeomagnetic Intensity and Climate Records in Deep Sea Sediments, *Nature*, **229**, 538–39, 7th, 1962
- Kent, D. and Opdyke, N., Palaeomagnetic Field Intensity Variations Recorded in a Brunhes Epoch Deep-sea Core, *Nature*, **266**, 156–159, 1977

- King, J., Banerjee, S. and Marvin, J., A New Rock-Magnetic Approach to Selecting Sediments for Geomagnetic Palaeointensity Studies: Application to Palaeointensities for the Last 4000 years, *J.G.R.*, **88**, B7, 5911-5921, 1983
- King, J., Banerjee, S., Marvin, J. and Özdemir, Ö, A Comparison of Different Magnetic Methods for Determining the Relative Grain Size of Magnetite in Natural Materials: Some Results from Lake Sediments, *E.P.S.L.*, **59**, 405-419, 1982
- Koenigsberg, J., Natural Residual Magnetism of Eruptive Rocks, *Terr. Magn. Atmos. electr.* **43**, 119-127, 1938
- Leeder, M., Sediment Deformation Structures and the Palaeotectonic Analysis of Sedimentary Basins, with a Case Study from the Carboniferous of Northern England. 137-146, *Deformation of Sediments and Sedimentary Rocks*, ed. by M. Jones and R. Preston, Geol. Soc. Special Publication, **29**, 1987
- Livingstone, D.A., A Lightweight Piston Sampler for Lake Deposits, *Ecology*, **36**, 137-139, 1955
- Lomb, N., Least-squares Frequency Analysis of Unequally Spaced Data, *Astrophys. Space. Sci.* **39**, 447-462, 1976
- Loper, D., Torque Balance and Energy Budget for the Precessionally Driven Dynamo, *P.E.P.I.*, **11**, 43-60, 1975
- Lorenz, V., On the Formation of Maars, *Bulletin Volcanologique* **37**, 183-204, 1973
- Louris. C., Jouzel, J., Ritz, C., Merlivat, L., Barkov, N., Kofgekvich, Y. and Kotlyakov, V., A 150,000 year Climatic Record from Antarctic Ice, *Nature*, **316**, 591-596, 1985
- Lovlie, R., Post-Depositional Remanent Magnetization in Re-deposited Deep-Sea Sediments. *Earth Planet. Sci. Lett.*, **21**, 315 - 320, 1974.
- Lowes, F.J., Spatial Power Spectrum of the Main Geomagnetic Field, and extrapolation to the Core, *Geophys. J. Roy. Astro. Soc.*, **36**, 717-730, 1974
- Mackereth, F.J., A Portable Core Sampler for Lake Deposits. *Limnol. Oceanog.* **3**, 181 - 191, 1958.
- Malkus, R., Precessional Torques as the Cause of Geomagnetism, *J.G .R* **68**, No **10**, 2871-2886, 1963